



WILEY

New Phase Space Formulations and Quantum Dynamics Approaches

Journal:	<i>WIREs Computational Molecular Science</i>
Manuscript ID	CMS-842
Wiley - Manuscript type:	Focus Article
Date Submitted by the Author:	05-Feb-2022
Complete List of Authors:	He, Xin; Peking University, College of Chemistry and Molecular Engineering Wu, Baihua; Peking University, College of Chemistry and Molecular Engineering Shang, Youhao; Peking University, College of Chemistry and Molecular Engineering Li, Binqi; Peking University, College of Chemistry and Molecular Engineering Cheng, Xiangsong; Peking University, College of Chemistry and Molecular Engineering Liu, Jian; Peking University, College of Chemistry and Molecular Engineering
Keywords:	quantum dynamics, nonadiabatic dynamics, phase space formulation, composite quantum systems, constraint phase space
Choose 1-3 topics to categorize your article:	Molecular Dynamics and Monte-Carlo Methods (CDAC) < Molecular and Statistical Mechanics (CDAA), Reaction Dynamics and Kinetics (CEAB) < Theoretical and Physical Chemistry (CEAA), Statistical Mechanics (CEAE) < Theoretical and Physical Chemistry (CEAA)

SCHOLARONE™
Manuscripts

1
2
3
4
5 **New Phase Space Formulations and Quantum Dynamics Approaches**
6
7 **(Invited Contribution)**
8
9

10 **Article Type:**
11
12

- 13 OPINION PRIMER OVERVIEW
14 ADVANCED REVIEW FOCUS ARTICLE SOFTWARE FOCUS
15
16
17
18

19 **Authors:**
20
21

22 **Xin He** (co-first author)
23
24 Beijing National Laboratory for Molecular Sciences, Institute of Theoretical and Computational
25 Chemistry, College of Chemistry and Molecular Engineering, Peking University, Beijing 100871,
26 China
27
28

29 **Baihua Wu** (co-first author)
30
31 Beijing National Laboratory for Molecular Sciences, Institute of Theoretical and Computational
32 Chemistry, College of Chemistry and Molecular Engineering, Peking University, Beijing 100871,
33 China
34
35

36 **Youhao Shang**
37
38 Beijing National Laboratory for Molecular Sciences, Institute of Theoretical and Computational
39 Chemistry, College of Chemistry and Molecular Engineering, Peking University, Beijing 100871,
40 China
41
42

43 **Bingqi Li**
44
45 Beijing National Laboratory for Molecular Sciences, Institute of Theoretical and Computational
46 Chemistry, College of Chemistry and Molecular Engineering, Peking University, Beijing 100871,
47 China
48
49

50 **Xiangsong Cheng**
51
52 Beijing National Laboratory for Molecular Sciences, Institute of Theoretical and Computational
53 Chemistry, College of Chemistry and Molecular Engineering, Peking University, Beijing 100871,
54 China
55
56

1
2
3
4
5
6
7
8
9
10
11
12
13
14
15
16
17
18
19
20
21
22
23
24
25
26
27
28
29
30
31
32
33
34
35
36
37
38
39
40
41
42
43
44
45
46
47
48
49
50
51
52
53
54
55
56
57
58
59
60

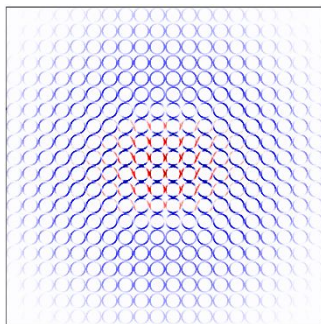
Jian Liu*

Beijing National Laboratory for Molecular Sciences, Institute of Theoretical and Computational Chemistry, College of Chemistry and Molecular Engineering, Peking University, Beijing 100871, China
ORCID ID: 0000-0002-2906-5858
Email: jianliupku@pku.edu.cn

Abstract

We report recent progress on the phase space formulation of quantum mechanics with coordinate-momentum variables, focusing more on new theory of (weighted) constraint coordinate-momentum phase space for discrete-variable quantum systems. This leads to a general coordinate-momentum phase space formulation of composite quantum systems, where conventional formulations on infinite phase space are employed for continuous variables. It is convenient to utilize (weighted) constraint coordinate-momentum phase space for representing the quantum state and describing nonclassical features. Various numerical tests demonstrate that the new trajectory-based quantum dynamics approaches with the (weighted) constraint phase space representation are useful and practical for describing processes of composite quantum systems in gas phase as well as in condensed phase.

Graphical/Visual Abstract and Caption



Schematic representation of a Bell entangled state of a composite quantum system

1. INTRODUCTION

Phase space with coordinate-momentum variables is a fundamental concept and offers a convenient tool to describe statistics as well as dynamics in classical mechanics. In comparison to other equivalent interpretations of quantum mechanics, phase space formulations offer more insight and understanding between quantum and

1
2
3 classical counterpart concepts, which are widely used in chemical and biological dynamics and spectroscopy¹⁻⁶⁰,
4 quantum optics^{51, 61-70}, cryogenic physics/chemistry⁷¹⁻⁷⁵, quantum information and computation⁷⁶⁻⁸⁷, etc.
5
6

7 Phase space formulations of quantum mechanics have been developed since two important pioneering works,
8 the Weyl transform in 1927, of which the original formulation converted a Hamiltonian on classical phase space
9 into a quantum mechanical operator⁸⁸, and the Wigner function in 1932 that in principle depicts the inverse
10 transform although a pure state was used for demonstration⁸⁹. The most essential element is the one-to-one
11 correspondence mapping between quantum operators and classical functions often defined on a smooth manifold,
12 namely, the phase space. Because of the commutation relation of conjugate operators, the mapping is not unique
13 in quantum mechanics^{90, 91}.
14
15

16 When infinite phase space is employed for a continuous-variable quantum system, most phase space
17 formulations can be described by Cohen's generalized form⁹² in 1966. Quantum dynamics with phase space
18 variables is expressed by the Moyal or Moyal-like bracket as first proposed by Groenewold⁹³ in 1946 and Moyal⁹⁴
19 in 1949. The Wigner and Husimi representations are most often used for the continuous-variable system. When
20 the Moyal bracket is approximated by the Poisson bracket in the phase space expression of the quantum Liouville
21 theorem, which was also derived as the linearized semiclassical initial value representation (LSC-IVR) or classical
22 Wigner model^{4-8, 11, 20, 23} for the quantum correlation function. It reproduces exact quantum correlation functions
23 even of nonlinear operators (i.e., nonlinear functions of the coordinate or momentum operator). The LSC-IVR is
24 similar to the truncated Wigner approximation⁷⁴ with the time-dependent generalization of the Bopp
25 representation^{90, 95}, but the latter requests evaluation of the stability matrix elements along the trajectory when
26 nonlinear operators are involved in the correlation function. Ref. ¹⁵ suggests a practical way to implement the
27 imaginary time path integral treatment of the Boltzmann density operator in the LSC-IVR for general molecular
28 systems that often contain imaginary frequencies. Its recent application illustrates that quantum dynamical effects
29 play a critical role in reproducing the peaks in the intermediate region between the librational and bending bands,
30 those between the bending and stretching bands, and the double-peak in the stretching band in the experimental
31 isotropic Raman spectrum of liquid water¹⁹ (as shown in Figure 1). In addition that more advanced versions of
32 SC-IVR⁹⁶⁻⁹⁹ are capable of improving over the LSC-IVR, in ref ¹¹ we first employed the quantum Liouville
33 theorem in the phase space formulation to develop trajectory-based approaches to satisfy the two fundamental
34 criteria: conservation of the quantum Boltzmann distribution for the thermal equilibrium system and being exact
35 for any quantum thermal correlation functions in the classical and harmonic limits. Such trajectory-based
36 approaches can in principle be further improved by higher order corrections of the exact series expansion of the
37 38 39 40 41 42 43 44 45 46 47 48 49 50 51 52 53 54 55 56 57 58 59 60

phase space propagator as demonstrated in ref⁴⁴. More progress along this line can be found in refs³⁷⁻⁴⁷. (Figure 2 shows molecular vibrational spectra reported along this line.)

Phase space representations of a finite discrete F -state quantum system were first independently described by Stratonovich¹⁰⁰ in 1956, Feynman¹⁰¹ in 1987, and Wootters¹⁰² in 1987. Further developments of Stratonovich's formulation have focused on an SU(2) or SU(F) structure of phase space¹⁰³⁻¹¹⁷, while those on the construction of a discrete phase space are described in Refs^{78, 118-126}. Other than the 2-state (or spin 1/2) system, the exact equations of motion (EOMs) of the phase variables (expressed by the Moyal-like bracket) involved in these approaches for the finite discrete multi-state system are often tedious (and nonlinear)^{109, 127-130}. Recent theoretical progress on exact mapping the finite discrete F -state quantum system onto *constraint* coordinate-momentum phase space suggests that there exists a novel unified framework to derive comprehensive exact mapping Hamiltonians^{44, 57, 131, 132}, of which the quantum EOMs of mapping coordinate-momentum variables are simply linear^{44, 57, 131-134}.

The unified mapping formulation on coordinate-momentum phase space^{44, 57, 131-134} then offers a useful tool to treat dynamics of a composite quantum system, in which both continuous and finite discrete degrees of freedom (DOFs) are involved and coupled with one another. Because a typical molecular system has vibrational, rotational, and translational motion, it is often much more convenient to employ continuous coordinate space rather than Hilbert space with dense states to describe the nuclear DOFs. On the other hand, the energy gap between different electronic states of interest is often significantly larger such that the (adiabatic or diabatic) state representation is more useful to depict the electronic DOFs. It is evident that a general description of the molecular system leads to a composite quantum system, especially in the nonadiabatic region¹³⁵⁻¹⁵². A comprehensive version of the Meyer-Miller mapping Hamiltonian model^{153, 154} can rigorously be formulated in the general coordinate-momentum phase space formulation^{44, 57, 131-134}.

In the Focus Article we focus on novel developments on the phase space formulation of quantum mechanics with coordinate-momentum variables for discrete-variable systems as well as for composite systems^{44, 57, 131-134}. In Section 2 we first review the general coordinate-momentum phase space formulation, where infinite space is used for describing continuous variables and constraint space is employed for mapping discrete variables. We then propose a weighted constraint phase space representation that is also an exact formulation for mapping discrete variables. Section 3 demonstrates several examples and discusses implications of the (weighted) constraint coordinate-momentum phase space for studying and illustrating discrete-variable or composite quantum systems. When we use the weighted constraint phase space representation for mapping the composite system, the

mapping Hamiltonian (we use the Meyer-Miller mapping Hamiltonian for demonstration throughout the article, albeit that other mapping Hamiltonians are also available^{57, 58, 131, 132}) yields a new trajectory-based approximate approaches for composite systems. Such a new method satisfies the frozen nuclei limit [i.e., the dynamics reproduces the exact evolution when only finite discrete (electronic) DOFs are involved]. In Section 4 the performance of new trajectory-based quantum dynamics approaches on (weighted) constraint phase space is extensively tested for a few typical benchmark composite systems in gas phase as well as in condensed phase. Finally, conclusion remarks are presented in Section 5.

2. GENERAL COORDINATE-MOMENTUM PHASE SPACE FORMULATION OF QUANTUM MECHANICS

Consider a (molecular) system with N continuous (nuclear) DOFs and F discrete (electronic) states, of which the Hamiltonian reads

$$\hat{H} = \sum_{n,m=1}^F H_{nm}(\hat{\mathbf{R}}, \hat{\mathbf{P}}) |n\rangle\langle m| = \sum_{n,m=1}^F \left[\frac{1}{2} \hat{\mathbf{P}}^T \mathbf{M}^{-1} \hat{\mathbf{P}} \delta_{nm} + V_{nm}(\hat{\mathbf{R}}, \hat{\mathbf{P}}) \right] |n\rangle\langle m| , \quad 2$$

where \mathbf{R} and \mathbf{P} are the nuclear coordinate and momentum variables, respectively, \mathbf{M} is the diagonal mass matrix, and the F states form an orthonormal complete basis sets, i.e.,

$$\langle m | n \rangle = \delta_{mn}, \quad \hat{I}_{ele} = \sum_{n=1}^F |n\rangle\langle n| . \quad 3$$

\hat{I}_{ele} and \hat{I}_{nuc} stand for the identity operator of the discrete (electronic) DOFs and that of the continuous (nuclear) DOFs. The potential term in the diabatic representation is a function of only the coordinate vector, i.e., $V_{nm}(\mathbf{R}, \mathbf{P}) = V_{nm}(\mathbf{R})$. In the adiabatic representation the term that includes \mathbf{P} in $V_{nm}(\mathbf{R}, \mathbf{P})$ is linearly dependent on \mathbf{P} (See Appendix 1).

The unified formulation of mapping phase space in the coordinate-momentum representation offers a useful exact approach to describe the composite system. The trace of a product of two quantum operators is expressed as an integral of two functions on mapping phase space, *i.e.*,

$$\text{Tr}_{n,e} [\hat{A}\hat{B}] = \int d\mu_{nuc}(\mathbf{R}, \mathbf{P}) \int_{S(x,p)} d\mu_{ele}(x, p) A_C(\mathbf{R}, \mathbf{P}; x, p) B_C^0(\mathbf{R}, \mathbf{P}; x, p) \quad 4$$

with

$$A_C(\mathbf{R}, \mathbf{P}; x, p) = \text{Tr}_{n,e} [\hat{A} \hat{K}_{nuc}(\mathbf{R}, \mathbf{P}) \otimes \hat{K}_{ele}(x, p)] , \quad 5$$

$$\hat{B}_C^0(\mathbf{R}, \mathbf{P}; \mathbf{x}, \mathbf{p}) = \text{Tr}_{n,e} \left[\hat{K}_{nuc}^{-1}(\mathbf{R}, \mathbf{P}) \otimes \hat{K}_{ele}^{-1}(\mathbf{x}, \mathbf{p}) \hat{B} \right], \quad 6$$

$d\mu_{nuc}(\mathbf{R}, \mathbf{P}) = (2\pi\hbar)^{-N} d\mathbf{R}d\mathbf{P}$ and $d\mu_{ele}(\mathbf{x}, \mathbf{p}) = F d\mathbf{x}d\mathbf{p}$ as the integration measure on nuclear phase space and that on electronic phase space, respectively, and $\text{Tr}_{n,e}$ represents the trace over the corresponding nuclear and electronic Hilbert space. The integral over the mapping phase space variables for the finite discrete (electronic) DOFs in eq 4 is performed as

$$\int_{S(x,p)} F d\mathbf{x}d\mathbf{p} g(\mathbf{x}, \mathbf{p}) = \int F d\mathbf{x}d\mathbf{p} \frac{1}{\Omega} S(\mathbf{x}, \mathbf{p}) g(\mathbf{x}, \mathbf{p}) = \int F d\mathbf{x}d\mathbf{p} \bar{S}(\mathbf{x}, \mathbf{p}) g(\mathbf{x}, \mathbf{p}), \quad 7$$

where the area of constraint space $S(\mathbf{x}, \mathbf{p})$

$$\Omega = \int d\mathbf{x}d\mathbf{p} S(\mathbf{x}, \mathbf{p}) \quad 8$$

is the normalization constant, and $\bar{S}(\mathbf{x}, \mathbf{p})$ is the normalized constraint space.

The normalization of the (inverse) mapping kernel reads

$$\text{Tr}_n \left[\hat{K}_{nuc}(\mathbf{R}, \mathbf{P}) \right] = \text{Tr}_n \left[\hat{K}_{nuc}^{-1}(\mathbf{R}, \mathbf{P}) \right] = 1 \quad 9$$

$$\text{Tr}_e \left[\hat{K}_{ele}(\mathbf{x}, \mathbf{p}) \right] = \text{Tr}_e \left[\hat{K}_{ele}^{-1}(\mathbf{x}, \mathbf{p}) \right] = 1 \quad 10$$

and

$$\int d\mu_{nuc}(\mathbf{R}, \mathbf{P}) \hat{K}_{nuc}(\mathbf{R}, \mathbf{P}) = \int d\mu_{nuc}(\mathbf{R}, \mathbf{P}) \hat{K}_{nuc}^{-1}(\mathbf{R}, \mathbf{P}) = \hat{I}_{nuc} \quad 11$$

$$\int_{S(x,p)} d\mu_{ele}(\mathbf{x}, \mathbf{p}) \hat{K}_{ele}(\mathbf{x}, \mathbf{p}) = \int_{S(x,p)} d\mu_{ele}(\mathbf{x}, \mathbf{p}) \hat{K}_{ele}^{-1}(\mathbf{x}, \mathbf{p}) = \hat{I}_{ele}. \quad 12$$

The one-to-one correspondence mapping from phase space function $A_C(\mathbf{R}, \mathbf{P}; \mathbf{x}, \mathbf{p})$ or $\hat{B}_C^0(\mathbf{R}, \mathbf{P}; \mathbf{x}, \mathbf{p})$ of Eq 5 back to operator \hat{A} or \hat{B} is

$$\begin{aligned} \hat{A} &= \int d\mu_{nuc}(\mathbf{R}, \mathbf{P}) \int_{S(x,p)} d\mu_{ele}(\mathbf{x}, \mathbf{p}) A_C(\mathbf{R}, \mathbf{P}; \mathbf{x}, \mathbf{p}) \hat{K}_{nuc}^{-1}(\mathbf{R}, \mathbf{P}) \otimes \hat{K}_{ele}^{-1}(\mathbf{x}, \mathbf{p}) \\ \hat{B} &= \int d\mu_{nuc}(\mathbf{R}, \mathbf{P}) \int_{S(x,p)} d\mu_{ele}(\mathbf{x}, \mathbf{p}) \hat{B}_C^0(\mathbf{R}, \mathbf{P}; \mathbf{x}, \mathbf{p}) \hat{K}_{nuc}(\mathbf{R}, \mathbf{P}) \otimes \hat{K}_{ele}(\mathbf{x}, \mathbf{p}) \end{aligned} \quad 13$$

The nuclear or electronic kernel should satisfy five criteria, namely, linearity, reality, standardization (normalization), traciality, and covariance^{93, 94, 100, 115}.

1
2
3 **2.1 Mapping kernel for continuous (nuclear) degrees of freedom**
4

5 The integrals for (\mathbf{R}, \mathbf{P}) in eqs 4, 11, and 13 are over infinite (nuclear) phase space. The mapping kernel
6
7 and its inverse for the nuclear DOFs are
8
9

$$\begin{aligned} \hat{K}_{nuc}(\mathbf{R}, \mathbf{P}) &= \left(\frac{\hbar}{2\pi} \right)^N \int d\zeta \int d\eta e^{i\zeta(\hat{\mathbf{R}}-\mathbf{R})+i\eta(\hat{\mathbf{P}}-\mathbf{P})} f(\zeta, \eta) \\ \hat{K}_{nuc}^{-1}(\mathbf{R}, \mathbf{P}) &= \left(\frac{\hbar}{2\pi} \right)^N \int d\zeta \int d\eta e^{i\zeta(\hat{\mathbf{R}}-\mathbf{R})+i\eta(\hat{\mathbf{P}}-\mathbf{P})} [f(\zeta, \eta)]^{-1} \end{aligned} \quad , \quad 14$$

18 where $f(\zeta, \eta)$ is a scalar function. E.g., we have the Wigner function^{89, 155}
19

$$f(\zeta, \eta) = 1 \quad , \quad 15$$

25 the Husimi function¹⁵⁶
26

$$f(\zeta, \eta) = \exp \left(-\frac{\zeta^T \Gamma^{-1} \zeta}{4} - \frac{\hbar^2}{4} \eta^T \Gamma \eta \right) , \quad 16$$

32 the anti-Husimi function
33

$$f(\zeta, \eta) = \exp \left(\frac{\zeta^T \Gamma^{-1} \zeta}{4} + \frac{\hbar^2}{4} \eta^T \Gamma \eta \right) , \quad 17$$

38 the Glauber-Sudarshan P function^{61, 62, 66} (with the characteristic frequency matrix ω of the system)
39

$$f(\zeta, \eta) = \exp \left[\frac{\hbar}{4} \zeta^T \mathbf{M}^{-1/2} \omega^{-1} \mathbf{M}^{-1/2} \zeta + \frac{\hbar}{4} \eta^T \mathbf{M}^{1/2} \omega \mathbf{M}^{1/2} \eta \right] \quad 18$$

45 and its generalized versions⁶⁶, the Glauber Q function¹⁵⁷
46

$$f(\zeta, \eta) = \exp \left[-\frac{\hbar}{4} \zeta^T \mathbf{M}^{-1/2} \omega^{-1} \mathbf{M}^{-1/2} \zeta - \frac{\hbar}{4} \eta^T \mathbf{M}^{1/2} \omega \mathbf{M}^{1/2} \eta \right] , \quad 19$$

52 the normal-antinormal ordered function⁹¹
53

$$f(\zeta, \eta) = \cosh \left[\frac{\hbar}{4} \zeta^T \mathbf{M}^{-1/2} \omega^{-1} \mathbf{M}^{-1/2} \zeta + \frac{\hbar}{4} \eta^T \mathbf{M}^{1/2} \omega \mathbf{M}^{1/2} \eta \right] , \quad 20$$

59 the Kirkwood antistandard-ordered function^{158, 159}
60

$$f(\zeta, \eta) = e^{i\hbar\zeta^T \eta/2}, \quad 21$$

the Mehta standard-ordered function¹⁶⁰

$$f(\zeta, \eta) = e^{-i\hbar\zeta^T \eta/2}, \quad 22$$

the Rivier function^{161, 162}

$$f(\zeta, \eta) = \cos\left[\frac{1}{2}\hbar\zeta^T \eta\right], \quad 23$$

and the distribution function of Born and Jordan¹⁶³

$$f(\zeta, \eta) = \frac{\sin\left[\frac{1}{2}\hbar\zeta^T \eta\right]}{\frac{1}{2}\hbar\zeta^T \eta}, \quad 24$$

etc.

2.2 Mapping kernel on constraint space for discrete (electronic) degrees of freedom

As derived first in Appendix A of ref¹³² and then in the Supporting Information of ref¹³⁴, the kernel that maps a set of F states onto constraint phase space $\mathbf{S}(\mathbf{x}, \mathbf{p})$ reads

$$\hat{K}_{ele}(\mathbf{x}, \mathbf{p}) = \sum_{n,m=1}^F \left[\frac{1}{2} (x^{(n)} + ip^{(n)}) (x^{(m)} - ip^{(m)}) - \gamma \delta_{nm} \right] |n\rangle\langle m| \quad 25$$

and the corresponding inverse kernel is

$$\hat{K}_{ele}^{-1}(\mathbf{x}, \mathbf{p}) = \sum_{n,m=1}^F \left[\frac{1+F}{2(1+F\gamma)^2} (x^{(n)} + ip^{(n)}) (x^{(m)} - ip^{(m)}) - \frac{1-\gamma}{1+F\gamma} \delta_{nm} \right] |n\rangle\langle m|. \quad 26$$

As naturally required by eq 10, constraint phase space $\mathbf{S}(\mathbf{x}, \mathbf{p})$ is defined by

$$\delta\left(\sum_{n=1}^F \frac{(x^{(n)})^2 + (p^{(n)})^2}{2} - (1+F\gamma)\right), \quad 27$$

of which the area is

$$\Omega(\gamma) = \int d\mathbf{x}d\mathbf{p} \delta\left(\sum_{n=1}^F \frac{(x^{(n)})^2 + (p^{(n)})^2}{2} - (1+F\gamma)\right). \quad 28$$

The normalized constraint phase space is $\bar{\mathbf{S}}(\mathbf{x}, \mathbf{p}) = \mathbf{S}(\mathbf{x}, \mathbf{p})/\Omega(\gamma)$.

Equations 25-28 define the mapping kernel and inverse kernel as well as constraint phase space, which are the key elements of the coordinate-momentum phase space formulation of the discrete-variable quantum system that we first established in refs^{131, 132} and further developed in refs^{57, 58, 134}. As yielded from eq 5, when the Wigner function eq 15 is used for the nuclear DOFs, the mapping Hamiltonian for the quantum Hamiltonian operator eq 2 reads

$$H_{map}(\mathbf{R}, \mathbf{P}; \mathbf{x}, \mathbf{p}; \gamma) = \frac{1}{2} \mathbf{P}^T \mathbf{M}^{-1} \mathbf{P} + \sum_{n,m=1}^F \left[\frac{1}{2} (x^{(n)} x^{(m)} + p^{(n)} p^{(m)}) - \gamma \right] V_{mn}(\mathbf{R}, \mathbf{P}) , \quad 29$$

which is the seminal Meyer-Miller Hamiltonian¹⁵³ that has extensively been implemented for nonadiabatic dynamics in the literature^{4, 56, 60, 138, 154, 164-218}. In refs^{58, 131, 132} it is shown that there also exist other mapping Hamiltonian models in the general coordinate-momentum phase space formulation of quantum mechanics. When the mapping Hamiltonian is employed to generate trajectory-based dynamics in the phase space formulation for a composite quantum system, we denote it the classical mapping model (CMM) approach. It satisfies the frozen nuclei limit. We use the Meyer-Miller Hamiltonian for demonstration throughout the Focus Article.

When Meyer and Miller proposed the original Meyer-Miller mapping Hamiltonian model for the nonadiabatic system in 1979, they did not invoke the phase space formulation. In 1997 Stock and Thoss¹⁵⁴ utilized the Schwinger oscillator theory of angular momentum^{219, 220} to derive the Meyer-Miller mapping Hamiltonian¹⁵³. Its LSC-IVR approximation⁴ in principle includes *infinite* Wigner phase space for the finite discrete (electronic) DOFs. The applications, however, suggest that the LSC-IVR approximation in the framework of Refs^{4, 154, 170} is not good^{172, 177, 181, 187, 195, 200, 202}. More advanced semiclassical approaches^{96, 97} improve the performance but request more computational effort^{172, 173}. The symmetric-window-function and other techniques have been introduced to practically overcome the drawbacks^{177, 181, 187, 195, 200, 202}.

Equation 27 indicates that parameter γ lies in region $(-1/F, \infty)$. It is shown that parameter γ can be either positive or negative^{131, 134} and should be interpreted as a special case of the commutator matrix^{57, 58, 131, 134} rather than the conventional zero-point-energy parameter^{153, 154}. There exist three key elements for a trajectory-based quantum dynamics to evaluate the evolution of the expectation/ensemble average of any physical properties, namely,

- 1) the EOMs of the trajectory,
- 2) the initial condition of the trajectory, and
- 3) the integral expression for the expectation/ensemble average of the physical property of interest.

In the frozen-nuclei limit, Hamilton's EOMs governed by the Meyer-Miller mapping Hamiltonian is isomorphic to exact dynamics. While it is reasonable to employ the mapping Hamiltonian to define the EOMs of the trajectory, the left two elements are also important to consider such that the trajectory-based dynamics method is consistent. The constraint coordinate-momentum phase space formulation then offers a more advanced platform to consider all the three key elements.

It is evident that eq 27 is a special choice of constraint phase space $\mathbf{S}(\mathbf{x}, \mathbf{p})$. The interpretation of parameter γ in refs^{57, 58, 131, 134} hints that a more comprehensive choice of normalized constraint phase space $\bar{\mathbf{S}}(\mathbf{x}, \mathbf{p})$ is

$$\int_{-1/F}^{\infty} d\gamma w(\gamma) \frac{1}{\Omega(\gamma)} \delta\left(\sum_{n=1}^F \frac{(x^{(n)})^2 + (p^{(n)})^2}{2} - (1+F\gamma)\right), \quad 30$$

with the *quasi*-probability distribution function

$$\int_{-1/F}^{\infty} d\gamma w(\gamma) = 1. \quad 31$$

Equation 7, the integral over the mapping phase space variables for the finite discrete (electronic) DOFs then becomes

$$\int_{\mathbf{S}(\mathbf{x}, \mathbf{p})} F d\mathbf{x} d\mathbf{p} g(\mathbf{x}, \mathbf{p}) = \int_{-1/F}^{\infty} d\gamma w(\gamma) \int F d\mathbf{x} d\mathbf{p} \frac{1}{\Omega(\gamma)} \delta\left(\sum_{n=1}^F \frac{(x^{(n)})^2 + (p^{(n)})^2}{2} - (1+F\gamma)\right) g(\mathbf{x}, \mathbf{p}). \quad 32$$

If we require that the kernel is the same as its inverse, i.e.,

$$\hat{K}_{ele}(\mathbf{x}, \mathbf{p}) = \hat{K}_{ele}^{-1}(\mathbf{x}, \mathbf{p}) = \sum_{n,m=1}^F \left[\frac{1}{2} (x^{(n)} + ip^{(n)}) (x^{(m)} - ip^{(m)}) - \gamma \delta_{nm} \right] |n\rangle \langle m|, \quad 33$$

it is then not difficult to obtain

$$\int_{-1/F}^{\infty} d\gamma w(\gamma) \chi(\gamma) = 1 \quad 34$$

with

$$\chi(\gamma) = F\gamma^2 + 2\gamma. \quad 35$$

(See Appendix 2 for more discussion.) Equations 30-35 define normalized constraint phase space $\bar{\mathbf{S}}(\mathbf{x}, \mathbf{p})$, the mapping kernel and inverse kernel, and the *quasi*-probability distribution function $w(\gamma)$ of parameter γ . The weighted constraint phase space formulation for the discrete-variable quantum system is the key new theoretical result of the Focus Article. When the Wigner function, eq 15, is used for the nuclear DOFs, where

$\hat{K}_{nuc}(\mathbf{x}, \mathbf{p}) = \hat{K}_{nuc}^{-1}(\mathbf{x}, \mathbf{p})$, eq 5 is then identical to eq 6. The mapping Hamiltonian for the quantum Hamiltonian operator eq 2 produced by either of eq 5 and eq 6 leads to the same expression as eq 29. When the mapping Hamiltonian is utilized to produce the trajectory-based dynamics for a composite system, it is denoted the weighted mapping model (wMM) approach. The frozen nuclei limit is satisfied in wMM.

Many choices are possible for the discrete or continuous version of the normalized quasi-probability distribution function $w(\gamma)$ in the weighted constraint phase space mapping theory. In the Focus Article we consider only the simplest cases of the discrete version. When but a single value of parameter γ is chosen in eq 34, i.e., $w(\gamma) = \delta(\gamma - \gamma_1)$, we obtain

$$F\gamma^2 + 2\gamma = 1 , \quad 36$$

of which the non-trivial solution is

$$\gamma = \frac{\sqrt{1+F} - 1}{F} . \quad 37$$

In this case, the weighted constraint phase space formulation is identical to the constraint phase space formulation, and wMM becomes CMM when trajectory-based dynamics is considered. When only two values of parameter γ are selected, i.e.,

$$w(\gamma) = \sum_{j=1}^2 w(\gamma_j) \delta(\gamma - \gamma_j) , \quad 38$$

eq 31 and eq 34 lead to

$$w(\gamma_1) = \frac{1 - \chi(\gamma_2)}{\chi(\gamma_1) - \chi(\gamma_2)} \quad 39$$

$$w(\gamma_2) = \frac{\chi(\gamma_1) - 1}{\chi(\gamma_1) - \chi(\gamma_2)}$$

When the values of parameter γ are close to zero or smaller than zero in region $(-1/F, \infty)$, trajectories produced by the Meyer-Miller mapping Hamiltonian eq 29 for nonadiabatic molecular dynamics are stable. For demonstration in the paper we choose

$$\gamma_1 = -\gamma_2 = \Delta \quad 40$$

with Δ a reasonably small positive real number. Figure 3 presents the constraint coordinate-momentum phase space formulation when a single value of parameter γ is used (Figure 3a) as well as the weighted formulation when two values of parameter γ suggested by eq 40 are used (Figure 3b).

3. PHASE SPACE REPRESENTATION OF NONCLASSICAL FEATURES IN QUANTUM SYSTEMS

Recent advance on quantum technologies makes it possible to control and manipulate quantum states in experiment. Because the phase space formulation offers an informationally complete description of the density matrix, direct measurements of phase space of the quantum system with continuous DOFs, those of the quantum system with discrete DOFs, and those of the composite quantum system have been realized in experiment^{70, 85, 221-234}. Stratonovich phase space has been used for illustration of nonclassical features of coupled spins^{113, 227, 235, 236}, as well as for visualization of nonclassical correlations or entanglement between the discrete DOF and the continuous DOF of the composite system^{237, 238}. However, the selection of the projection surface or slice and corresponding interpretation for multi-state systems are far from trivial as well as far from convenient.

As coordinate-momentum phase space is well-established in classical mechanics, the formulation of (weighted) constraint coordinate-momentum phase space described in Section 2 offers a novel and convenient approach for describing correlations and dynamics in the discrete-variable system as well as the composite system in quantum mechanics. When (weighted) constraint coordinate-momentum phase space is used for mapping a finite set of F states, eq 24 or eq 33 suggests that the correlation between state $|n\rangle$ and state $|m\rangle$ is described by the term of $|n\rangle\langle m|$, i.e.,

$$f_{(n,m)}(\mathbf{x}, \mathbf{p}) = \frac{1}{\Omega(\gamma)} \left[\frac{1}{2} (x_n + ip_n)(x_m - ip_m) - \gamma \delta_{nm} \right]. \quad 41$$

The density matrix in quantum mechanics can rigorously be decomposed by a summation of $f_{(n,m)}(\mathbf{x}, \mathbf{p})$. (See Appendix 3 for more discussion.) So it will be possible as well as convenient to reconstruct the full density matrix based on direct measurements of phase points^{70, 85, 221-234} on (weighted) constraint space.

For tomographic illustration the key is to reduce phase space variables (\mathbf{x}, \mathbf{p}) to two relevant variables. We define the marginal function of (x_n, x_m) or of (x_n, p_m) to describe the correlation. For example, the marginal function on constraint coordinate-momentum phase space (Figure 4) is

$$f_{(n,m)}(x_n, x_m) = \int F d\mathbf{x}' d\mathbf{p}' \frac{1}{\Omega(\gamma)} \delta \left(\sum_{j=1}^F \frac{(x^{(j)})^2 + (p^{(j)})^2}{2} - (1+F\gamma) \right) f_{(n,m)}(\mathbf{x}, \mathbf{p}; \gamma) \quad 42$$

and that on weighted constraint phase space is

$$f_{(n,m)}(x_n, x_m) = \int_{-1/F}^{\infty} d\gamma w(\gamma) \frac{1}{\Omega(\gamma)} \int F dx' dp \delta \left(\sum_{j=1}^F \frac{(x^{(j)})^2 + (p^{(j)})^2}{2} - (1+F\gamma) \right) f_{(n,m)}(\mathbf{x}, \mathbf{p}; \gamma), \quad 43$$

where \mathbf{x}' includes any x_k other than $\{x_n, x_m\}$, and $f_{(n,m)}(\mathbf{x}, \mathbf{p}; \gamma)$ is defined by eq 41. Figure 5 demonstrates the case of eq 43 when the quasi-probability distribution function $w(\gamma)$ is defined by eqs 38-40 where two symmetrical values of parameter γ are used. Similarly, one can define the marginal function of (x_n, p_m) . Because $2F$ -dimensional Euclidean phase space is used to obtain the marginal function, it is convenient to describe the correlation/entanglement between any arbitrary two states when F is large. The manipulation complexity is the same for any pair of variables (x_n, x_m) or (x_n, p_m) . This feature bypasses the difficulty of choosing a special slice of a high-dimensional space (when F is large) in such as the Stratonovich representation. Another important advantage is that exact dynamics in the formulation of (weighted) constraint coordinate-momentum phase space for the discrete-variable quantum system (e.g., a finite set of F states) is equivalent to Hamilton's EOMs produced by the mapping Hamiltonian eq 29. Such EOMs are simply linear on (weighted) constraint coordinate-momentum phase space. In comparison, exact EOMs on Stratonovich phase space are much more difficult to obtain for general discrete-variable systems (when F is large).

Figures 4-5 demonstrate a composite system that consists of a discrete variable for spin-1/2 and a continuous variable for a harmonic oscillator. The marginal quasi-probability distribution functions of the continuous variable for both the pure state and the mixed state are presented in Figure 4a, where infinite Wigner phase space is employed. More interestingly, the marginal functions for the discrete variable are demonstrated on constraint coordinate-momentum phase space in Figure 4b and on weighted constraint space in Figure 5b. The marginal functions of the discrete variable (based on eq 41) read

$$\begin{pmatrix} f_{(\uparrow,\uparrow)}(x_1, x_2) & f_{(\uparrow,\downarrow)}(x_1, x_2) \\ f_{(\downarrow,\uparrow)}(x_1, x_2) & f_{(\downarrow,\downarrow)}(x_1, x_2) \end{pmatrix} = \begin{pmatrix} \frac{F}{4\pi(1+F\gamma)} \left((1+F\gamma) - 2\gamma + \frac{1}{2}x_1^2 - \frac{1}{2}x_2^2 \right) & \frac{F}{4\pi(1+F\gamma)} x_1 x_2 \\ \frac{F}{4\pi(1+F\gamma)} x_1 x_2 & \frac{F}{4\pi(1+F\gamma)} \left((1+F\gamma) - 2\gamma - \frac{1}{2}x_1^2 + \frac{1}{2}x_2^2 \right) \end{pmatrix}. \quad 44$$

The difference between the Schrodinger cat state and the mixed state is distinct in either Figure 4b on constraint space or Figure 5b on weighted constraint space.

The joint marginal function of a pure Bell entangled state, $(|0\rangle|\downarrow\rangle+|1\rangle|\uparrow\rangle)/2$, of the composite system is demonstrated in Figure 4c where constraint coordinate-momentum phase space is used for the discrete DOF at each grid, as well as in Figure 5c where weighted constraint space is employed for the discrete DOF at each grid. The two-dimensional grids represent variables (R, P) of infinite Wigner phase space for the continuous DOF in either of Figure 4c and Figure 5c. When the pure Bell entangled state is studied, both Figure 4c and Figure 5c clearly demonstrate a Gaussian decay of the joint marginal function against Wigner phase space variables (R, P) of the continuous DOF. Either Figure 4c or Figure 5c also shows the pattern of the correlation between the continuous DOF and the discrete variable. It is convenient to distinguish the pure Bell entangled state, $(|0\rangle|\downarrow\rangle+|1\rangle|\uparrow\rangle)/2$, from the direct product of the Schrodinger cat states, $(|0\rangle+|1\rangle)\otimes(|\uparrow\rangle+|\downarrow\rangle)/2$, when the hybrid representation of the general coordinate-momentum phase space is used.

4. DYNAMICS OF COMPOSITE QUANTUM SYSTEMS

The quantum Liouville theorem can be expressed as a generalized Moyal bracket on hybrid coordinate-momentum phase space. When the Poisson bracket for classical Hamilton's EOMs governed by the mapping Hamiltonian, eq 29, is used to approximate the generalized Moyal bracket on phase space, we have CMM when constraint space is used, and wMM when weighted constraint space is employed.

We compare the new wMM and CMM approaches to Ehrenfest dynamics^{239, 240} as well as the fewest-switches surface hopping (FSSH) method²⁴¹⁻²⁴³, two prevailing trajectory-based dynamics methods for a range of benchmark systems, including two-site dissipative models, Tully's scattering models, atomic systems in cavity interacted with a number of field modes, and linear vibronic coupling model systems that involve the conical intersection^{135, 244-246}. They are typical composite quantum systems in chemistry, physics, condensed matter science, quantum optics, and quantum information.

4.1 Spin-boson models at low-temperature in condensed phase

The first model illustrated is the spin-boson model, which describes a two-site system interacted with an environmental bath in condense phase. It is also a simplified model for electron transfer and energy transfer in chemical and biological reactions. Several numerically exact benchmark methods for solving the spin-boson model include quasi-adiabatic propagator path integral (QuAPI)²⁴⁷⁻²⁵⁰, hierarchy equations of motion (HEOM)²⁵¹⁻²⁵⁹, (multi-layer) multi-configuration time-dependent Hartree [(ML-)MCTDH]²⁶⁰⁻²⁶⁶, but their numerical costs typically increase exponentially as the number of DOFs increases. Quantum dynamics of the spin-boson model exhibits interesting dissipative characters, of which the asymptotic behaviours are often missed by either of

Ehrenfest dynamics and FSSH in the low temperature regime⁵⁸. Spin-boson models with strong coupling in the low temperature regime presents challenging tests for trajectory-based dynamics methods.

The Hamiltonian of the spin-boson model is divided to three parts, $\hat{H} = \hat{H}_s + \hat{H}_b + \hat{H}_{sb}$. Here $\hat{H}_s = \varepsilon \hat{\sigma}_z + \Delta_c \hat{\sigma}_x$ describes a two-site system with the bias ε and tunneling Δ_c , while the bath part of the Hamiltonian is discretized into a combination of a number of quantum oscillators $\hat{H}_b = \sum_{j=1}^{N_b} (\hat{P}_j^2 + \omega_j^2 \hat{R}_j^2) / 2$. The system-bath coupling adopts a bilinear interaction, $\hat{H}_{sb} = \sum_{j=1}^{N_b} c_j \hat{R}_j \hat{\sigma}_z$. Here we use an Ohmic bath spectral density $J(\omega) = (\pi / 2) \alpha \omega e^{-\omega/\omega_c}$, where α is the Kondo parameter and ω_c the cut-off frequency, from which discrete frequencies and coupling strengths $\{\omega_j, c_j\}$ are sampled^{267, 268} from

$$\begin{cases} \omega_j = -\omega_c \ln[1 - j / (1 + N_b)] \\ c_j = \omega_j \sqrt{\alpha \omega_c / (1 + N_b)} \end{cases}, \quad j = 1, \dots, N_b . \quad 45$$

The initial density is set as $|1\rangle_s \langle 1|_s \otimes \hat{\rho}_b$, where the system is in excited state $|1\rangle_s$ while all oscillation bath modes are at thermal equilibrium with $\hat{\rho}_b = e^{-\beta \hat{H}_b} / Z_b$. Initial nuclear DOFs are sampled from the Wigner distribution of $\hat{\rho}_b$, while initial electronic DOFs are sampled from (weighted) constraint coordinate-momentum phase space $\mathbf{S}(\mathbf{x}, \mathbf{p})$. The continuous spectral density is discretized into $N_b = 300$ effective bath modes to guarantee numerical convergence in simulations.

In Figure 6, we demonstrate results produced by wMM with parameter $\Delta = 0.05$, by wMM with $\Delta = 0.1$, and by CMM with $\gamma = (\sqrt{F+1} - 1) / F = 0.366$ which is a special case of CMM of Ref.¹³⁴. Numerically exact results, as well as results yielded by Ehrenfest dynamics and FSSH, are shown for comparison. Figure 6 demonstrates that wMM, as well as CMM, outperforms both Ehrenfest dynamics and FSSH dynamics, either for short-time coherences or for long-time dissipations.

4.2 Tully's gas phase scattering models

Tully's scattering models²⁴¹ mimic different intersection types of molecular systems, which have widely been tested for various nonadiabatic dynamics methods. They describe a two-state Hamiltonian with a central coupling area and asymptotic plateau regions where diabatic potential function $V_{nn}(R \rightarrow \pm\infty)$ is flat. All the three

models, including the single avoided crossing (SAC), dual avoided crossing (DAC), and extended coupling region (ECR) problems, are used in our numerical tests.

Atomic units are used in the simulations of the Tully models. The SAC model (Panel (a1) of Figure 7) describes the simplest but essential surface crossing in molecular systems. In the diabatic representation, its diagonal potential energy surfaces (PESes) are $V_{11} = -V_{22} = A(1 - e^{-B|R|})\text{sgn}(R)$ and off-diagonal coupling terms are $V_{12} = V_{21} = Ce^{-DR^2}$. Here, the parameters are $A = 0.01$, $B = 1.6$, $C = 0.005$, and $D = 1.0$. The DAC model (Panel (b1) of Figure 7) includes two crossing points, thus different (electronic) paths are interfered with the dependence on the initial momentum. Its diagonal PESes are $V_{11} = 0$ and $V_{22} = -Ae^{-BR^2} + E_0$, and off-diagonal coupling terms are $V_{12} = V_{21} = Ce^{-DR^2}$ in the diabatic representation with parameters $A = 0.10$, $B = 0.28$, $E_0 = 0.05$, $C = 0.015$ and $D = 0.06$. The ECR model in the diabatic representation (Panel (c1) of Figure 7) has diagonal PESes $V_{11} = -V_{22} = E_0$ and coupling terms $V_{12} = V_{21} = C[e^{BR}\Theta(-R) + (2 - e^{-BR})\Theta(R)]$, with $E_0 = -0.0006$, $B = 0.9$, $C = 0.1$. Here $\Theta(R)$ is the Heaviside function of coordinate R . The adiabatic PESes and nonadiabatic coupling vector of the ECR model are also illustrated in Panel (c2) of Figure 7.

We investigate the transmission and reflection coefficients of each state. In the simulations, the initial condition is a nuclear wavepacket, $\Psi(R; t = 0) \propto \exp[-\alpha(R - R_0)^2/2 + i(R - R_0)P_0/\hbar]$, occupied on state 1, where $\alpha = 1$ is the Gaussian width parameter, and R_0 and P_0 are the initial average coordinate and momentum. The initial average coordinate is set at $R_0 = -3.8$, -10 , and -13 for the SAC, DAC and ECR models, respectively. The initial Wigner distribution for the nuclear DOF is then $\rho_W^{\text{nuc}}(R, P) \propto \exp[-\alpha(R - R_0)^2 - (P - P_0)^2 / (\alpha\hbar^2)]$.

Figure 7a shows that all methods are capable of quantitatively describing transmission coefficients on (diabatic) state 1 and state 2 of the SAC model. Figure 7b demonstrates that either wMM or CMM outperforms Ehrenfest dynamics and FSSH in predicting the peak shape when the initial momentum is relatively high, e.g., $P_0 \geq 15$ au. This indicates that the trajectory-based approximate dynamics approaches in the mapping phase space formulation are good for fast processes in the gas phase composite/nonadiabatic system. However, the performance of either wMM or CMM in the low initial momentum region should be improved. It is important to

note that the EOMs of wMM/CMM are invariant with the representation of the electronic state, as described in the Supporting Information of ref⁵⁷. (More discussion is available in Appendix 1.) That is, both the diabatic and adiabatic representations produce the same results for wMM or CMM, which is often not satisfied in FSSH and other nonadiabatic dynamics approaches.

For the ECR model of Figure 7c, the numerically exact DVR solution indicates an energy threshold for a bifurcation. Ehrenfest dynamics totally misses the step-like behaviours for the transmission coefficient on state 1, and for the reflection coefficient on either state 1 or state 2. CMM greatly improves over Ehrenfest dynamics. It is more encouraging that wMM is capable of faithfully describing such step-like behaviours. Tully's original FSSH algorithm is not able to well describe the ECR model²⁴¹, but a modified version for treating frustrated hopping of FSSH (e.g., see ref.²⁴³) is capable of qualitatively capturing the step-like behaviours. As shown in Figure 7c, in comparison to the traditional FSSH approach^{241, 243}, the overall performance of wMM for the ECR model is better.

4.3 Atom/molecule-in-cavity models of quantum electrodynamic light-matter systems

The cavity quantum electrodynamics (cQED) focuses on studying the interaction between light and a multi-level system (e.g., an atom or a molecule) in an optical cavity, which has many applications in the field of quantum information and quantum computation. There exist many interesting and important phenomena in cQED, e.g., the Purcell effect when coupling is weak and vacuum Rabi splitting when coupling becomes strong²⁶⁹⁻²⁸³. When the general atomic/molecular system is coupled to multi-cavity modes, it is often intractable to solve the exact evolution in real time due to the curse of dimensionality. We test wMM for two typical models that describe an imprisoned multi-level atom coupled with a series of optical modes in a one-dimensional lossless cavity^{57, 204, 284-287}.

The total Hamiltonian consists of three parts. The optical field is depicted by N effective modes

$$\hat{H}_p = \sum_{j=1}^N \frac{1}{2} \left(\hat{P}_j^2 + \omega_j^2 \hat{R}_j^2 \right), \quad 46$$

where $\{\hat{P}_j, \hat{R}_j\}$ denote the canonical variables of j -th optical field mode with the corresponding photonic frequency ω_j . The atomic system is described by $\hat{H}_a = \sum_{n=1}^F \varepsilon_n |n\rangle\langle n|$ with ε_n representing the atomic energy level of n -th state. Employing the dipole approximation, one can formulate the coupling between atom and optical field as

$$\hat{H}_c = \sum_{n \neq m}^F \left(\sum_{j=1}^N \omega_j \lambda_j(r_0) \hat{R}_j \right) \mu_{nm} |n\rangle\langle m| . \quad 47$$

Here μ_{nm} denotes the transitional dipole moment between the n -th and m -th atomic levels, and the coupling vector is

$$\lambda_j(r_0) = \sqrt{\frac{2}{\epsilon_0 L}} \sin\left(\frac{j\pi r_0}{L}\right) \quad 48$$

along the direction of coupling between the j -th mode and the atom, where L is the volume length of cavity, ϵ_0 denotes the vacuum permittivity, and r_0 represents the location of the atom. In the simulation, the volume length of the cavity is set to 236200 au and the atom is frozen at the central location, i.e., $r_0 = L / 2$. The optical field is depicted by 400 standing-wave modes in cavity, of which the j -th frequency is $\omega_j = j\pi c / L$ with c the light speed in vacuum. We use two benchmark models for studying cQED processes, a three-level model with $\epsilon_1 = -0.6738$, $\epsilon_2 = -0.2798$, $\epsilon_3 = -0.1547$, $\mu_{12} = -1.034$, $\mu_{23} = -2.536$ (all in atomic units), and a reduced two-level model where only the two lowest atomic levels are employed.

The highest atomic level is initially occupied with no photon in cavity, i.e., all cavity modes are in the corresponding vacuum state. The spontaneous emission occurs at the beginning, the released photon evolves in the cavity, and the re-absorption and re-emission happen later when the photon is reflected to meet the atom. Figure 8 shows the population transfer of each atomic level of the two models. The wMM results are compared with CMM, Ehrenfest dynamics, FSSH, and exact results^{285, 286}. Results of Ehrenfest dynamics and of FSSH significantly deviate from exact results even since very short time, while CMM and wMM yield much more reasonable descriptions for all levels, including the transfer behaviour at short time and the revival at around $t = 1800$ au. The wMM approach shows overall better performance than CMM in most of the cases. Figure 8 implies that the trajectory-based methods in the general coordinate-momentum phase space formulation will be useful for studying cQED phenomena in the field of quantum optics and quantum information.

4.4 Linear vibronic coupling model for the molecular system involving the conical intersection

The conical intersection widely exists in molecular systems and plays a central role in many photophysical and photochemical phenomena^{135, 139, 214, 244, 245, 288-291}. The linear vibronic coupling model (LVCM) is the simplest but effective model widely used to describe dynamic properties around the conical intersection region, of which Hamiltonian in the diabatic representation is

$$\hat{H} = \hat{H}_0 + \hat{H}_l + \hat{H}_c . \quad 49$$

Here, $\hat{H}_0 = \sum_{k=1}^N \omega_k (\hat{P}_k^2 + \hat{R}_k^2) / 2$ is the zeroth-order harmonic oscillator Hamiltonian for describing the electronic ground state in normal-mode space, where $\hat{P}_k, \hat{R}_k (k = 1, \dots, N)$ denote the k -th effective weighted normal-mode variables with frequency ω_k (i.e., $P_k = p_k / \sqrt{m_k \omega_k}$, $R_k = \sqrt{m_k \omega_k} r_k$, where p_k, r_k, m_k are the canonical momentum, canonical coordinate, and mass of k -th normal-mode). In eq 49, $\hat{H}_l = \sum_{n=1}^F \left(E_n + \sum_{k=1}^N \kappa_k^{(n)} \hat{R}_k \right) |n\rangle\langle n|$ contains the vertical excitation energy, $E_n (n = 1, \dots, F)$ of F electronic states, and the linear coupling term $\kappa_k^{(n)}$ of each nuclear DOF for diagonal Hamiltonian elements, while $\hat{H}_c = \sum_{n \neq m}^F \left(\sum_{k=1}^N \lambda_k^{(nm)} \hat{R}_k \right) |n\rangle\langle m|$ includes linear coupling $\lambda_k^{(nm)}$ for each normal-mode between two different electronic states, $|n\rangle$ and $|m\rangle$.

A typical two-level 3-mode LVCM describes the S1/S2 conical intersection of the pyrazine molecule. The parameters of this model are fitted from semi-empirical electronic structure calculations by Schneiders and Domcke in ref²⁹². The excitation energies for the two electronic states are $E_1 = 3.94$ eV and $E_2 = 4.84$ eV. The diagonal linear coupling terms of first two modes $\{\hat{R}_1, \hat{R}_2\}$ are $\kappa_1^{(1)} = 0.037$ eV, $\kappa_2^{(1)} = -0.105$ eV for the first electronic state, and $\kappa_1^{(2)} = -0.254$ eV, $\kappa_2^{(2)} = 0.149$ eV for the second electronic state, respectively. The off-diagonal linear coupling of third mode \hat{R}_3 is $\lambda_3^{(12)} = \lambda_3^{(21)} = 0.262$ eV. The normal-mode vibronic frequency of each mode is $\omega_1 = 0.126$ eV, $\omega_2 = 0.074$ eV, and $\omega_3 = 0.118$ eV, respectively. Initial conditions of nuclear DOFs are sampled from the corresponding Wigner function of the vibronic ground state while the second electronic state is occupied. All simulations employ 10^5 trajectories as well as time stepsize $\Delta t = 0.01$ fs for fully converged results. Numerically exact result of this model calculated by ML-MCTDH are available in ref²¹².

Figure 9 shows population dynamics on state 2 yielded by wMM, CMM, Ehrenfest dynamics, FSSH and ML-MCTDH. It is evident that Ehrenfest dynamics fails to describe the short-time behaviour (before 100 fs). In comparison, wMM, CMM, and FSSH more reasonably describe the radiationless energy transfer process at short time. Interestingly, wMM describes the oscillating behaviours in the long-time region (after 300 fs) better than

other approximate methods do. Such oscillating characters are significant for calculating linear and nonlinear optical spectra of molecular systems. It is expected that trajectory-based dynamics methods on weighted constraint phase space for the discrete DOFs will be useful for studying both dynamics and spectroscopy of conical intersection-involved systems.

Figures 6-9 demonstrate that the overall performance of wMM is better than CMM, especially in the gas phase scattering case of Figure 7c and the quantum electrodynamic light-matter systems of Figure 8. Both wMM and CMM approaches are able to outperform Ehrenfest dynamics as well as FSSH for condensed phase systems (e.g., in Figure 6 and Figure 8).

5. CONCLUSION REMARKS

The phase space formulation of quantum mechanics not only presents a type of convenient interpretation to describe quantum-classical correspondences as well as nonclassical correlations/entanglement, but also sets the insightful scene for developing practical and useful trajectory-based quantum dynamics approaches.

The constraint coordinate-momentum phase space formulation for the discrete-variable system which we have recently developed, and the weighted representation that we propose in the Focus Article are expected to be useful for future measurements of phase points in experiment^{70, 85, 221-234} as well as tomography in the field of quantum information and computation. In comparison to such as Stratonovich phase space, (weighted) constraint coordinate-momentum phase space is more convenient to reconstruct the density matrix and to interpret (nonclassical) correlations as the number of discrete states increases.

When the general Moyal bracket of the quantum Liouville theorem is approximated by the corresponding Poisson bracket on (weighted) constraint phase space, it reproduces the correct frozen-nuclei limit of composite/nonadiabatic systems. Various benchmark model tests of from gas phase to condensed phase quantum systems (as shown in Figures 6-9) indicate that wMM, the new trajectory-based approximate approach with the weighted constraint coordinate-momentum phase space representation, demonstrates overall better performance than FSSH as well as Ehrenfest dynamics. It is expected that more investigations on the (weighted) constraint phase space formulation will shed light on more numerically favourable dynamics approaches with the Meyer-Miller mapping Hamiltonian or other mapping Hamiltonians.

We note that the (weighted) constraint coordinate-momentum phase space formulation is established for any systems with a finite set of states, not only limited to discrete electronic states, but also for finite discrete nuclear states. The weighted phase space strategy that we propose can also be applied to other types of phase space formulations of the discrete-variable system, such as Stratonovich phase space with an either SU(2) or SU(F)

1
2
3 structure, and Wootters phase space, albeit that the general coordinate-momentum phase space formulation
4 presented in the Focus Article will be more convenient, for experimental measurements, tomography, or
5 characterizations of fidelity, coherence, inequalities, displaced parity, atomic/molecular/optical Schrodinger cat
6 states, and entanglement in quantum information and computation^{70, 85, 221-234, 293, 294} as well as for studying
7 dynamic processes of composite systems in physics, chemistry, materials, biology, and environmental science.
8
9
10
11
12
13
14
15
16
17
18
19
20
21
22
23
24
25
26
27
28
29
30
31
32
33
34
35
36
37
38
39
40
41
42
43
44
45
46
47
48
49
50
51
52
53
54
55
56
57
58
59
60

For Peer Review

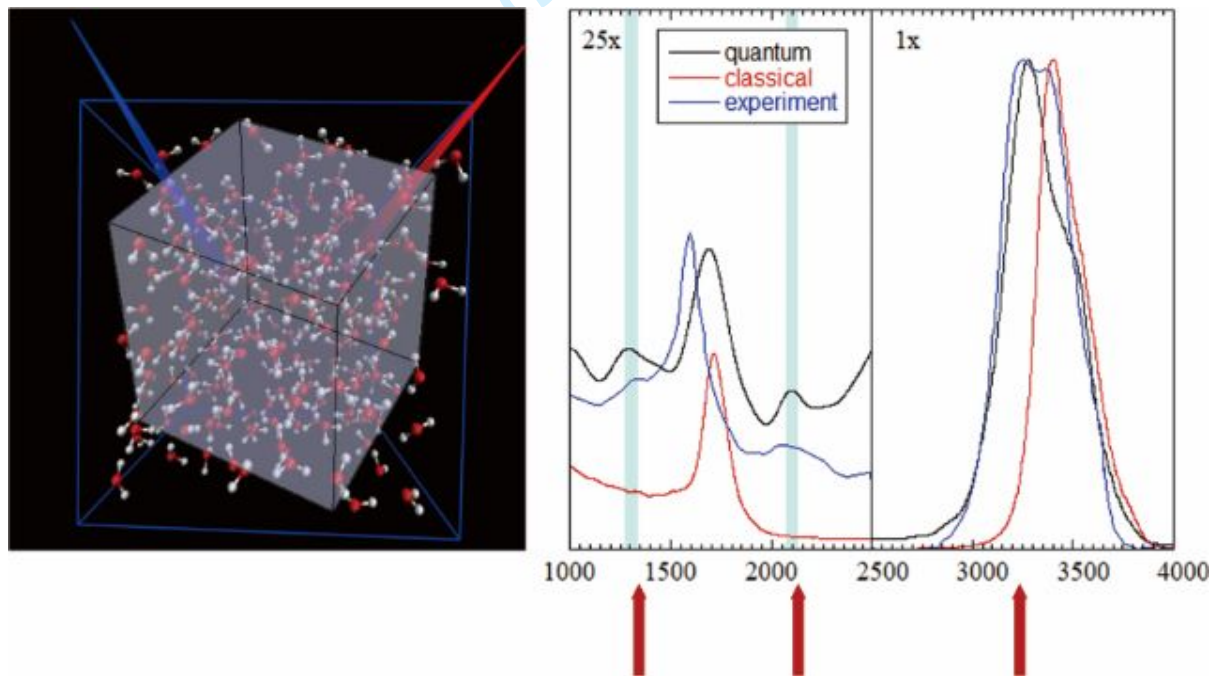
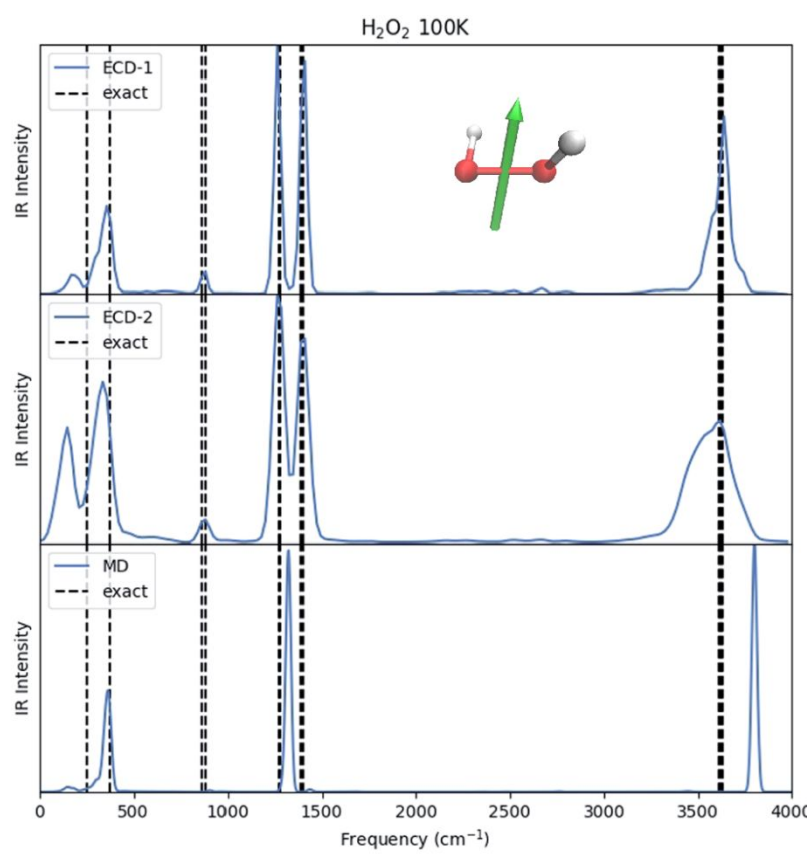
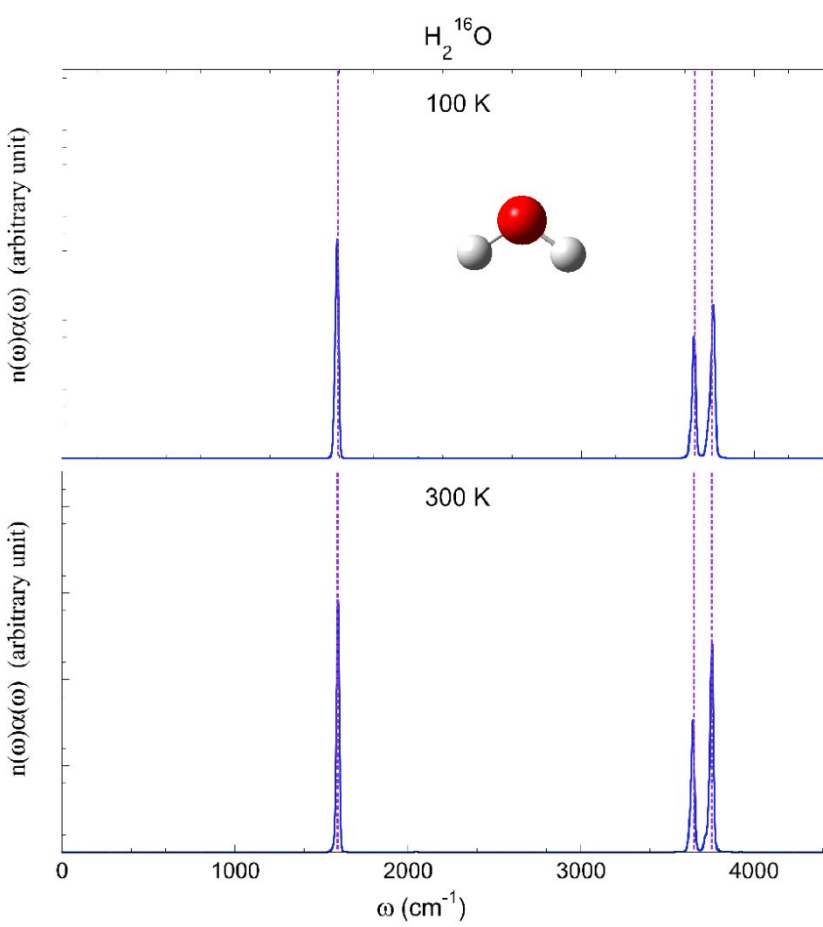
Figures and Tables

Figure 1. Quantum dynamical effects are decisive in reproducing the experimental isotropic Raman spectrum of liquid water at room temperature, as illustrated by the LSC-IVR simulation where infinite (Wigner) phase space for nuclear DOFs is used. Converged results were obtained with 216 water molecules in a box with periodic boundary conditions. (Reprinted with permission from ref¹⁹. Copyright 2018 Taylor & Francis.)

1
2
3
4
5
6
7
8
9
10
11
12
13
14
15
16
17
18
19
20
21
22
23
24
25
26
27
28
29
30
31
32
33
34
35
36
37
38
39
40
41
42
43
44
45
46
47
48
49
50
51
52
53
54
55
56
57
58
59
60

For Peer Review



1
2
3 **Figure 2.** Molecular vibrational spectra produced by more advanced trajectory-based dynamics methods with
4 infinite (Wigner) phase space used for nuclear DOFs, which satisfy the two fundamental criteria: conservation of
5 the quantum Boltzmann distribution for the thermal equilibrium system and being exact for any quantum thermal
6 correlation functions in the classical and harmonic limits. (a) Vibrational spectrum of the H₂O molecule at
7 100K and that at 300K. Adapted with permission from ref ⁴¹. Copyright 2016 American Institute of Physics
8 Publishing. (b) Vibrational spectrum of the H₂O₂ molecule at 100K. Adapted with permission from ref ⁴⁴.
9
10
11
12
13
14
15
16 Copyright 2021 American Institute of Physics Publishing.
17
18
19
20
21
22
23
24
25
26
27
28
29
30
31
32
33
34
35
36
37
38
39
40
41
42
43
44
45
46
47
48
49
50
51
52
53
54
55
56
57
58
59
60

For Peer Review

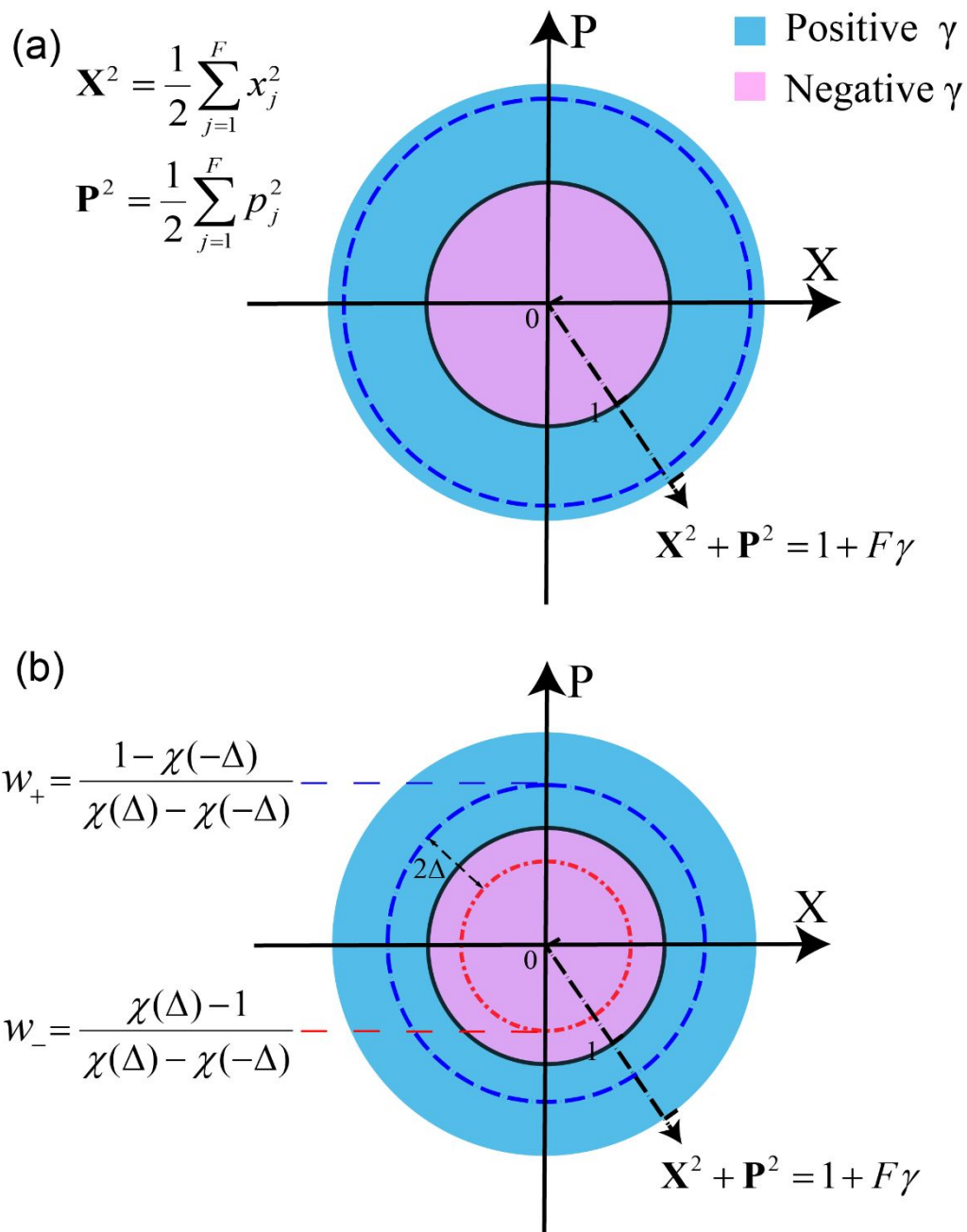
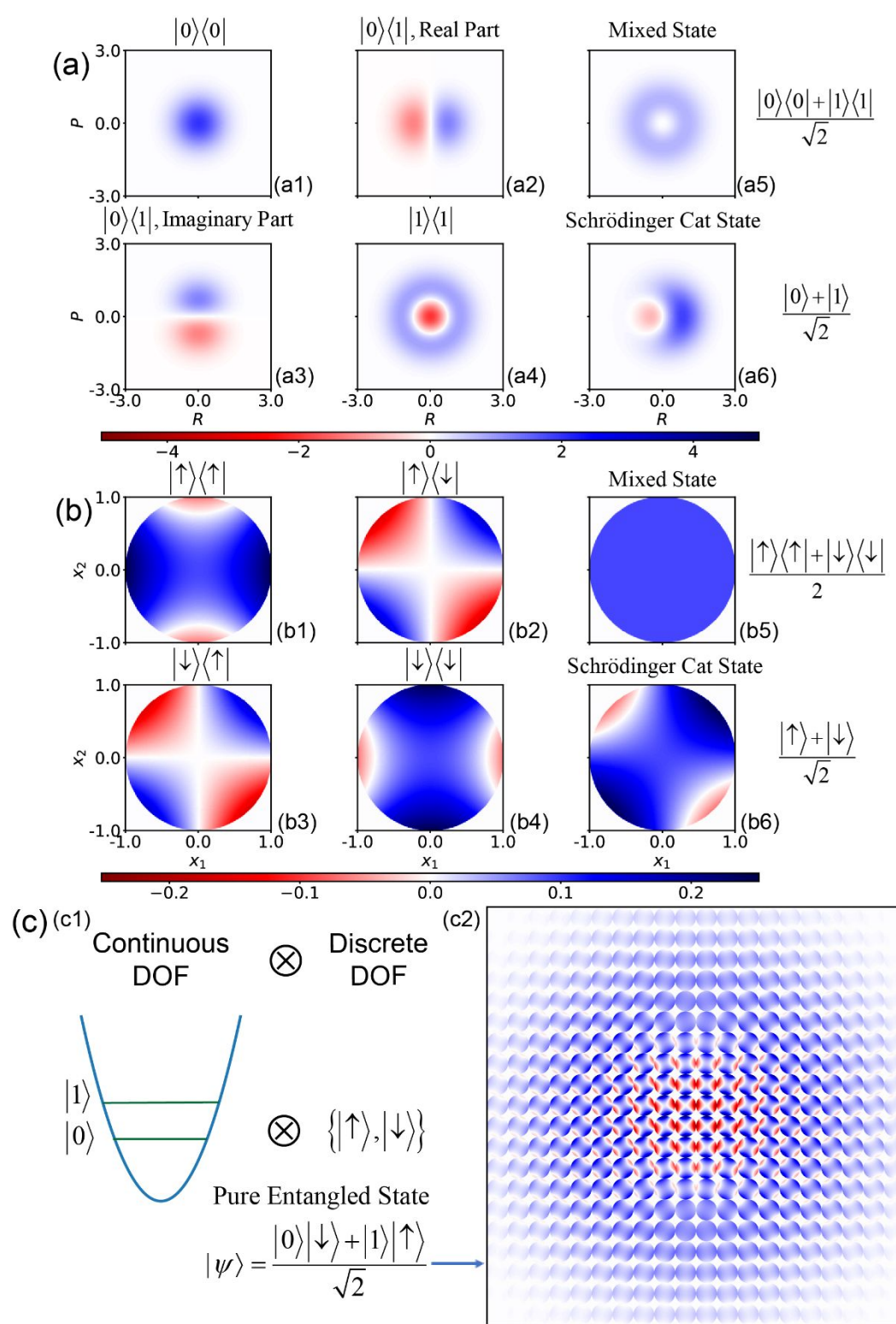
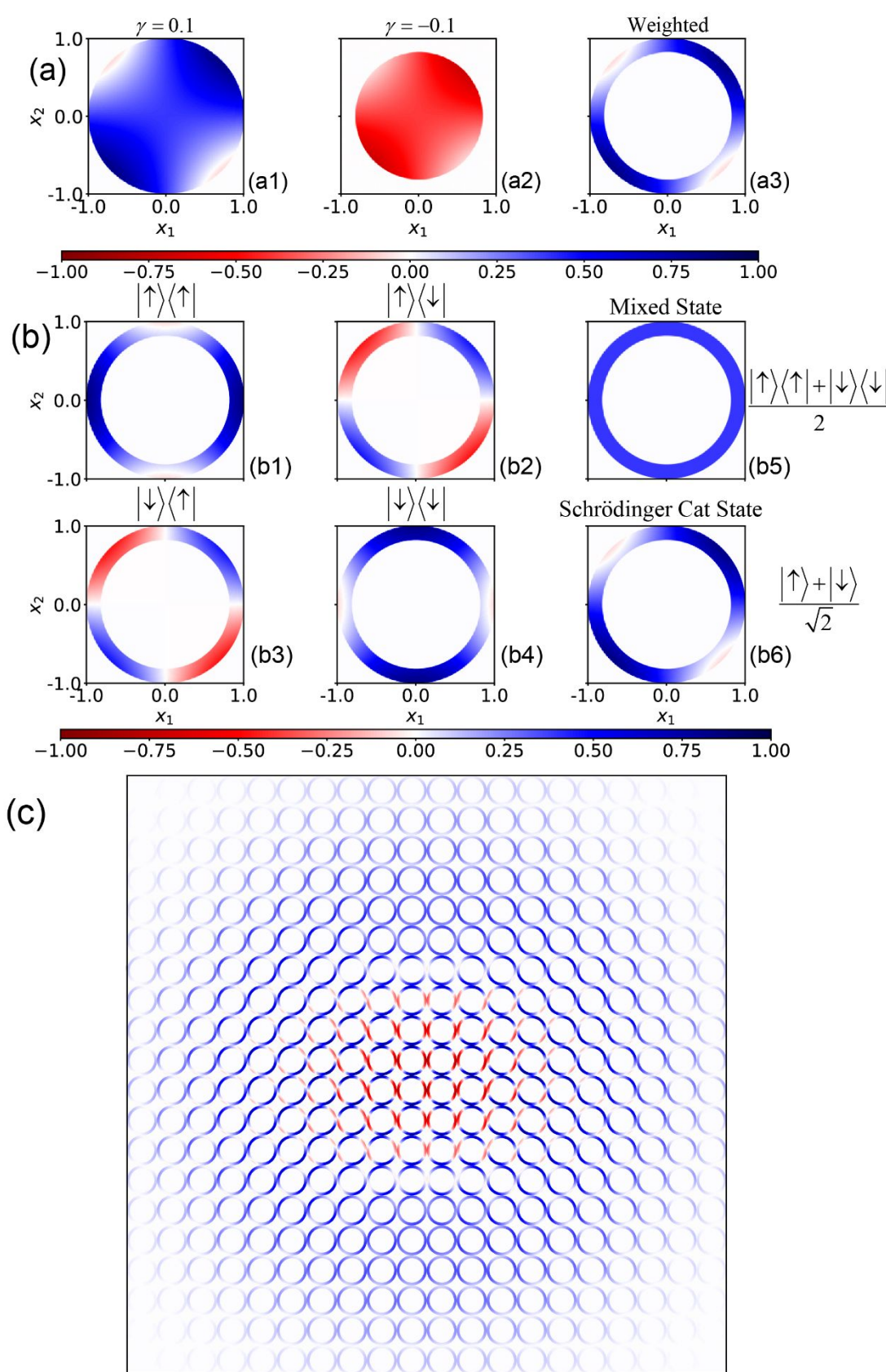


Figure 3: Illustration of the exact mapping formulation with constraint coordinate-momentum phase space. Panel (a) presents constraint phase space with only a single value of parameter γ . Panel (b) demonstrates weighted constraint phase space with two values of parameter γ , where the quasi-probability distribution function is $w(\gamma) = w_+ \delta(\gamma - \Delta) + w_- \delta(\gamma + \Delta)$. Constraint phase space with the positive weight is blue-dashed, while that with the negative weight is red dot-dashed. (Panel (a) is adapted with permission from ref¹³⁴. Copyright 2021 American Chemical Society.)



1
2
3 **Figure 4:** Illustrations of (a) Wigner representation of a continuous-variable system, (b) constraint phase space
4 representation of a discrete-variable system, and (c) hybrid coordinate-momentum phase space representation of
5 a composite system with both discrete and continuous DOFs.
6
7

- 8 (a) Wigner distribution for $|0\rangle\langle 0|$ (Panel a1), that for $|1\rangle\langle 1|$ (Panel a4), real part (Panel a2) and imaginary part
9 (Panel a3) of the Wigner distribution for $|0\rangle\langle 1|$, wigner distribution for mixed state $(|0\rangle\langle 0|+|1\rangle\langle 1|)/2$
10 (Panel a5), and that for Schrödinger cat state $(|0\rangle+|1\rangle)/\sqrt{2}$ (Panel a6). Here, $|0\rangle$ and $|1\rangle$ are two energy
11 levels of a continuous-variable system.
12
13 (b) Marginal distribution of constraint phase space coordinates (x_1, x_2) for $|\uparrow\rangle\langle \uparrow|$ (Panel b1), $|\downarrow\rangle\langle \downarrow|$ (Panel
14 b2), that for $|\uparrow\rangle\langle \downarrow|$ (Panel b4), that for $|\downarrow\rangle\langle \uparrow|$ (Panel b3), that for mixed state $(|\uparrow\rangle\langle \uparrow|+|\downarrow\rangle\langle \downarrow|)/2$
15 (Panel b5), and that for Schrödinger cat state $(|\uparrow\rangle+|\downarrow\rangle)/\sqrt{2}$ (Panel b6). Here, $|\uparrow\rangle$ and $|\downarrow\rangle$ represent
16 two discrete states of a discrete-variable system.
17
18 (c) Panel c1: Schematic representaton of the composite system and the pure entangled state
19 $(|0\rangle|\downarrow\rangle+|1\rangle|\uparrow\rangle)/2$; Panel c2: hybrid coordinate-momentum phase space representation of the entangled
20 state. The grid is on the Wigner phase space (R, P) for the continous DOF, and each circle of a grid stands
21 for the local marginal distribution function of constraint phase space variables (x_1, x_2) . The notations are
22 identical to those in Panels (a)-(b).



1
2
3 **Figure 5:** Illustrations of (a) components and (b) marginal distribution functions of the weighted constraint phase
4 space representation of a discrete-variable system, and (c) weighted hybrid representation of the same composite
5 system as that of Figure 4(c).

- 6
7
8
9 (a) Marginal distribution of constraint phase space coordinates (x_1, x_2) for Schrödinger cat state
10
11 $(|\uparrow\rangle + |\downarrow\rangle)/\sqrt{2}$ with $\gamma = \Delta$ weighted by w_+ (Panel a1), with $\gamma = -\Delta$ weighted by w_- (Panel a2). The
12
13 sum of the two components yields the marginal distribution of constraint phase space coordinates (x_1, x_2)
14
15 of the weighted representation with two values of parameter γ for the Schrödinger cat state (Panel a3).
16
17 Coordinates are scaled by the larger radius $\sqrt{2(1+F\Delta)}$.
18
19
20 (b) Weighted marginal distribution of constraint phase space coordinates (x_1, x_2) for the same properties as
21
22 those in Figure 4(b).
23
24 (c) Same as Figure 4(c), but using weighted marginal distribution for the discrete DOF.
25
26
27
28
29
30
31
32
33
34
35
36
37
38
39
40
41
42
43
44
45
46
47
48
49
50
51
52
53
54
55
56
57
58
59
60

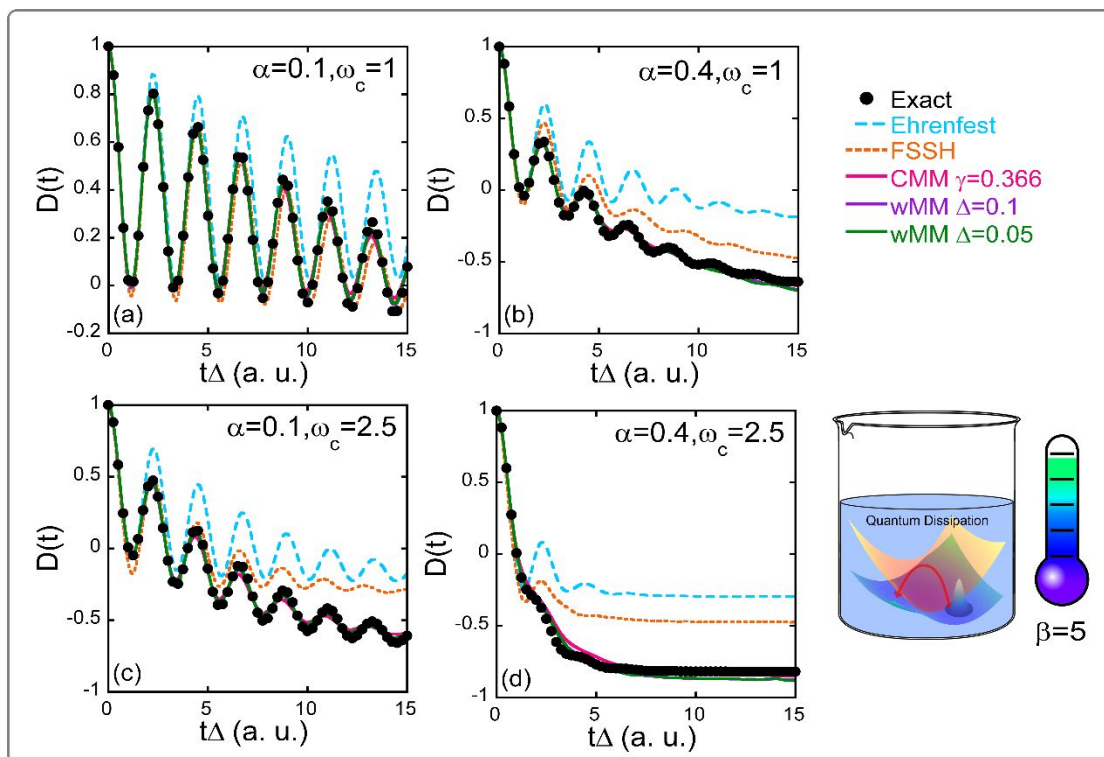
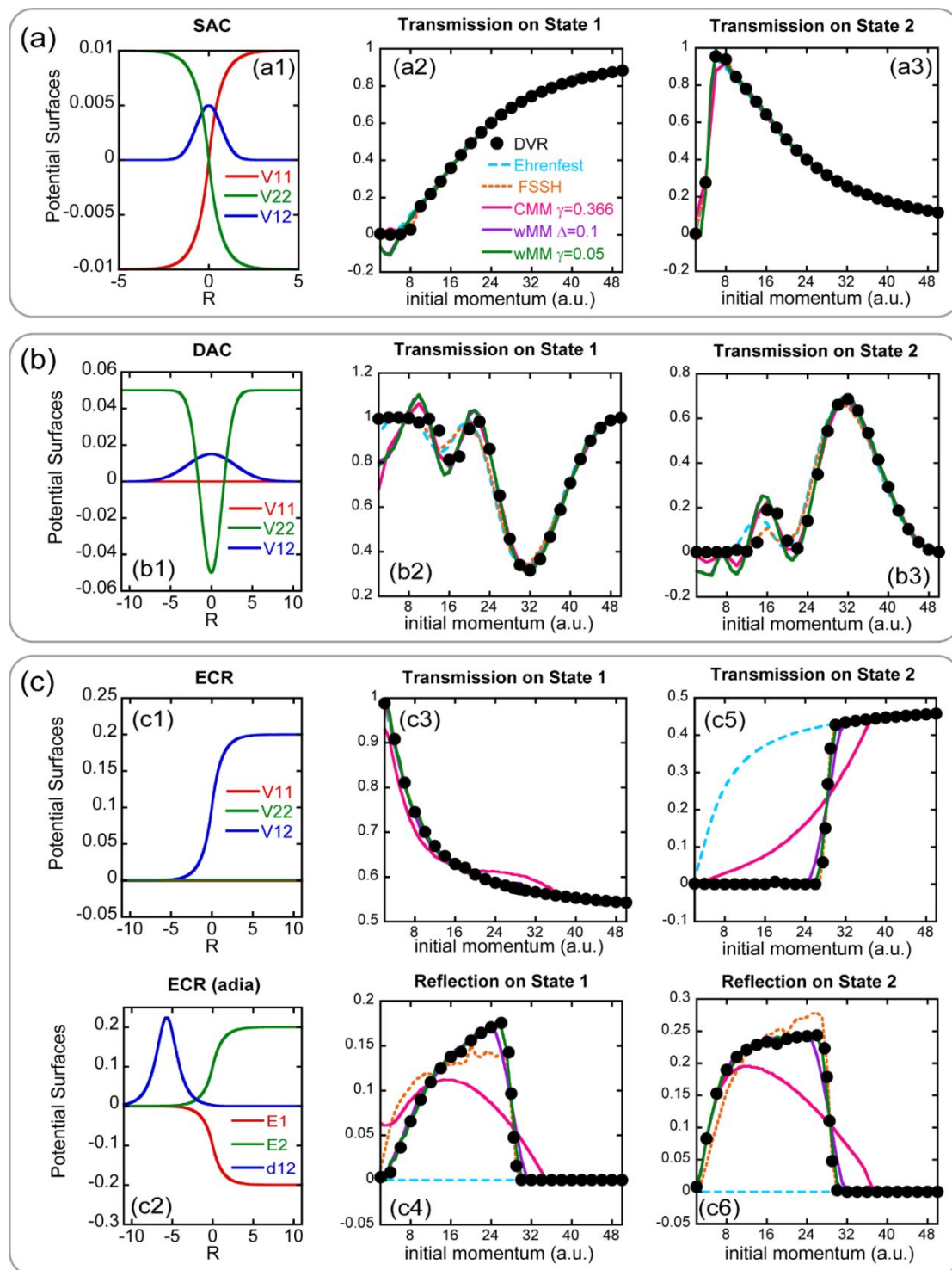


Figure 6: Results of population difference $D(t) = P_1(t) - P_0(t)$ between two states for the spin-boson model at low-temperature ($\beta = 1/(k_B T) = 5$) with the Ohmic bath. Panel (a) reports the population dynamics of the spin-boson model with parameters $\varepsilon = \Delta_c = 1$, $\beta = 5$, $\omega_c = 1$, $\alpha = 0.1$ in Panel (a). Solid circles: Exact results produced by eHEOM reported in ref¹³⁴. Cyan dashed lines: Ehrenfest dynamics. Orange dashed lines: FSSH. Magenta solid lines: CMM with $\gamma = 0.366$. Purple and green solid lines: wMM with $\Delta = 0.1$ and 0.05 , respectively. Panel (b) is similar to Panel (a) but for $\alpha = 0.4$; Panel (c) is similar to Panel (a) but for $\omega_c = 2.5$; Panel (d) is similar to Panel (a) but for $\omega_c = 2.5$, $\alpha = 0.4$. In each model 300 continuous DOFs (i.e., effective bath modes) are used.



1
2
3
4
5 **Figure 7:** Illustration of three Tully models and simulation results. Panel (a1) denotes diabatic PESes $V_{11}(R)$
6 and $V_{22}(R)$, as well as coupling term $V_{12}(R)$ for the SAC model; Panel (b1) does so for the DAC model; Panel
7
8
9 (c1) does so for the ECR model. Panel (c2) demonstrates adiabatic PESes $E_1(R)$ and $E_2(R)$, as well as
10 nonadiabatic coupling vector $d_{12}(R)$.
11
12

13 Panels (a2)-(a3): transmission coefficients on diabatic state 1, and those on diabatic state 2 of the SAC model,
14 respectively. Panels (b2)-(b3): similar to Panels (a2)-(a3), but for the DAC model. Panels (c3) and (c4):
15 transmission/reflection coefficients on adiabatic state 1 of the ECR model; Panels (c5) and (c6): those on adiabatic
16 state 2.
17
18

19 In Panels (a2)-(a3), (b2)-(b3), and (c3)-(c6), magenta, purple and green lines stand for transmission coefficients
20 results for CMM with $\gamma = 0.366$, wMM with $\Delta = 0.1$, and wMM with $\Delta = 0.05$, respectively. Long-dashed
21 blue lines: Ehrenfest dynamics; Short-dashed orange lines: FSSH; Black points: exact DVR benchmarks.
22
23
24
25
26
27
28
29
30
31
32
33
34
35
36
37
38
39
40
41
42
43
44
45
46
47
48
49
50
51
52
53
54
55
56
57
58
59
60

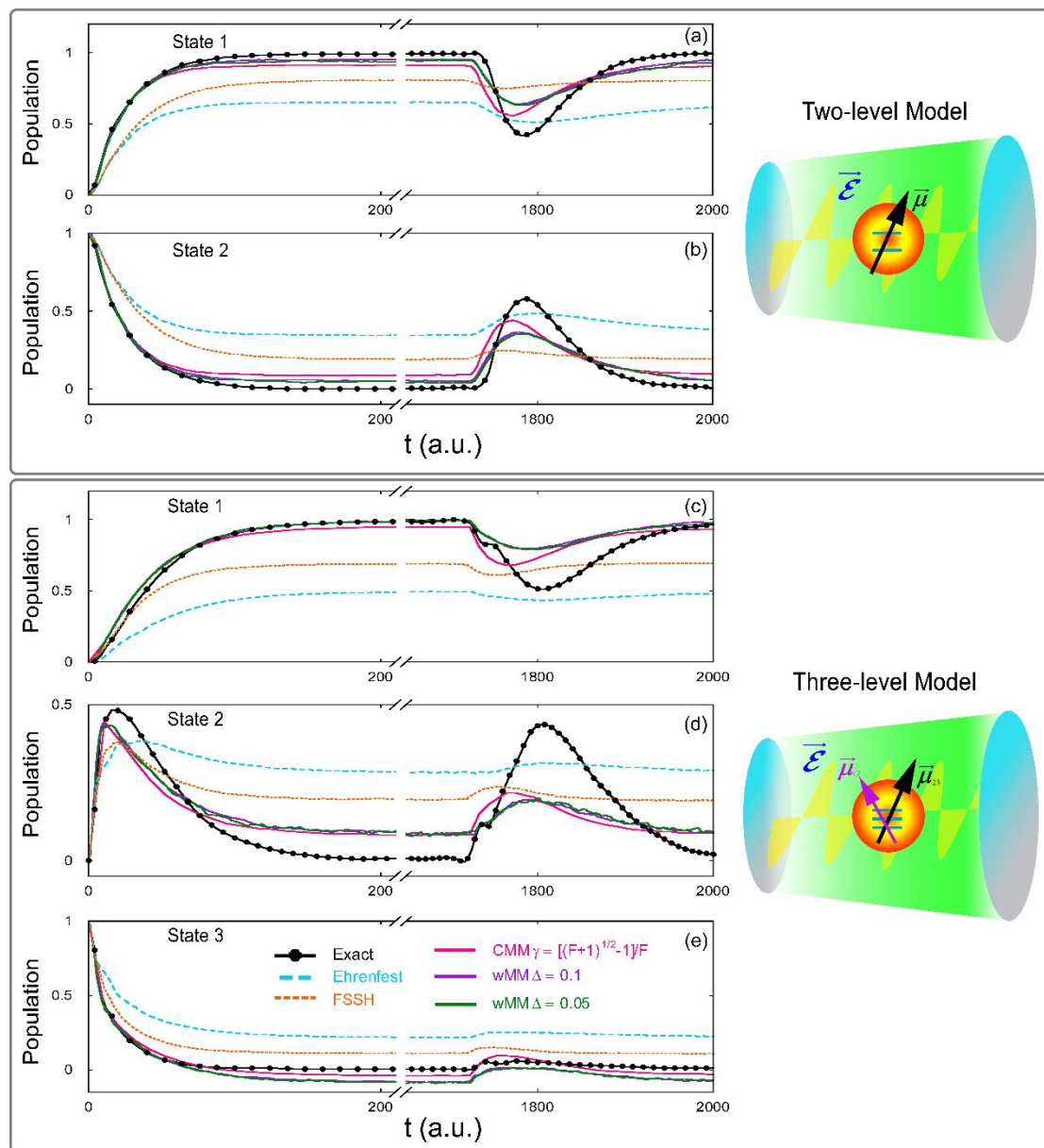


Figure 8: Results of population dynamics for the atom-in-cavity models. Panels (a)-(b) represent data of the first and second states of the two-level model, respectively. Panels (c)-(e) denote data of the first, second and third states of the three-level model, respectively. Magenta solid lines: CMM with $\gamma = (\sqrt{F+1} - 1)/F$; Purple solid lines: wMM with $\Delta = 0.1$; Green solid line: wMM with $\Delta = 0.05$; Cyan long-dashed lines: Ehrenfest dynamics; Orange short-dashed lines: FSSH; Black solid-dotted lines: exact results from refs^{285, 286}. In each model 400 continuous DOFs (i.e., standing-wave modes) are involved.

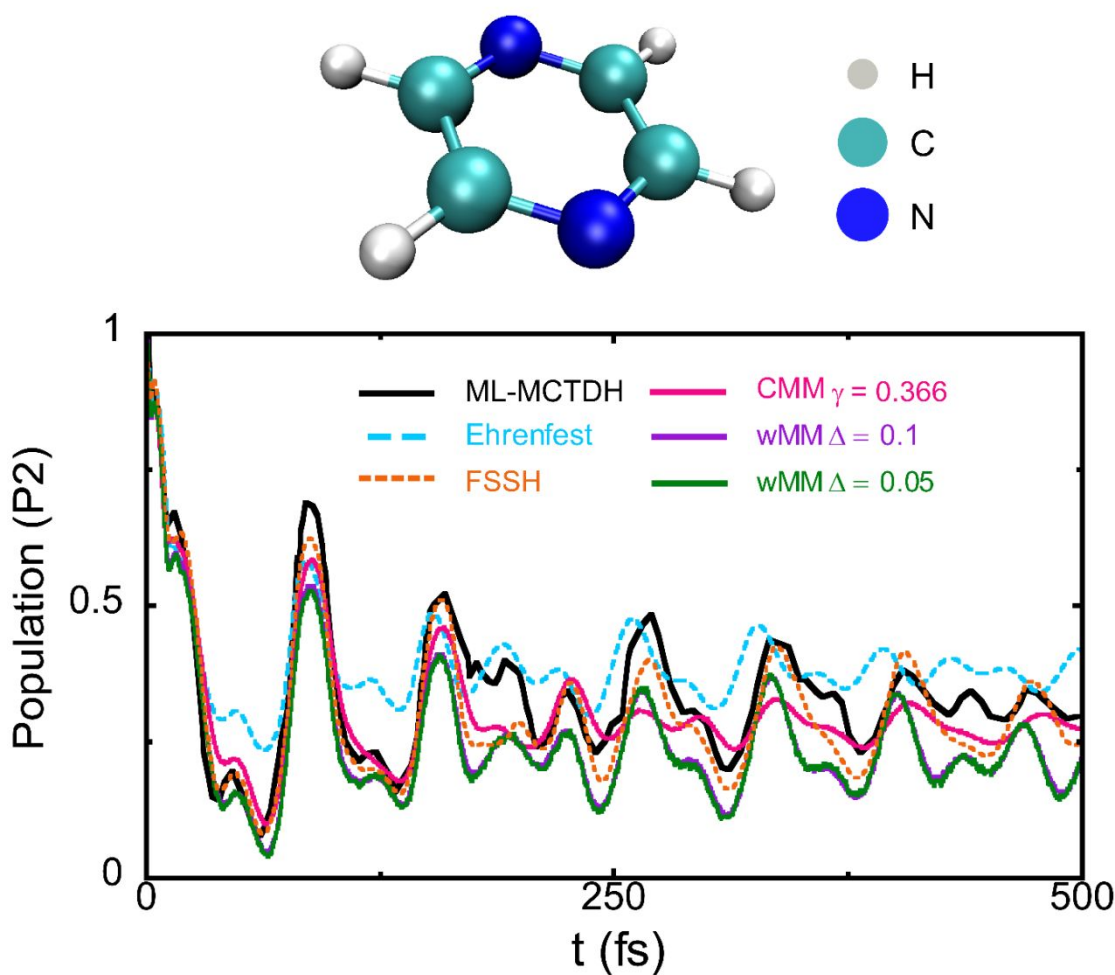


Figure 9: Results of population dynamics of the second electronic state of the 2-level 3-mode pyrazine model.

Magenta solid lines: CMM with $\gamma = (\sqrt{F+1} - 1) / F \approx 0.366$; Purple solid lines: wMM with $\Delta = 0.1$;

Green solid lines: wMM with $\Delta = 0.05$. Cyan dashed lines: Ehrenfest dynamics; Orange short-dashed lines:

FSSH; Black solid lines: ML-MCTDH results of ref²¹².

Funding Information

National Natural Science Foundation of China (NSFC) Grant No. 21961142017; Ministry of Science and Technology of China (MOST) Grant No. 2017YFA0204901

Research Resources

High-performance Computing Platform of Peking University, Beijing PARATERA Tech CO., Ltd., and Guangzhou supercomputer center

Acknowledgments

This work was supported by the National Natural Science Foundation of China (NSFC) Grant No. 21961142017, and by the Ministry of Science and Technology of China (MOST) Grant No. 2017YFA0204901. We acknowledge the High-performance Computing Platform of Peking University, Beijing PARATERA Tech CO., Ltd., and Guangzhou supercomputer center for providing computational resources.

Notes

The authors declare no competing financial interest.

Further Reading**Appendices****1. Equations of motion in the adiabatic representation**

We show EOMs in the adiabatic representation for applying phase space mapping dynamics methods with on-the-fly ab initio calculations. The realistic molecular Hamiltonian *via* the Born-Huang expansion is

$$\hat{H}_{nm} = \left[-\sum_{I=1}^N \frac{\hbar^2}{2M_I} \frac{\partial^2}{\partial R_I^2} + E_m(\mathbf{R}) \right] \delta_{nm} - \sum_n \sum_{I=1}^N \frac{\hbar^2}{2M_I} \left[2d_{mn}^{(I)}(\mathbf{R}) \frac{\partial}{\partial R_I} + D_{mn}^{(I)}(\mathbf{R}) \right]. \quad 50$$

Here, $d_{mn}^{(I)}(\mathbf{R}) = \left\langle \phi_m(\mathbf{R}) \left| \frac{\partial \phi_n(\mathbf{R})}{\partial R_I} \right. \right\rangle$ and $D_{mn}^{(I)}(\mathbf{R}) = \left\langle \phi_m(\mathbf{R}) \left| \frac{\partial^2 \phi_n(\mathbf{R})}{\partial R_I^2} \right. \right\rangle$ denote the first order and second

order nonadiabatic coupling terms, respectively, on adiabatic basis $\{\phi_n(\mathbf{R})\}$. It is trivial to show the relation,

$$D_{nm}^{(I)}(\mathbf{R}) = \sum_{k=1}^F d_{nk}^{(I)} d_{km}^{(I)} + \frac{\partial}{\partial R_I} \cdot d_{nm}^{(I)} . \quad 51$$

We use the momentum operator $\hat{\mathbf{P}} = -i\hbar\nabla_{\mathbf{R}}$ to simplify $V_{mn}(\hat{\mathbf{R}}, \hat{\mathbf{P}})$, the element of the effective potential matrix that is the second term of the right-hand side of eq 50,

$$V_{mn}(\hat{\mathbf{R}}, \hat{\mathbf{P}}) = E_n(\hat{\mathbf{R}}) \delta_{mn} - i\hbar \sum_{I=1}^N d_{mn}^{(I)}(\hat{\mathbf{R}}) \frac{\hat{P}_I}{2M_I} - i\hbar \sum_{I=1}^N \frac{\hat{P}_I}{2M_I} \cdot d_{mn}^{(I)}(\hat{\mathbf{R}}) - \sum_{I=1}^N \sum_{k=1}^F \frac{\hbar^2 d_{mk}^{(I)}(\hat{\mathbf{R}}) d_{kn}^{(I)}(\hat{\mathbf{R}})}{2M_I} . \quad 52$$

When infinite Wigner phase space for continuous (nuclear) DOFs, because the Wigner-Weyl correspondence leads to

$$i\hbar \sum_{I=1}^N d_{mn}^{(I)}(\hat{\mathbf{R}}) \frac{\hat{P}_I}{2M_I} + i\hbar \sum_{I=1}^N \frac{\hat{P}_I}{2M_I} \cdot d_{mn}^{(I)}(\hat{\mathbf{R}}) \approx i\hbar \sum_{I=1}^N \frac{P_I}{M_I} \cdot d_{mn}^{(I)}(\mathbf{R}) , \quad 53$$

the total Hamiltonian (matrix) on nuclear phase space becomes

$$\mathbf{H}(\mathbf{R}, \mathbf{P}) = \sum_{I=1}^N \frac{P_I^2}{2M_I} \mathbf{I}_{ele}(\mathbf{R}) + \mathbf{V}(\mathbf{R}, \mathbf{P}) \quad 54$$

with the element of the effective potential matrix,

$$V_{mn}(\mathbf{R}, \mathbf{P}) = \sum_{I=1}^N \left(-\frac{i\hbar}{M_I} P_I \cdot d_{mn}^{(I)}(\mathbf{R}) - \frac{\hbar^2}{2M_I} \sum_{k=1}^F d_{mk}^{(I)}(\mathbf{R}) d_{kn}^{(I)}(\mathbf{R}) \right) + E_n(\mathbf{R}) \delta_{mn} , \quad 55$$

and the identity matrix in the adiabatic representation $\mathbf{I}_{ele}(\mathbf{R}) = \sum_{n=1}^F |\phi_n(\mathbf{R})\rangle\langle\phi_n(\mathbf{R})|$.

Define (adiabatic) potential matrix $\mathbf{E}_{ele}(\mathbf{R}) = \sum_{n=1}^F E_n(\mathbf{R}) |\phi_n(\mathbf{R})\rangle\langle\phi_n(\mathbf{R})|$, and nonadiabatic coupling matrix of the I -th nuclear DOF $\mathbf{d}^{(I)}(\mathbf{R}) = \sum_{m,n=1}^F d_{mn}^{(I)}(\mathbf{R}) |\phi_m(\mathbf{R})\rangle\langle\phi_n(\mathbf{R})|$. Using the kinematic momentum matrix

$$\mathbf{P}_{kin,I}(\mathbf{R}, \mathbf{P}) @ P_I \mathbf{I}_{ele} - i\hbar \mathbf{d}^{(I)}(\mathbf{R}) , \quad 56$$

we then obtain an alternative expression of the effective potential (matrix)

$$\mathbf{V}(\mathbf{R}, \mathbf{P}) = -\sum_{I=1}^N \frac{i\hbar}{M_I} \mathbf{P}_{kin,I}(\mathbf{R}, \mathbf{P}) \cdot \mathbf{d}^{(I)}(\mathbf{R}) + \mathbf{E}(\mathbf{R}) . \quad 57$$

Or equivalently, eq 54 becomes

$$\mathbf{H}(\mathbf{R}, \mathbf{P}) = \sum_{I=1}^N \frac{\mathbf{P}_{kin,I}^T \mathbf{P}_{kin,I}}{2M_I} + \mathbf{E}(\mathbf{R}) . \quad 58$$

In eq 58 only the first-order nonadiabatic coupling term is involved.

In ref.¹⁸⁴ Cotton and Miller proposed a strategy of using the kinematic momentum in the EOMs of the Meyer-Miller mapping Hamiltonian, which can also be applied here to avoid the derivative of the first-order nonadiabatic coupling. Such EOMs read

$$\begin{aligned} \dot{\mathbf{R}}_I &= \frac{P_{kin,I}}{M_I} \\ \dot{\mathbf{P}}_{kin,I} &= - \sum_{n,m=1}^F \left[\frac{1}{2} \left(x^{(n)} x^{(m)} + p^{(n)} p^{(m)} \right) - \gamma \right] \left[\frac{\partial E_n(\mathbf{R})}{\partial R_I} \delta_{mn} + (E_n(\mathbf{R}) - E_m(\mathbf{R})) d_{mn}^{(I)}(\mathbf{R}) \right], \end{aligned} \quad 59$$

for mapping phase space variables for the continuous (nuclear) DOFs, and

$$\begin{aligned} \dot{\mathbf{x}}^{(m)} &= \sum_{n=1}^F V_{mn}(\mathbf{R}, \mathbf{P}) p^{(n)} \\ \dot{\mathbf{p}}^{(m)} &= - \sum_{n=1}^F V_{mn}(\mathbf{R}, \mathbf{P}) x^{(n)} \end{aligned}, \quad 60$$

for mapping phase space variables for the discrete (electronic) DOFs. The EOMs, eqs 59-60, are invariant with the transformation of the electronic state basis, which faithfully reproduce Hamilton's EOMs governed by the mapping Hamiltonian eq 29 in the diabatic representation. More discussion and extension along this line are available in the Supporting Information of ref⁵⁷.

A symplectic and convenient approach for solving eq 60 is to construct an exact propagator on electronic phase space at each nuclear phase space point, i.e.,

$$\mathbf{U}(\mathbf{R}, \mathbf{P}; \Delta t) = \exp[-i\Delta t \mathbf{V}(\mathbf{R}, \mathbf{P})/\hbar], \quad 61$$

such that the electronic phase space variables evolve as $\mathbf{g}(t + \Delta t) = \mathbf{U}(\mathbf{R}, \mathbf{P}; \Delta t) \mathbf{g}(t)$ with the definition, $\mathbf{g}(t) = \mathbf{x}(t) + i\mathbf{p}(t)$.

2. On the quasi-probability distribution function of the weighted constraint phase space formulation

As presented in eq (S15) of the Supporting Information of ref¹³⁴, the second order moment and fourth order moment on constraint space defined by eq 27 are

$$\begin{aligned} \int_{\mathbb{S}_\gamma(\mathbf{x}, \mathbf{p})} d\mathbf{X} (X_i X_j) &= \frac{1+F\gamma}{F} \delta_{ij} \\ \int_{\mathbb{S}_\gamma(\mathbf{x}, \mathbf{p})} d\mathbf{X} (X_i X_j X_k X_l) &= \frac{(1+F\gamma)^2}{F(F+1)} (\delta_{ij}\delta_{kl} + \delta_{ik}\delta_{jl} + \delta_{il}\delta_{jk}) \end{aligned}. \quad 62$$

Here, we use $\mathbf{S}_\gamma(\mathbf{x}, \mathbf{p})$ for eq 27 because the constraint space is parameterized by γ . When the kernel is required to be symmetrical, i.e., eq 33, we denote the element of the (inverse) kernel operator

$$K_{nm}(\mathbf{x}, \mathbf{p}) = [K^{-1}]_{nm}(\mathbf{x}, \mathbf{p}) = \frac{1}{2}(x_n + ip_n)(x_m - ip_m) - \gamma\delta_{nm} . \quad 63$$

Employing eq (S20) of the Supporting Information of ref¹³⁴, we obtain

$$\begin{aligned} & F \int_{\mathbf{S}_\gamma(\mathbf{x}, \mathbf{p})} d\mathbf{X} K_{nm}(\mathbf{x}, \mathbf{p}) K_{lk}^{-1}(\mathbf{x}, \mathbf{p}) \\ &= \int_{\mathbf{S}_\gamma(\mathbf{x}, \mathbf{p})} d\mathbf{X} \left[\frac{1}{2}(x_n + ip_n)(x_m - ip_m) - \gamma\delta_{nm} \right] \left[\frac{1}{2}(x_l + ip_l)(x_k - ip_k) - \gamma\delta_{lk} \right] . \quad 64 \\ &= \frac{(1+F\gamma)^2}{(F+1)} \delta_{nk} \delta_{ml} + \left[\frac{(1+F\gamma)^2}{(F+1)} - 2\gamma - F\gamma^2 \right] \delta_{lk} \delta_{nm} \end{aligned}$$

The orthonormal relation of the kernel function of the exact mapping on weighted constraint space is

$$F \int d\gamma w(\gamma) \int_{\mathbf{S}_\gamma(\mathbf{x}, \mathbf{p})} d\mathbf{X} K_{nm}(\mathbf{x}, \mathbf{p}) K_{lk}^{-1}(\mathbf{x}, \mathbf{p}) = \delta_{nk} \delta_{ml} . \quad 65$$

Substitution of eq 64 into eq 65 yields

$$\int d\gamma w(\gamma) (F\gamma^2 + 2\gamma) = \int d\gamma w(\gamma) \chi(\gamma) = 1 , \quad 66$$

which is eq 34 of the main text.

3. The matrix bases for mapping between the density matrix and phase space functions

The Hermitian mapping kernels can also be expressed as

$$\hat{K}(\mathbf{X}) = \sum_\mu f_\mu(\mathbf{X}) \hat{\mathbf{M}}_\mu^\dagger = \sum_\mu f_\mu^*(\mathbf{X}) \hat{\mathbf{M}}_\mu , \quad 67$$

where $\hat{\mathbf{M}}_\mu$ is an arbitrary basis (operator basis) on the $F \times F$ operator space satisfying

$$\text{Tr}[\hat{\mathbf{M}}_\mu^\dagger \hat{\mathbf{M}}_\nu] = \delta_{\mu\nu} , \quad 68$$

and $f_\mu(\mathbf{X})$ is an orthonormal function basis on the mapping space,

$$\int F d\mathbf{X} \frac{1}{\Omega(\gamma)} \delta \left(\sum_{n=1}^F \frac{(x^{(n)})^2 + (p^{(n)})^2}{2} - (1+F\gamma) \right) f_\mu^*(\mathbf{X}) f_\nu(\mathbf{X}) = \delta_{\mu\nu} . \quad 69$$

Any operator \hat{A} and the corresponding phase space function can be decomposed into

$$\hat{A} = \sum_\mu A_\mu \hat{\mathbf{M}}_\mu, \quad A(\mathbf{X}) = \text{Tr}[\hat{A} \hat{K}(\mathbf{X})] = \sum_\mu A_\mu f_\mu(\mathbf{X}) . \quad 70$$

A natural option for the matrix bases is $\{ |n\rangle\langle m| \}$, which satisfies the criterion of eq 68 and is used for the formulation of (weighted) constraint coordinate-momentum phase space of Section 2.

References

1. Lee, H. W.; Scully, M. O., A new approach to molecular-collisions - statistical quasiclassical method. *The Journal of Chemical Physics* **1980**, *73* (5), 2238-2242.
2. Lee, H. W.; Scully, M. O., The Wigner phase-space description of collision processes. *Foundations of Physics* **1983**, *13* (1), 61-72.
3. Heller, E. J., Wigner phase space method: Analysis for semiclassical applications. *The Journal of Chemical Physics* **1976**, *65*, 1289.
4. Sun, X.; Wang, H.; Miller, W. H., Semiclassical theory of electronically nonadiabatic dynamics: Results of a linearized approximation to the initial value representation. *The Journal of Chemical Physics* **1998**, *109* (17), 7064-7074.
5. Wang, H.; Sun, X.; Miller, W. H., Semiclassical approximations for the calculation of thermal rate constants for chemical reactions in complex molecular systems. *The Journal of Chemical Physics* **1998**, *108* (23), 9726-9736.
6. Pollak, E.; Liao, J. L., A new quantum transition state theory. *The Journal of Chemical Physics* **1998**, *108* (7), 2733-2743.
7. Shao, J.; Liao, J.-L.; Pollak, E., Quantum transition state theory: Perturbation expansion. *The Journal of Chemical Physics* **1998**, *108* (23), 9711-9725.
8. Hernandez, R.; Voth, G. A., Quantum time correlation functions and classical coherence. *Chemical Physics* **1998**, *233* (2-3), 243-255.
9. Liu, J.; Miller, W. H., Using the thermal Gaussian approximation for the Boltzmann operator in semiclassical initial value time correlation functions. *The Journal of Chemical Physics* **2006**, *125* (22), 224104.
10. Liu, J.; Miller, W. H., Linearized semiclassical initial value time correlation functions using the thermal Gaussian approximation: applications to condensed phase systems. *The Journal of Chemical Physics* **2007**, *127* (11), 114506.
11. Liu, J.; Miller, W. H., Real time correlation function in a single phase space integral beyond the linearized semiclassical initial value representation. *The Journal of Chemical Physics* **2007**, *126* (23), 234110.
12. Liu, J.; Miller, W. H., Linearized semiclassical initial value time correlation functions with maximum entropy analytic continuation. *The Journal of Chemical Physics* **2008**, *129* (12), 124111.
13. Liu, J.; Miller, W. H., Test of the consistency of various linearized semiclassical initial value time correlation functions in application to inelastic neutron scattering from liquid para-hydrogen. *The Journal of Chemical Physics* **2008**, *128* (14), 144511.
14. Liu, J.; Miller, W. H.; Paesani, F.; Zhang, W.; Case, D. A., Quantum dynamical effects in liquid water: A semiclassical study on the diffusion and the infrared absorption spectrum. *The Journal of Chemical Physics* **2009**, *131* (16), 164509.
15. Liu, J.; Miller, W. H., A simple model for the treatment of imaginary frequencies in chemical reaction rates and molecular liquids. *The Journal of Chemical Physics* **2009**, *131* (7), 074113.
16. Liu, J.; Alder, B. J.; Miller, W. H., A semiclassical study of the thermal conductivity of low temperature liquids. *The Journal of Chemical Physics* **2011**, *135* (11), 114105.
17. Liu, J.; Miller, W. H.; Fanourgakis, G. S.; Xantheas, S. S.; Imoto, S.; Saito, S., Insights in quantum dynamical effects in the infrared spectroscopy of liquid water from a semiclassical study with an ab initio-based flexible and polarizable force field. *The Journal of Chemical Physics* **2011**, *135* (24), 244503.
18. Liu, J., Recent advances in the linearized semiclassical initial value representation/classical Wigner model for the thermal correlation function. *International Journal of Quantum Chemistry* **2015**, *115* (11), 657-670.
19. Liu, X.; Liu, J., Critical role of quantum dynamical effects in the Raman spectroscopy of liquid water. *Molecular Physics* **2018**, *116* (7-8), 755-779.
20. Shi, Q.; Geva, E., Semiclassical theory of vibrational energy relaxation in the condensed phase. *Journal of Physical Chemistry A* **2003**, *107*, 9059-9069.
21. Shi, Q.; Geva, E., A relationship between semiclassical and centroid correlation functions. *The Journal of Chemical Physics* **2003**, *118* (18), 8173-8184.
22. Ka, B. J.; Geva, E., Vibrational energy relaxation of polyatomic molecules in liquid solution via the linearized semiclassical method. *Journal of Physical Chemistry A* **2006**, *110* (31), 9555-9567.

- 1
2
3 23. Poulsen, J. A.; Nyman, G.; Rossky, P. J., Practical evaluation of condensed phase quantum correlation
4 functions: A Feynman-Kleinert variational linearized path integral method. *The Journal of Chemical Physics*
5 **2003**, *119* (23), 12179-12193.
- 6 24. Poulsen, J. A.; Nyman, G.; Rossky, P. J., Feynman-Kleinert linearized path integral (FK-LPI) algorithms
7 for quantum molecular dynamics, with application to water and He(4). *Journal of Chemical Theory and*
8 *Computation* **2006**, *2* (6), 1482-1491.
- 9 25. Shao, J.; Makri, N., Forward-Backward Semiclassical Dynamics with Linear Scaling. *The Journal of*
10 *Physical Chemistry A* **1999**, *103* (47), 9479-9486.
- 11 26. Shao, J.; Makri, N., Forward-Backward Semiclassical Dynamics without Prefactors. *The Journal of*
12 *Physical Chemistry A* **1999**, *103* (39), 7753-7756.
- 13 27. Liu, J.; Nakayama, A.; Makri, N., Long-time behaviour of quantized distributions in forward-backward
14 semiclassical dynamics. *Molecular Physics* **2006**, *104* (8), 1267-1274.
- 15 28. Liu, J.; Makri, N., Symmetries and detailed balance in forward-backward semiclassical dynamics.
16 *Chemical Physics* **2006**, *322* (1), 23-29.
- 17 29. Makri, N.; Nakayama, A.; Wright, N. J., Forward-backward semiclassical simulation of dynamical
18 properties in liquids. *Journal of Theoretical and Computational Chemistry* **2004**, *3* (03), 391-417.
- 19 30. Makri, N., Quantum-classical path integral: A rigorous approach to condensed phase dynamics.
20 *International Journal of Quantum Chemistry* **2015**, *115* (18), 1209-1214.
- 21 31. Walters, P. L.; Makri, N., Quantum-Classical Path Integral Simulation of Ferrocene-Ferrocenium Charge
22 Transfer in Liquid Hexane. *Journal of Physical Chemistry Letters* **2015**, *6* (24), 4959-4965.
- 23 32. Kryvohuz, M.; Cao, J. S., Quantum-classical correspondence in response theory. *Physical Review Letters*
24 **2005**, *95* (18), 180405.
- 25 33. Donoso, A.; Martens, C. C., Quantum tunneling using entangled classical trajectories. *Physical Review*
26 *Letters* **2001**, *87* (22).
- 27 34. Donoso, A.; Zheng, Y. J.; Martens, C. C., Simulation of quantum processes using entangled trajectory
28 molecular dynamics. *Journal of Chemical Physics* **2003**, *119* (10), 5010-5020.
- 29 35. Wang, A.; Zheng, Y.; Martens, C. C.; Ren, W., Quantum tunneling dynamics using entangled
30 trajectories: general potentials. *Physical Chemistry Chemical Physics* **2009**, *11* (10), 1588-1594.
- 31 36. Xu, F.; Martens, C. C.; Zheng, Y., Entanglement dynamics with a trajectory-based formulation. *Physical*
32 *Review A* **2017**, *96* (2).
- 33 37. Liu, J.; Miller, W. H., An approach for generating trajectory-based dynamics which conserves the
34 canonical distribution in the phase space formulation of quantum mechanics. I. Theories. *The Journal of Chemical*
35 *Physics* **2011**, *134* (10), 104101.
- 36 38. Liu, J.; Miller, W. H., An approach for generating trajectory-based dynamics which conserves the
37 canonical distribution in the phase space formulation of quantum mechanics. II. Thermal correlation functions.
38 *The Journal of Chemical Physics* **2011**, *134* (10), 104102.
- 39 39. Liu, J., Two more approaches for generating trajectory-based dynamics which conserves the canonical
40 distribution in the phase space formulation of quantum mechanics. *The Journal of Chemical Physics* **2011**, *134*
41 (19), 194110.
- 42 40. Liu, J., Path integral Liouville dynamics for thermal equilibrium systems. *The Journal of Chemical*
43 *Physics* **2014**, *140* (22), 224107.
- 44 41. Liu, J.; Zhang, Z., Path integral Liouville dynamics: Applications to infrared spectra of OH, water,
45 ammonia, and methane. *The Journal of Chemical Physics* **2016**, *144* (3), 034307.
- 46 42. Liu, J.; Li, D.; Liu, X., Further study of path integral Liouville dynamics. *Scientia Sinica Chimica* **2016**,
47 *46*, 27-37.
- 48 43. Zhang, Z.-j.; Chen, Z.-f.; Liu, J., Path integral Liouville dynamics simulations of vibrational spectra of
49 formaldehyde and hydrogen peroxide. *Chinese Journal of Chemical Physics* **2020**, *33* (5), 613-622.
- 50 44. Liu, X.; Zhang, L.; Liu, J., Machine learning phase space quantum dynamics approaches. *The Journal*
51 *of Chemical Physics* **2021**, *154* (18), 184104.
- 52 45. Smith, K. K. G.; Poulsen, J. A.; Nyman, G.; Cunsolo, A.; Rossky, P. J., Application of a new ensemble
53 conserving quantum dynamics simulation algorithm to liquid para-hydrogen and ortho-deuterium. *Journal of*
54 *Chemical Physics* **2015**, *142* (24).
- 55 46. Smith, K. K. G.; Poulsen, J. A.; Nyman, G.; Rossky, P. J., A new class of ensemble conserving
56 algorithms for approximate quantum dynamics: Theoretical formulation and model problems. *Journal of*
57 *Chemical Physics* **2015**, *142* (24).
- 58 47. Willatt, M. J.; Ceriotti, M.; Althorpe, S. C., Approximating Matsubara dynamics using the planetary
59 model: Tests on liquid water and ice. *Journal of Chemical Physics* **2018**, *148* (10).
- 60 48. Orr, L.; de la Pena, L. H.; Roy, P.-N., Formulation of state projected centroid molecular dynamics:
Microcanonical ensemble and connection to the Wigner distribution. *Journal of Chemical Physics* **2017**, *146* (21).

- 1
2
3
4
5
6
7
8
9
10
11
12
13
14
15
16
17
18
19
20
21
22
23
24
25
26
27
28
29
30
31
32
33
34
35
36
37
38
39
40
41
42
43
44
45
46
47
48
49
50
51
52
53
54
55
56
57
58
59
60
49. Bonella, S.; Montemayor, D.; Coker, D. F., Linearized path integral approach for calculating nonadiabatic time correlation functions. *Proc. Natl. Acad. Sci. U.S.A.* **2005**, *102* (19), 6715-6719.
50. Nassimi, A.; Bonella, S.; Kapral, R., Analysis of the quantum-classical Liouville equation in the mapping basis. *The Journal of Chemical Physics* **2010**, *133* (13), 134115.
51. Weinrib, J.; Ferry, D. K., Recent advances in Wigner function approaches. *Applied Physics Reviews* **2018**, *5* (4).
52. Pie, T.; Huppert, S.; Finocchi, F.; Depondt, P.; Bonella, S., Sampling the thermal Wigner density via a generalized Langevin dynamics. *Journal of Chemical Physics* **2019**, *151* (11).
53. Kapral, R.; Ciccotti, G., Mixed quantum-classical dynamics. *The Journal of Chemical Physics* **1999**, *110* (18), 8919-8929.
54. Kapral, R., Quantum dynamics in open quantum-classical systems. *Journal of Physics: Condensed Matter* **2015**, *27* (7), 073201.
55. Bai, S.; Xie, W.; Zhu, L.; Shi, Q., Calculation of absorption spectra involving multiple excited states: Approximate methods based on the mixed quantum classical Liouville equation. *Journal of Chemical Physics* **2014**, *140* (8).
56. Tao, G.; Miller, W. H., Semiclassical Description of Electronic Excitation Population Transfer in a Model Photosynthetic System. *Journal of Physical Chemistry Letters* **2010**, *1* (6), 891-894.
57. He, X.; Wu, B.; Gong, Z.; Liu, J., Commutator Matrix in Phase Space Mapping Models for Nonadiabatic Quantum Dynamics. *The Journal of Physical Chemistry A* **2021**, *125* (31), 6845-6863.
58. Liu, J.; He, X.; Wu, B., Unified Formulation of Phase Space Mapping Approaches for Nonadiabatic Quantum Dynamics. *Accounts of chemical research* **2021**, *54* (23), 4215-4228.
59. Orioli, A. P.; Safavi-Naini, A.; Wall, M. L.; Rey, A. M., Nonequilibrium dynamics of spin-boson models from phase-space methods. *Physical Review A* **2017**, *96* (3).
60. Lang, H. F.; Vendrell, O.; Hauke, P., Generalized discrete truncated Wigner approximation for nonadiabatic quantum-classical dynamics. *Journal of Chemical Physics* **2021**, *155* (2).
61. Glauber, R. J., Coherent and Incoherent States of Radiation Field. *Physical Review* **1963**, *131* (6), 2766.
62. Sudarshan, E. C. G., Equivalence of Semiclassical and Quantum Mechanical Descriptions of Statistical Light Beams. *Physical Review Letters* **1963**, *10* (7), 277.
63. Cahill, K. E.; Glauber, R. J., Ordered expansions in boson amplitude operators. *Physical Review* **1969**, *177* (5P1), 1857-+.
64. Cahill, K. E.; Glauber, R. J., Density operators and quasiprobability distributions. *Physical Review* **1969**, *177* (5P1), 1882-+.
65. Arrechi, F. T.; Thomas, H.; Gilmore, R.; Courtens, E., Atomic coherent states in quantum optics. *Physical Review A* **1972**, *6* (6), 2211-&.
66. Drummond, P. D.; Gardiner, C. W., Generalized P-Representations in Quantum Optics. *Journal of Physics a-Mathematical and General* **1980**, *13* (7), 2353-2368.
67. Walls, D.; Millburn, G., *Quantum Optics*. Springer-Verlag: Berlin, 1994.
68. Gardiner, C.; Zoller, P., *Quantum Noise*. 3rd edition ed.; Springer-Verlag: Berlin Heidelberg, 2004.
69. Schleich, W. P., Quantum Optics in Phase Space. *Quantum Optics in Phase Space* **2001**, 716.
70. Deleglise, S.; Dotsenko, I.; Sayrin, C.; Bernu, J.; Brune, M.; Raimond, J. M.; Haroche, S., Reconstruction of non-classical cavity field states with snapshots of their decoherence. *Nature* **2008**, *455* (7212), 510-514.
71. Steel, M. J.; Olsen, M. K.; Plimak, L. I.; Drummond, P. D.; Tan, S. M.; Collett, M. J.; Walls, D. F.; Graham, R., Dynamical quantum noise in trapped Bose-Einstein condensates. *Physical Review A* **1998**, *58* (6), 4824-4835.
72. Sinatra, A.; Lobo, C.; Castin, Y., The truncated Wigner method for Bose-condensed gases: limits of validity and applications. *Journal of Physics B-Atomic Molecular and Optical Physics* **2002**, *35* (17), 3599-3631.
73. Blakie, P. B.; Bradley, A. S.; Davis, M. J.; Ballagh, R. J.; Gardiner, C. W., Dynamics and statistical mechanics of ultra-cold Bose gases using c-field techniques. *Advances in Physics* **2008**, *57* (5), 363-455.
74. Polkovnikov, A., Phase space representation of quantum dynamics. *Annals of Physics* **2010**, *325* (8), 1790-1852.
75. Mukherjee, R.; Mirasola, A. E.; Hollingsworth, J.; White, I. G.; Hazzard, K. R. A., Geometric representation of spin correlations and applications to ultracold systems. *Physical Review A* **2018**, *97* (4), 043606.
76. Zurek, W. H., Sub-Planck structure in phase space and its relevance for quantum decoherence. *Nature* **2001**, *412* (6848), 712-717.
77. Miquel, C.; Paz, J. P.; Saraceno, M., Quantum computers in phase space. *Physical Review A* **2002**, *65* (6).
78. Wootters, W. K., Picturing Qubits in Phase Space. *{IBM} Journal of Research and Development* **2004**, *48* (1), 99-110.

- 1
2
3 79. Paz, J. P.; Roncaglia, A. J.; Saraceno, M., Qubits in phase space: Wigner-function approach to quantum-
4 error correction and the mean-king problem. *Physical Review A* **2005**, *72* (1), 19.
5 80. Braunstein, S. L.; van Loock, P., Quantum information with continuous variables. *Reviews of Modern
6 Physics* **2005**, *77* (2), 513-577.
7 81. Delfosse, N.; Guerin, P. A.; Bian, J.; Raussendorf, R., Wigner function negativity and contextuality in
8 quantum computation on rebits. *Physical Review X* **2015**, *5* (2), 23.
9 82. Schachenmayer, J.; Pikovski, A.; Rey, A. M., Many-Body Quantum Spin Dynamics with Monte-Carlo
10 Trajectories on a Discrete Phase Space. *Physical Review X* **2015**, *5* (1), 011022.
11 83. Schachenmayer, J.; Pikovski, A.; Rey, A. M., Dynamics of correlations in two-dimensional quantum
12 spin models with long-range interactions: a phase-space Monte-Carlo study. *New Journal of Physics* **2015**, *17* (6),
13 065009.
14 84. Bermejo-Vega, J.; Delfosse, N.; Browne, D. E.; Okay, C.; Raussendorf, R., Contextuality as a resource
15 for models of quantum computation with qubits. *Physical Review Letters* **2017**, *119* (12), 5.
16 85. Rundle, R. P.; Mills, P. W.; Tilma, T.; Samson, J. H.; Everitt, M. J., Simple procedure for phase-space
17 measurement and entanglement validation. *Physical Review A* **2017**, *96* (2), 022117.
18 86. Zhu, B.; Rey, A. M.; Schachenmayer, J., A generalized phase space approach for solving quantum spin
19 dynamics. *New Journal of Physics* **2019**, *21* (8), 082001.
20 87. Rundle, R. P.; Everitt, M. J., Overview of the Phase Space Formulation of Quantum Mechanics with
21 Application to Quantum Technologies. *Advanced Quantum Technologies* **2021**, *4* (6), 2100016.
22 88. Weyl, H., Quantum mechanics and Group theory. *Zeitschrift Fur Physik* **1927**, *46* (1-2), 1-46.
23 89. Wigner, E., On the Quantum Correction For Thermodynamic Equilibrium. *Physical Review* **1932**, *40*
(5), 749-759.
24 90. Hillery, M.; Oconnell, R. F.; Scully, M. O.; Wigner, E. P., Distribution-functions in physics -
25 fundamentals. *Physics Reports-Review Section of Physics Letters* **1984**, *106* (3), 121-167.
26 91. Lee, H. W., Theory and Application of the Quantum Phase-Space Distribution Functions. *Physics
Reports-Review Section of Physics Letters* **1995**, *259* (3), 147-211.
27 92. Cohen, L., Generalized Phase-Space Distribution Functions. *Journal of Mathematical Physics* **1966**, *7*
(5), 781-786.
28 93. Groenewold, H. J., On the Principles of Elementary Quantum Mechanics. *Physica* **1946**, *12* (7), 405-
31 460.
32 94. Moyal, J. E., Quantum mechanics as a statistical theory. *Mathematical Proceedings of the Cambridge
Philosophical Society* **1949**, *45* (1), 99-124.
34 95. Bopp, F., *Werner Heisenberg und die Physik unserer Zeit*. Vieweg: Braunschweig, 1961.
35 96. Miller, W. H., Quantum dynamics of complex molecular systems. *Proceedings of the National Academy
of Sciences* **2005**, *102* (19), 6660-6664.
37 97. Miller, W. H., Including quantum effects in the dynamics of complex (i.e., large) molecular systems. *The
Journal of Chemical Physics* **2006**, *125* (13), 132305.
38 98. Miller, W. H., Classical-limit quantum mechanics and the theory of molecular collisions. *Advances in
Chemical Physics* **1974**, *25*, 69-177.
41 99. Miller, W. H., The classical S-matrix in molecular collisions. *Advances in Chemical Physics*
42 **1975**, *30*, 77.
44 100. Stratonovich, R. L., On distributions in representation space. *Zh. Eksp. Teor. Fiz.* **1956**, *31*, 1012.
45 101. Feynman, R. P., Negative probability. In *Quantum Implications: Essays in Honour of David Bohm*,
Hiley, B. J.; Peat, D., Eds. Routledge: New York, 1987; pp 235-248.
46 102. Wootters, W. K., A Wigner-function formulation of finite-state quantum mechanics. *Annals of Physics*
47 **1987**, *176* (1), 1-21.
48 103. Várilly, J. C.; Gracia-Bonda, J., The Moyal representation for spin. *Annals of Physics* **1989**, *190* (1), 107-
49 148.
50 104. Amiet, J. P.; Cibils, M. B., DESCRIPTION OF QUANTUM SPIN USING FUNCTIONS ON THE
51 SPHERE J2. *Journal of Physics a-Mathematical and General* **1991**, *24* (7), 1515-1535.
52 105. Amiet, J. P.; Weigert, S., Discrete Q- and P-symbols for spin s. *J. Opt. B-Quantum Semicl. Opt.* **2000**, *2*
53 (2), 118-121.
54 106. Dowling, J. P.; Agarwal, G. S.; Schleich, W. P., Wigner distribution of a general angular-momentum
55 state - Applications to a collection of 2-level atoms. *Physical Review A* **1994**, *49* (5), 4101-4109.
56 107. Brif, C.; Mann, A., Phase-space Formulation of Quantum Mechanics and Quantum-state Reconstruction
57 for Physical Systems with Lie-group Symmetries. *Physical Review A* **1999**, *59* (2), 971-987.
58 108. Cunha, M. O. T.; Man'ko, V. I.; Scully, M. O., Quasiprobability and probability distributions for spin-
59 1/2 states. *Found. Phys. Lett.* **2001**, *14* (2), 103-117.

- 1
2
3 109. Klimov, A. B.; Espinoza, P., Moyal-like form of the star product for generalized SU(2) Stratonovich-Weyl symbols. *Journal of Physics A: Mathematical and General* **2002**, *35* (40), 8435-8447.
4
5 110. Klimov, A. B.; Romero, J. L., A Generalized Wigner Function for Quantum Systems with the SU(2) Dynamical Symmetry Group. *Journal of Physics A: Mathematical and Theoretical* **2008**, *41* (5), 055303.
6
7 111. Klimov, A. B.; Romero, J. L.; de Guise, H., Generalized SU(2) Covariant Wigner Functions and Some of Their Applications. *Journal of Physics A: Mathematical and Theoretical* **2017**, *50* (32), 323001.
8
9 112. Adam, P.; Andreev, V. A.; Man'ko, M. A.; Man'ko, V. I.; Mechler, M., SU(2) Symmetry of Qubit States and Heisenberg-Weyl Symmetry of Systems with Continuous Variables in the Probability Representation of Quantum Mechanics. *Symmetry-Basel* **2020**, *12* (7), 23.
10
11 113. Koczor, B.; Zeier, R.; Glaser, S. J., Continuous Phase-space Representations for Finite-dimensional Quantum States and Their Tomography. *Physical Review A* **2020**, *101* (2), 022318.
12
13 114. Tilma, T.; Nemoto, K., SU(N)-symmetric quasi-probability distribution functions. *J. Phys. A-Math. Theor.* **2012**, *45* (1), 14.
14
15 115. Tilma, T.; Everitt, M. J.; Samson, J. H.; Munro, W. J.; Nemoto, K., Wigner Functions for Arbitrary Quantum Systems. *Physical Review Letters* **2016**, *117* (18), 180401.
16
17 116. Marchiolli, M. A.; Galetti, D., On the discrete Wigner function for SU(N). *Journal of Physics A: Mathematical and Theoretical* **2019**, *52* (40), 405305.
18
19 117. Rundle, R. P.; Tilma, T.; Samson, J. H.; Dwyer, V. M.; Bishop, R. F.; Everitt, M. J., General Approach to Quantum Mechanics As a Statistical Theory. *Physical Review A* **2019**, *99* (1), 012115.
20
21 118. Cohendet, O.; Combe, P.; Sirugue, M.; Siruguecollin, M., A stochastic treatment of the dynamics of an integer spin. *Journal of Physics a-Mathematical and General* **1988**, *21* (13), 2875-2883.
22
23 119. Leonhardt, U., Quantum-state tomography and discrete Wigner function. *Physical Review Letters* **1995**, *74* (21), 4101-4105.
24
25 120. Leonhardt, U., Discrete Wigner function and quantum-state tomography. *Physical Review A* **1996**, *53* (5), 2998-3013.
26
27 121. Gibbons, K. S.; Hoffman, M. J.; Wootters, W. K., Discrete phase space based on finite fields. *Physical Review A* **2004**, *70* (6), 062101.
28
29 122. Wootters, W. K., Quantum Measurements and Finite Geometry. *Foundations of Physics* **2006**, *36* (1), 112-126.
30
31 123. Ruzzi, M.; Marchiolli, M. A.; Galetti, D., Extended Cahill-Glauber formalism for finite-dimensional spaces: I. Fundamentals. *Journal of Physics a-Mathematical and General* **2005**, *38* (27), 6239-6251.
32
33 124. Chaturvedi, S.; Ercolessi, E.; Marmo, G.; Morandi, G.; Mukunda, N.; Simon, R., Wigner distributions for finite dimensional quantum systems: An algebraic approach. *Pramana* **2005**, *65* (6), 981-993.
34
35 125. Chaturvedi, S.; Ercolessi, E.; Marmo, G.; Morandi, G.; Mukunda, N.; Simon, R., Wigner-Weyl correspondence in quantum mechanics for continuous and discrete systems}a Dirac-inspired view. *Journal of Physics A: Mathematical and General* **2006**, *39* (6), 1405-1423.
36
37 126. Gross, D., Hudson's theorem for finite-dimensional quantum systems. *Journal of Mathematical Physics* **2006**, *47* (12), 25.
38
39 127. Valtierra, I. F.; Romero, J. L.; Klimov, A. B., TWA versus semiclassical unitary approximation for spin-like systems. *Annals of Physics* **2017**, *383*, 620-634.
40
41 128. Valtierra, I. F.; Klimov, A. B.; Leuchs, G.; Sánchez-Soto, L. L., Quasiprobability currents on the sphere. *Physical Review A* **2020**, *101* (3), 033803.
42
43 129. Czischek, S., Discrete Truncated Wigner Approximation. In *Springer Theses*, Springer International Publishing: 2020; pp 85-109.
44
45 130. Morales-Hernández, G. E.; Castellanos, J. C.; Romero, J. L.; Klimov, A. B., Semi-classical Discretization and Long-time Evolution of Variable Spin Systems. *Entropy* **2021**, *23* (6), 684.
46
47 131. Liu, J., A unified theoretical framework for mapping models for the multi-state Hamiltonian. *The Journal of Chemical Physics* **2016**, *145* (20), 204105.
48
49 132. He, X.; Liu, J., A new perspective for nonadiabatic dynamics with phase space mapping models. *The Journal of Chemical Physics* **2019**, *151* (2), 024105.
50
51 133. Liu, J., Isomorphism between the multi-state Hamiltonian and the second-quantized many-electron Hamiltonian with only 1-electron interactions. *The Journal of Chemical Physics* **2017**, *146* (2), 024110.
52
53 134. He, X.; Gong, Z.; Wu, B.; Liu, J., Negative Zero-Point-Energy Parameter in the Meyer-Miller Mapping Model for Nonadiabatic Dynamics. *The journal of physical chemistry letters* **2021**, *12* (10), 2496-2501.
54
55 135. Domcke, W.; Yarkony, D. R.; Köppel, H., *Conical Intersections: Theory, Computation and Experiment*. World Scientific: Singapore, 2011.
56
57 136. Yonehara, T.; Hanasaki, K.; Takatsuka, K., Fundamental Approaches to Nonadiabaticity: Toward a Chemical Theory beyond the Born-Oppenheimer Paradigm. *Chemical Reviews* **2011**, *112* (1), 499-542.
58
59 137. Tully, J. C., Perspective: Nonadiabatic dynamics theory. *The Journal of Chemical Physics* **2012**, *137* (22), 22A301.
60

- 1
2
3 138. Miller, W. H.; Cotton, S. J., Classical molecular dynamics simulation of electronically non-adiabatic
4 processes. *Faraday Discussions* **2016**, *195*, 9-30.
- 5 139. Levine, B. G.; Martinez, T. J., Isomerization through conical intersections. *Annual Review of Physical
6 Chemistry* **2007**, *58*, 613-634.
- 7 140. Martinez, T. J., Seaming is believing. *Nature* **2010**, *467* (7314), 412-413.
- 8 141. Sisto, A.; Glowacki, D. R.; Martinez, T. J., Ab Initio Nonadiabatic Dynamics of Multichromophore
9 Complexes: A Scalable Graphical-Processing-Unit-Accelerated Exciton Framework. *Accounts of Chemical
10 Research* **2014**, *47* (9), 2857-2866.
- 11 142. Makhov, D. V.; Glover, W. J.; Martinez, T. J.; Shalashilin, D. V., Ab initio multiple cloning algorithm
12 for quantum nonadiabatic molecular dynamics. *The Journal of Chemical Physics* **2014**, *141* (5), 054110.
- 13 143. Mai, S.; Marquetand, P.; Gonzalez, L., Nonadiabatic dynamics: The SHARC approach. *Wiley
14 Interdisciplinary Reviews-Computational Molecular Science* **2018**, *8* (6).
- 15 144. Mai, S.; Gonzalez, L., Molecular Photochemistry: Recent Developments in Theory. *Angew Chem Int
16 Edit* **2020**, *59* (39), 16832-16846.
- 17 145. Subotnik, J. E.; Jain, A.; Landry, B.; Petit, A.; Ouyang, W.; Bellonzi, N., Understanding the Surface
18 Hopping View of Electronic Transitions and Decoherence. In *Annual Review of Physical Chemistry*, Vol 67,
19 Johnson, M. A.; Martinez, T. J., Eds. Annual Reviews: 2016; Vol. 67, pp 387-417.
- 20 146. Fang, W.-H., Ab Initio Determination of Dark Structures in Radiationless Transitions for Aromatic
21 Carbonyl Compounds. *Accounts of Chemical Research* **2008**, *41* (3), 452-457.
- 22 147. Long, R.; Prezhdo, O. V.; Fang, W., Nonadiabatic charge dynamics in novel solar cell materials. *Wiley
23 Interdisciplinary Reviews-Computational Molecular Science* **2017**, *7*, e1305.
- 24 148. Feng, W.; Xu, L.; Li, X.-Q.; Fang, W.; Yan, Y., Nonadiabatic molecular dynamics simulation: An
25 approach based on quantum measurement picture. *AIP Advances* **2014**, *4* (7).
- 26 149. Lan, Z.; Shao, J., Approximate Theoretical Methods for Nonadiabatic Dynamics of Polyatomic
27 Molecules. *Progress in Chemistry* **2012**, *24* (6), 1105-1119.
- 28 150. Wang, Y. C.; Ke, Y. L.; Zhao, Y., The hierarchical and perturbative forms of stochastic Schrodinger
29 equations and their applications to carrier dynamics in organic materials. *Wiley Interdisciplinary Reviews-
30 Computational Molecular Science* **2019**, *9* (1), e1375.
- 31 151. Nelson, T.; Fernandez-Alberti, S.; Roitberg, A. E.; Tretiak, S., Nonadiabatic Excited-State Molecular
32 Dynamics: Modeling Photophysics in Organic Conjugated Materials. *Accounts of Chemical Research* **2014**, *47*
(4), 1155-1164.
- 33 152. Crespo-Otero, R.; Barbatti, M., Recent Advances and Perspectives on Nonadiabatic Mixed Quantum-
34 Classical Dynamics. *Chemical Reviews* **2018**, *118* (15), 7026-7068.
- 35 153. Meyer, H.-D.; Miller, W. H., A classical analog for electronic degrees of freedom in nonadiabatic
36 collision processes. *The Journal of Chemical Physics* **1979**, *70* (7), 3214-3223.
- 37 154. Stock, G.; Thoss, M., Semiclassical description of nonadiabatic quantum dynamics. *Physical Review
38 Letters* **1997**, *78* (4), 578-581.
- 39 155. Wigner, E. P., *Perspectives in Quantum Theory*. MIT: Cambridge, 1971.
- 40 156. Husimi, K., Some Formal Properties of the Density Matrix. *Proceedings of the Physico-Mathematical
41 Society of Japan* **1940**, *22* (4), 264-314.
- 42 157. Glauber, R. J., Optical Coherence and Photon Statistics. In *Quantum Optics and Electronics*, deWitt, C.;
Blandin, A.; C., C.-T., Eds. Gordon and Breach: New York, 1965.
- 43 158. Kirkwood, J. G., Quantum Statistics of Almost Classical Assemblies. *Physical Review* **1933**, *44* (1), 31.
- 44 159. Rihaczek, A. W., Signal Energy Distribution in Time and Frequency. *IEEE Transactions on Information
45 Theory* **1968**, *14* (3), 369-374.
- 46 160. Mehta, C. L., Phase-Space Formulation of the Dynamics of Canonical Variables. *Journal of
47 Mathematical Physics* **1964**, *5* (5), 677-686.
- 48 161. Rivier, D. C., On a One-to-One Correspondence between Infinitesimal Canonical Transformations and
49 Infinitesimal Unitary Transformations. *Physical Review* **1951**, *83* (4), 862.
- 50 162. Margenau, H.; Hill, R. N., Correlation between Measurements in Quantum Theory. *Progress of
51 Theoretical Physics* **1961**, *26* (5), 722-738.
- 52 163. Born, M.; Jordan, P., On quantum mechanics. *Zeitschrift fur Physik* **1925**, *34*, 858-888.
- 53 164. Meyer, H. D.; Miller, W. H., Classical-Models for Electronic Degrees of Freedom: Derivation Via Spin
54 Analogy and Application to F*+H2→F+H2. *The Journal of Chemical Physics* **1979**, *71* (5), 2156-2169.
- 55 165. Gray, S. K.; Miller, W. H., Classical model for electronic degrees of freedom: charge transfer in Na + I
56 collisions. *Chemical Physics Letters* **1982**, *93* (4), 341-344.
- 57 166. Ali, D. P.; Miller, W. H., Effect of electronic transition dynamics on iodine atom recombination in
58 liquids. *The Journal of Chemical Physics* **1983**, *78* (11), 6640-6645.
- 59 167. Ali, D. P.; Miller, W. H., Classical models for electronic degrees of freedom: Quenching of Br*(2P1/2)
60 by collision with H2 in three dimensions. *Chemical Physics Letters* **1984**, *103* (6), 470-474.

- 1
2
3 168. Stock, G.; Miller, W. H., A classical model for time- and frequency-resolved spectroscopy of
4 nonadiabatic excited-state dynamics. *Chemical Physics Letters* **1992**, *197* (4-5), 396-404.
5 169. Stock, G.; Miller, W. H., Classical formulation of the spectroscopy of nonadiabatic excited-state
6 dynamics. *The Journal of Chemical Physics* **1993**, *99* (3), 1545-1555.
7 170. Sun, X.; Miller, W. H., Semiclassical initial value representation for electronically nonadiabatic
8 molecular dynamics. *The Journal of Chemical Physics* **1997**, *106* (15), 6346-6353.
9 171. Coronado, E. A.; Batista, V. S.; Miller, W. H., Nonadiabatic photodissociation dynamics of ICN in the A
10 continuum: A semiclassical initial value representation study. *The Journal of Chemical Physics* **2000**, *112* (13),
11 5566-5575.
12 172. Coronado, E. A.; Xing, J.; Miller, W. H., Ultrafast non-adiabatic dynamics of systems with multiple
13 surface crossings: a test of the Meyer-Miller Hamiltonian with semiclassical initial value representation methods.
14 *Chemical Physics Letters* **2001**, *349* (5-6), 521-529.
15 173. Ananth, N.; Venkataraman, C.; Miller, W. H., Semiclassical description of electronically nonadiabatic
16 dynamics via the initial value representation. *The Journal of Chemical Physics* **2007**, *127* (8), 084114.
17 174. Miller, W. H., Electronically Nonadiabatic Dynamics via Semiclassical Initial Value Methods. *Journal
18 of Physical Chemistry A* **2009**, *113* (8), 1405-1415.
19 175. Ananth, N.; Miller, T. F., Exact quantum statistics for electronically nonadiabatic systems using
20 continuous path variables. *The Journal of Chemical Physics* **2010**, *133* (23), 234103.
21 176. Cotton, S. J.; Miller, W. H., Symmetrical Windowing for Quantum States in Quasi-Classical Trajectory
22 Simulations. *Journal of Physical Chemistry A* **2013**, *117* (32), 7190-7194.
23 177. Cotton, S. J.; Miller, W. H., Symmetrical windowing for quantum states in quasi-classical trajectory
24 simulations: Application to electronically non-adiabatic processes. *The Journal of Chemical Physics* **2013**, *139*
(23), 234112.
25 178. Cotton, S. J.; Igumenshchev, K.; Miller, W. H., Symmetrical windowing for quantum states in quasi-
26 classical trajectory simulations: Application to electron transfer. *The Journal of Chemical Physics* **2014**, *141* (8),
27 084104.
28 179. Cotton, S. J.; Miller, W. H., A Symmetrical Quasi-Classical Spin-Mapping Model for the Electronic
29 Degrees of Freedom in Non-Adiabatic Processes. *Journal of Physical Chemistry A* **2015**, *119* (50), 12138-12145.
30 180. Miller, W. H.; Cotton, S. J., Communication: Note on detailed balance in symmetrical quasi-classical
31 models for electronically non-adiabatic dynamics. *The Journal of Chemical Physics* **2015**, *142* (13), 131103.
32 181. Cotton, S. J.; Miller, W. H., A new symmetrical quasi-classical model for electronically non-adiabatic
33 processes: Application to the case of weak non-adiabatic coupling. *The Journal of Chemical Physics* **2016**, *145*
34 (14), 144108.
35 182. Cotton, S. J.; Miller, W. H., The Symmetrical Quasi-Classical Model for Electronically Non-Adiabatic
36 Processes Applied to Energy Transfer Dynamics in Site-Exciton Models of Light-Harvesting Complexes. *Journal
37 of Chemical Theory and Computation* **2016**, *12* (3), 983-991.
38 183. Miller, W. H.; Cotton, S. J., Communication: Wigner functions in action-angle variables, Bohr-
39 Sommerfeld quantization, the Heisenberg correspondence principle, and a symmetrical quasi-classical approach
40 to the full electronic density matrix. *The Journal of Chemical Physics* **2016**, *145* (8), 081102.
41 184. Cotton, S. J.; Liang, R.; Miller, W. H., On the adiabatic representation of Meyer-Miller electronic-
42 nuclear dynamics. *The Journal of Chemical Physics* **2017**, *147* (6), 064112.
43 185. Liang, R.; Cotton, S. J.; Binder, R.; Hegger, R.; Burghardt, I.; Miller, W. H., The symmetrical quasi-
44 classical approach to electronically nonadiabatic dynamics applied to ultrafast exciton migration processes in
45 semiconducting polymers. *The Journal of Chemical Physics* **2018**, *149* (4), 044101.
46 186. Cotton, S. J.; Miller, W. H., A symmetrical quasi-classical windowing model for the molecular dynamics
47 treatment of non-adiabatic processes involving many electronic states. *The Journal of Chemical Physics* **2019**,
48 *150* (10), 104101.
49 187. Cotton, S. J.; Miller, W. H., Trajectory-adjusted electronic zero point energy in classical Meyer-Miller
50 vibronic dynamics: Symmetrical quasiclassical application to photodissociation. *The Journal of Chemical Physics*
51 **2019**, *150* (19), 194110.
52 188. Muller, U.; Stock, G., Flow of zero-point energy and exploration of phase space in classical simulations
53 of quantum relaxation dynamics. II. Application to nonadiabatic processes. *Journal of Chemical Physics* **1999**,
54 *111* (1), 77-88.
55 189. Stock, G.; Muller, U., Flow of zero-point energy and exploration of phase space in classical simulations
56 of quantum relaxation dynamics. *Journal of Chemical Physics* **1999**, *111* (1), 65-76.
57 190. Stock, G.; Muller, U., Flow of zero-point energy and exploration of phase space in classical simulations
58 of quantum relaxation dynamics. ii. allication to nonadiabatic processes. *The Journal of Chemical Physics* **1999**,
59 *111*.
60 191. Stock, G.; Thoss, M., Classical Description of Nonadiabatic Quantum Dynamics. In *Advances in
Chemical Physics*, Rice, S. A., Ed. John Wiley & Sons, Inc.: 2005; Vol. 131, pp 243-375.

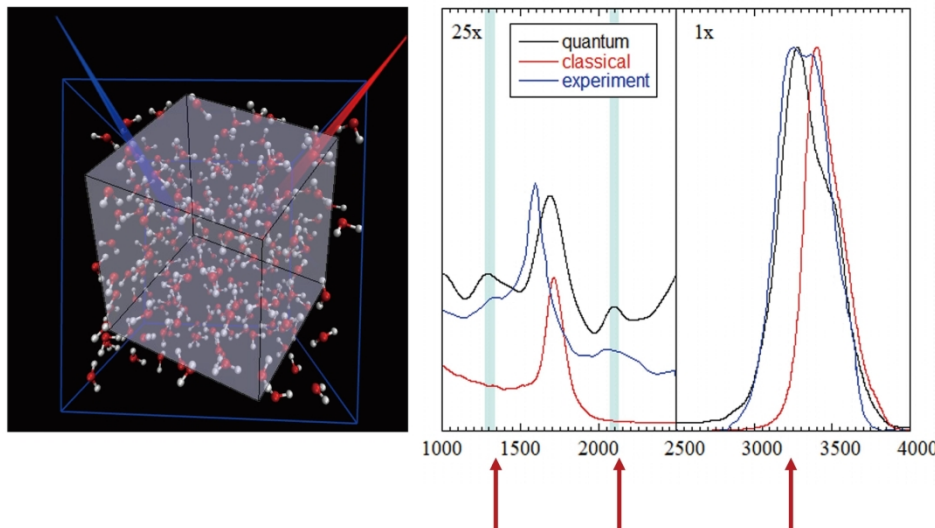
- 1
2
3 192. Thoss, M.; Miller, W. H.; Stock, G., Semiclassical description of nonadiabatic quantum dynamics:
4 Application to the S1-S2 conical intersection in pyrazine. *The Journal of Chemical Physics* **2000**, *112* (23), 10282-
5 10292.
- 6 193. Thoss, M.; Stock, G., Mapping approach to the semiclassical description of nonadiabatic quantum
7 dynamics. *Physical Review A* **1999**, *59* (1), 64-79.
- 8 194. Golosov, A. A.; Reichman, D. R., Classical mapping approaches for nonadiabatic dynamics: Short time
9 analysis. *The Journal of Chemical Physics* **2001**, *114* (3), 1065-1074.
- 10 195. Saller, M. A. C.; Kelly, A.; Richardson, J. O., On the identity of the identity operator in nonadiabatic
11 linearized semiclassical dynamics. *The Journal of Chemical Physics* **2019**, *150* (7), 071101.
- 12 196. Saller, M. A. C.; Kelly, A.; Richardson, J. O., Improved population operators for multi-state nonadiabatic
13 dynamics with the mixed quantum-classical mapping approach. *Faraday Discussions* **2020**, *221*, 150-167.
- 14 197. Runeson, J. E.; Richardson, J. O., Generalized spin mapping for quantum-classical dynamics. *The
15 Journal of Chemical Physics* **2020**, *152* (8), 084110.
- 16 198. Kananenka, A. A.; Hsieh, C. Y.; Cao, J. S.; Geva, E., Nonadiabatic Dynamics via the Symmetrical
17 Quasi-Classical Method in the Presence of Anharmonicity. *Journal of Physical Chemistry Letters* **2018**, *9* (2),
18 319-326.
- 19 199. Mulvihill, E.; Gao, X.; Liu, Y.; Schubert, A.; Dunietz, B. D.; Geva, E., Combining the mapping
20 Hamiltonian linearized semiclassical approach with the generalized quantum master equation to simulate
21 electronically nonadiabatic molecular dynamics. *The Journal of Chemical Physics* **2019**, *151* (7), 074103.
- 22 200. Gao, X.; Geva, E., Improving the Accuracy of Quasiclassical Mapping Hamiltonian Methods by Treating
23 the Window Function Width as an Adjustable Parameter. *Journal of Physical Chemistry A* **2020**, *124* (52), 11006-
11016.
- 24 201. Gao, X.; Lai, Y. F.; Geva, E., Simulating Absorption Spectra of Multiexcitonic Systems via
25 Quasiclassical Mapping Hamiltonian Methods. *Journal of Chemical Theory and Computation* **2020**, *16* (10),
26 6465-6480.
- 27 202. Gao, X.; Sailer, M. A. C.; Liu, Y. D.; Kelly, A.; Richardson, J. O.; Geva, E., Benchmarking
28 Quasiclassical Mapping Hamiltonian Methods for Simulating Electronically Nonadiabatic Molecular Dynamics.
29 *Journal of Chemical Theory and Computation* **2020**, *16* (5), 2883-2895.
- 30 203. Liu, Y. D.; Gao, X.; Lai, Y. F.; Mulvihill, E.; Geva, E., Electronic Dynamics through Conical
31 Intersections via Quasiclassical Mapping Hamiltonian Methods. *Journal of Chemical Theory and Computation*
32 **2020**, *16* (7), 4479-4488.
- 33 204. Saller, M. A. C.; Kelly, A.; Geva, E., Benchmarking Quasiclassical Mapping Hamiltonian Methods for
34 Simulating Cavity-Modified Molecular Dynamics. *Journal of Physical Chemistry Letters* **2021**, *12* (12), 3163-
35 3170.
- 36 205. Bonella, S.; Coker, D. F., A semiclassical limit for the mapping Hamiltonian approach to electronically
37 nonadiabatic dynamics. *The Journal of Chemical Physics* **2001**, *114* (18), 7778-7789.
- 38 206. Bonella, S.; Coker, D. F., Semiclassical implementation of the mapping Hamiltonian approach for
39 nonadiabatic dynamics using focused initial distribution sampling. *The Journal of Chemical Physics* **2003**, *118*
40 (10), 4370-4385.
- 41 207. Bonella, S.; Coker, D. F., LAND-map, a linearized approach to nonadiabatic dynamics using the
42 mapping formalism. *The Journal of Chemical Physics* **2005**, *122* (19), 194102.
- 43 208. Huo, P. F.; Coker, D. F., Semi-classical path integral non-adiabatic dynamics: a partial linearized
44 classical mapping Hamiltonian approach. *Molecular Physics* **2012**, *110* (9-10), 1035-1052.
- 45 209. Tang, D. D.; Fang, W. H.; Shen, L.; Cui, G. L., Combining Meyer-Miller Hamiltonian with electronic
46 structure methods for on-the-fly nonadiabatic dynamics simulations: implementation and application. *Physical
Chemistry Chemical Physics* **2019**, *21* (31), 17109-17117.
- 47 210. Zheng, J.; Xie, Y.; Jiang, S.-s.; Long, Y.-z.; Ning, X.; Lan, Z.-g., Ultrafast Electron Transfer with
48 Symmetrical Quasi-classical Dynamics based on Mapping Hamiltonian and Quantum Dynamics based on ML-
49 MCTDH. *Chinese Journal of Chemical Physics* **2017**, *30* (6), 800-810.
- 50 211. Xie, Y.; Zheng, J.; Lan, Z., Performance evaluation of the symmetrical quasi-classical dynamics method
51 based on Meyer-Miller mapping Hamiltonian in the treatment of site-exciton models. *The Journal of Chemical
52 Physics* **2018**, *149* (17), 174105.
- 53 212. Zheng, J.; Xie, Y.; Jiang, S.; Long, Y.; Ning, X.; Lan, Z., Initial sampling in symmetrical quasiclassical
54 dynamics based on Li-Miller mapping Hamiltonian. *Physical Chemistry Chemical Physics* **2019**, *21* (48), 26502-
55 26514.
- 56 213. Zheng, J.; Peng, J. W.; Xie, Y.; Long, Y. Z.; Ning, X.; Lan, Z. G., Study of the exciton dynamics in
57 perylene bisimide (PBI) aggregates with symmetrical quasiclassical dynamics based on the Meyer-Miller mapping
58 Hamiltonian. *Physical Chemistry Chemical Physics* **2020**, *22* (32), 18192-18204.
- 59 214. Peng, J.; Xie, Y.; Hu, D.; Lan, Z., Analysis of bath motion in MM-SQC dynamics via dimensionality
60 reduction approach: Principal component analysis. *The Journal of Chemical Physics* **2021**, *154* (9), 094122.

- 1
2
3 215. Hu, D. P.; Xie, Y.; Peng, J. W.; Lan, Z. G., On-the-Fly Symmetrical Quasi-Classical Dynamics with
4 Meyer–Miller Mapping Hamiltonian for the Treatment of Nonadiabatic Dynamics at Conical Intersections.
5 *Journal of Chemical Theory and Computation* **2021**, *17* (6), 3267–3279.
- 6 216. Tao, G., A multi-state trajectory method for non-adiabatic dynamics simulations. *The Journal of
7 Chemical Physics* **2016**, *144* (9), 094108.
- 8 217. Tao, G. H., Coherence-Controlled Nonadiabatic Dynamics via State-Space Decomposition: A Consistent
9 Way To Incorporate Ehrenfest and Born–Oppenheimer-Like Treatments of Nuclear Motion. *Journal of Physical
10 Chemistry Letters* **2016**, *7* (21), 4335–4339.
- 11 218. Tao, G., Multi-state trajectory approach to non-adiabatic dynamics: General formalism and the active
12 state trajectory approximation. *The Journal of Chemical Physics* **2017**, *147* (4), 044107.
- 13 219. Schwinger, J., In *Quantum Theory of Angular Momentum*, Biedenharn, L. C.; VanDam, H., Eds.
14 Academic: New York, 1965.
- 15 220. Sakurai, J. J., *Modern Quantum Mechanics*. Addison-Wesley: New York, 1994.
- 16 221. Flammia, S. T.; Liu, Y.-K., Direct Fidelity Estimation from Few Pauli Measurements. *Physical Review
17 Letters* **2011**, *106* (23).
- 18 222. Sperling, J.; Walmsley, I. A., Quasiprobability representation of quantum coherence. *Physical Review A*
19 **2018**, *97* (6), 062327.
- 20 223. Bohmann, M.; Agudelo, E.; Sperling, J., Probing nonclassicality with matrices of phase-space
21 distributions. *Quantum* **2020**, *4*, 16.
- 22 224. Bohmann, M.; Agudelo, E., Phase-space inequalities beyond negativities. *Physical Review Letters* **2020**,
23 *124* (13), 6.
- 24 225. Lütterbach, L. G.; Davidovich, L., Method for direct measurement of the Wigner function in cavity QED
25 and ion traps. *Physical Review Letters* **1997**, *78* (13), 2547–2550.
- 26 226. Signoles, A.; Facon, A.; Grossi, D.; Dotsenko, I.; Haroche, S.; Raimond, J. M.; Brune, M.; Gleyzes,
27 S., Confined quantum Zeno dynamics of a watched atomic arrow. *Nat. Phys.* **2014**, *10* (10), 715–719.
- 28 227. Leiner, D.; Glaser, S. J., Wigner process tomography: Visualization of spin propagators and their spinor
29 properties. *Physical Review A* **2018**, *98* (1), 16.
- 30 228. Tian, Y. L.; Wang, Z. H.; Zhang, P. F.; Li, G.; Li, J.; Zhang, T. C., Measurement of complete and
31 continuous Wigner functions for discrete atomic systems. *Physical Review A* **2018**, *97* (1), 6.
- 32 229. Chen, B.; Geng, J.; Zhou, F.; Song, L.; Shen, H.; Xu, N., Quantum state tomography of a single
33 electron spin in diamond with Wigner function reconstruction. *Applied Physics Letters* **2019**, *114* (4).
- 34 230. Jing, Y.; Fadel, M.; Ivannikov, V.; Byrnes, T., Split spin-squeezed Bose-Einstein condensates. *New
35 Journal of Physics* **2019**, *21*.
- 36 231. Song, C.; Xu, K.; Li, H.; Zhang, Y.-R.; Zhang, X.; Liu, W.; Guo, Q.; Wang, Z.; Ren, W.; Hao, J.;
37 Feng, H.; Fan, H.; Zheng, D.; Wang, D.-W.; Wang, H.; Zhu, S.-Y., Generation of multicomponent atomic
38 Schrödinger cat states of up to 20 qubits. *Science* **2019**, *365* (6453), 574–577.
- 39 232. Eichler, C.; Lang, C.; Fink, J. M.; Govenius, J.; Filipp, S.; Wallraff, A., Observation of Entanglement
40 between Itinerant Microwave Photons and a Superconducting Qubit. *Physical Review Letters* **2012**, *109* (24).
- 41 233. Morin, O.; Huang, K.; Liu, J. L.; Le Jeannic, H.; Fabre, C.; Laurat, J., Remote creation of hybrid
42 entanglement between particle-like and wave-like optical qubits. *Nature Photonics* **2014**, *8* (7), 570–574.
- 43 234. Agudelo, E.; Sperling, J.; Costanzo, L. S.; Bellini, M.; Zavatta, A.; Vogel, W., Conditional Hybrid
44 Nonclassicality. *Physical Review Letters* **2017**, *119* (12), 120403.
- 45 235. Garon, A.; Zeier, R.; Glaser, S. J., Visualizing operators of coupled spin systems. *Physical Review A*
46 **2015**, *91* (4), 28.
- 47 236. Koczor, B.; Zeier, R.; Glaser, S. J., Time evolution of coupled spin systems in a generalized Wigner
48 representation. *Annals of Physics* **2019**, *408*, 1–50.
- 49 237. Davies, B. I.; Rundle, R. P.; Dwyer, V. M.; Samson, J. H.; Tilma, T.; Everitt, M. J., Visualizing spin
50 degrees of freedom in atoms and molecules. *Physical Review A* **2019**, *100* (4), 9.
- 51 238. Rundle, R. P.; Davies, B. I.; Dwyer, V. M.; Tilma, T.; Everitt, M. J., Visualization of correlations in
52 hybrid discrete—continuous variable quantum systems. *Journal of Physics Communications* **2020**, *4* (2), 025002.
- 53 239. Ehrenfest, P., Bemerkung über die angenäherte Gültigkeit der klassischen Mechanik innerhalb der
54 Quantenmechanik. *Zeitschrift für Physik* **1927**, *45* (7), 455–457.
- 55 240. Li, X.; Tully, J. C.; Schlegel, H. B.; Frisch, M. J., Ab initio Ehrenfest dynamics. *The Journal of Chemical
56 Physics* **2005**, *123* (8), 084106.
- 57 241. Tully, J. C., Molecular dynamics with electronic transitions. *The Journal of Chemical Physics* **1990**, *93*
58 (2), 1061–1071.
- 59 242. Wang, L. J.; Akimov, A.; Prezhdo, O. V., Recent Progress in Surface Hopping: 2011–2015. *Journal of
60 Physical Chemistry Letters* **2016**, *7* (11), 2100–2112.
243. Peng, J. W.; Xie, Y.; Hu, D. P.; Du, L. K.; Lan, Z. G., Treatment of Nonadiabatic Dynamics by On-The-Fly Trajectory Surface Hopping Dynamics. *Acta Phys-Chim Sin* **2019**, *35* (1), 28–48.

- 1
2
3 244. Yarkony, D. R., Conical Intersections: Diabolical and Often Misunderstood. *Accounts of Chemical*
4 *Research* **1998**, *31* (8), 511-518.
- 5 245. Paterson, M. J.; Bearpark, M. J.; Robb, M. A.; Blancafort, L.; Worth, G. A., Conical intersections: A
6 perspective on the computation of spectroscopic Jahn-Teller parameters and the degenerate 'intersection space'.
7 *Physical Chemistry Chemical Physics* **2005**, *7* (10), 2100-2115.
- 8 246. Matsika, S.; Krause, P., Nonadiabatic Events and Conical Intersections. In *Annual Review of Physical*
9 *Chemistry*, Vol 62, Leone, S. R.; Cremer, P. S.; Groves, J. T.; Johnson, M. A., Eds. Annual Reviews: 2011; Vol.
10 62, pp 621-643.
- 11 247. Makarov, D. E.; Makri, N., Path-Integrals for Dissipative Systems by Tensor Multiplication -
12 Condensed-Phase Quantum Dynamics for Arbitrarily Long-Time. *Chemical Physics Letters* **1994**, *221* (5-6), 482-
13 491.
- 14 248. Makri, N.; Makarov, D. E., Tensor Propagator for Iterative Quantum Time Evolution of Reduced
15 Density-Matrices .2. Numerical Methodology. *Journal of Chemical Physics* **1995**, *102* (11), 4611-4618.
- 16 249. Makri, N.; Makarov, D. E., Tensor Propagator for Iterative Quantum Time Evolution of Reduced
17 Density-Matrices .1. Theory. *Journal of Chemical Physics* **1995**, *102* (11), 4600-4610.
- 18 250. Topaler, M.; Makri, N., Path integral calculation of quantum nonadiabatic rates in model condensed
19 phase reactions. *Journal of Physical Chemistry* **1996**, *100* (11), 4430-4436.
- 20 251. Tanimura, Y.; Kubo, R., Time Evolution of a Quantum System in Contact with a Nearly Gaussian-
21 Markoffian Noise Bath. *Journal of the Physical Society of Japan* **1989**, *58* (1), 101-114.
- 22 252. Yan, Y.-a.; Yang, F.; Liu, Y.; Shao, J., Hierarchical approach based on stochastic decoupling to
dissipative systems. *Chemical Physics Letters* **2004**, *395* (4-6), 216-221.
- 23 253. Xu, R.-X.; Cui, P.; Li, X.-Q.; Mo, Y.; Yan, Y., Exact quantum master equation via the calculus on path
integrals. *The Journal of Chemical Physics* **2005**, *122* (4), 041103.
- 24 254. Shao, J., Stochastic description of quantum open systems: Formal solution and strong dissipation limit.
25 *Chemical Physics* **2006**, *322* (1-2), 187-192.
- 26 255. Moix, J. M.; Cao, J., A hybrid stochastic hierarchy equations of motion approach to treat the low
27 temperature dynamics of non-Markovian open quantum systems. *The Journal of Chemical Physics* **2013**, *139*
28 (13), 134106.
- 29 256. Tanimura, Y., Reduced hierarchical equations of motion in real and imaginary time: Correlated initial
30 states and thermodynamic quantities. *The Journal of Chemical Physics* **2014**, *141* (4), 044114.
- 31 257. Yan, Y., Theory of open quantum systems with bath of electrons and phonons and spins: Many-
32 dissipaton density matrixes approach. *The Journal of Chemical Physics* **2014**, *140* (5), 054105.
- 33 258. Tang, Z.; Ouyang, X.; Gong, Z.; Wang, H.; Wu, J., Extended hierarchy equation of motion for the spin-
34 boson model. *The Journal of Chemical Physics* **2015**, *143* (22), 224112.
- 35 259. Tanimura, Y., Real-time and imaginary-time quantum hierachal Fokker-Planck equations. *The Journal*
36 *of Chemical Physics* **2015**, *142* (14), 144110.
- 37 260. Meyer, H.-D.; Manthe, U.; Cederbaum, L. S., The multi-configurational time-dependent Hartree
38 approach. *Chemical Physics Letters* **1990**, *165* (1), 73-78.
- 39 261. Thoss, M.; Wang, H. B.; Miller, W. H., Self-consistent hybrid approach for complex systems:
40 Application to the spin-boson model with Debye spectral density. *The Journal of Chemical Physics* **2001**, *115* (7),
2991-3005.
- 41 262. Wang, H. B.; Thoss, M.; Miller, W. H., Systematic convergence in the dynamical hybrid approach for
42 complex systems: A numerically exact methodology. *The Journal of Chemical Physics* **2001**, *115* (7), 2979-2990.
- 43 263. Wang, H. B.; Thoss, M., Multilayer formulation of the multiconfiguration time-dependent Hartree
44 theory. *The Journal of Chemical Physics* **2003**, *119* (3), 1289-1299.
- 45 264. Wang, H. B.; Thoss, M., From coherent motion to localization: dynamics of the spin-boson model at zero
46 temperature. *New Journal of Physics* **2008**, *10*, 115005.
- 47 265. Worth, G. A.; Meyer, H.-D.; Köppel, H.; Cederbaum, L. S.; Burghardt, I., Using the MCTDH
48 wavepacket propagation method to describe multimode non-adiabatic dynamics. *International Reviews in*
49 *Physical Chemistry* **2008**, *27* (3), 569-606.
- 50 266. Wang, H.; Thoss, M., From coherent motion to localization: II. Dynamics of the spin-boson model with
51 sub-Ohmic spectral density at zero temperature. *Chemical Physics* **2010**, *370* (1-3), 78-86.
- 52 267. Craig, I. R.; Thoss, M.; Wang, H., Proton transfer reactions in model condensed-phase environments:
53 Accurate quantum dynamics using the multilayer multiconfiguration time-dependent Hartree approach. *The*
54 *Journal of Chemical Physics* **2007**, *127* (14), 144503.
- 55 268. Wang, H. B., Iterative Calculation of Energy Eigenstates Employing the Multi layer Multiconfiguration
56 Time-Dependent Hartree Theory. *Journal of Physical Chemistry A* **2014**, *118* (39), 9253-9261.
- 57 269. Purcell, E. M., Spontaneous Emission Probabilities at Radio Frequencies. In *Confined Electrons and*
58 *Photons: New Physics and Applications*, Burstein, E.; Weisbuch, C., Eds. Springer US: Boston, MA, 1995; pp
59 839-839.

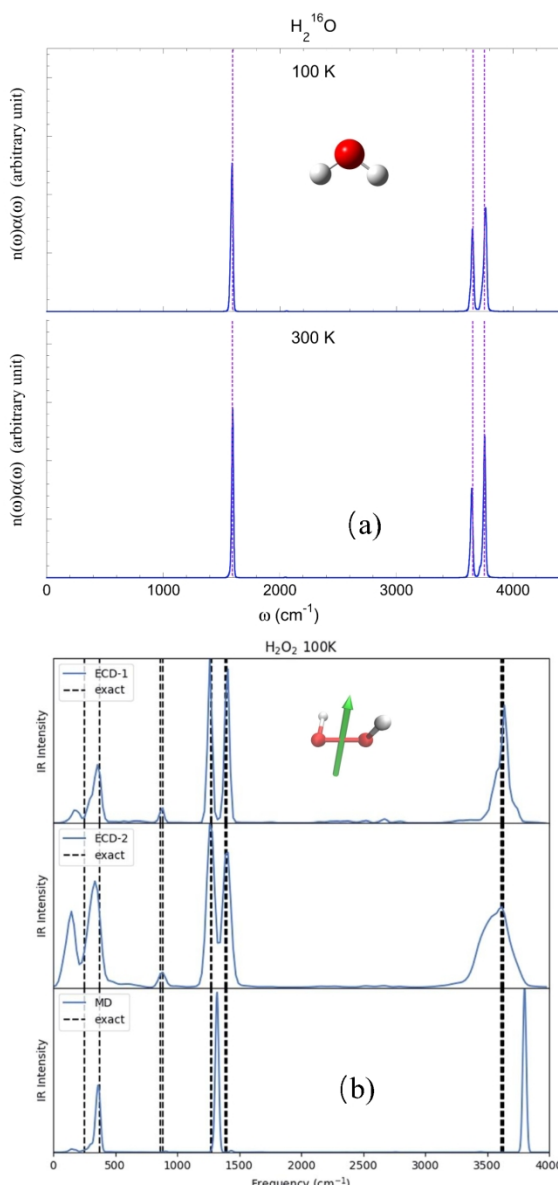
- 1
2
3 270. Krasnok, A. E.; Slobozhanyuk, A. P.; Simovski, C. R.; Tretyakov, S. A.; Poddubny, A. N.;
4 Miroshnichenko, A. E.; Kivshar, Y. S.; Belov, P. A., An antenna model for the Purcell effect. *Sci Rep* **2015**, *5*,
5 12956.
- 6 271. Rybin, M. V.; Mingaleev, S. F.; Limonov, M. F.; Kivshar, Y. S., Purcell effect and Lamb shift as
7 interference phenomena. *Sci Rep* **2016**, *6*, 20599.
- 8 272. Holsteen, A. L.; Raza, S.; Fan, P.; Kik, P. G.; Brongersma, M. L., Purcell effect for active tuning of
9 light scattering from semiconductor optical antennas. *Science* **2017**, *358* (6369), 1407-1410.
- 10 273. Alagappan, G.; Krivitsky, L. A.; Png, C. E., Diamond in a Nanopocket: A New Route to a Strong Purcell
11 Effect. *ACS Omega* **2018**, *3* (5), 4733-4742.
- 12 274. Gallego, J.; Alt, W.; Macha, T.; Martinez-Dorantes, M.; Pandey, D.; Meschede, D., Strong Purcell
13 Effect on a Neutral Atom Trapped in an Open Fiber Cavity. *Phys Rev Lett* **2018**, *121* (17), 173603.
- 14 275. Ren, T.; Dong, Y.; Xu, S.; Gong, X., Strong Purcell effect in deep subwavelength coaxial cavity with
15 GeSn active medium. *Opt Lett* **2021**, *46* (16), 3889-3892.
- 16 276. Carmichael, H. J.; Brecha, R. J.; Raizen, M. G.; Kimble, H. J.; Rice, P. R., Subnatural linewidth
17 averaging for coupled atomic and cavity-mode oscillators. *Phys Rev A Gen Phys* **1989**, *40* (10), 5516-5519.
- 18 277. Zhu, Y.; Gauthier, D. J.; Morin, S. E.; Wu, Q.; Carmichael, H. J.; Mossberg, T. W., Vacuum Rabi
19 splitting as a feature of linear-dispersion theory: Analysis and experimental observations. *Phys Rev Lett* **1990**, *64*
(21), 2499-2502.
- 20 278. Field, J. E., Vacuum-Rabi-splitting-induced transparency. *Phys Rev A* **1993**, *47* (6), 5064-5067.
- 21 279. Abram, I. I.; Oudar, J. L., Spontaneous emission in planar semiconductor microcavities displaying
22 vacuum Rabi splitting. *Phys Rev A* **1995**, *51* (5), 4116-4122.
- 23 280. Li, K.; Wang, W.; Chen, Z.; Gao, N.; Yang, W.; Li, W.; Chen, H.; Li, S.; Li, H.; Jin, P.; Kang, J.,
24 Vacuum Rabi splitting of exciton-polariton emission in an AlN film. *Sci Rep* **2013**, *3*, 3551.
- 25 281. Toida, H.; Nakajima, T.; Komiyama, S., Vacuum Rabi splitting in a semiconductor circuit QED system.
26 *Phys Rev Lett* **2013**, *110* (6), 066802.
- 27 282. Guerin, W.; Santo, T.; Weiss, P.; Cipris, A.; Schachenmayer, J.; Kaiser, R.; Bachelard, R., Collective
28 Multimode Vacuum Rabi Splitting. *Phys Rev Lett* **2019**, *123* (24), 243401.
- 29 283. Yan, Y.; Ergogo, T. T.; Lu, Z.; Chen, L.; Luo, J.; Zhao, Y., Lamb Shift and the Vacuum Rabi Splitting
30 in a Strongly Dissipative Environment. *J Phys Chem Lett* **2021**, *12* (40), 9919-9925.
- 31 284. Meystre, P., *Elements of quantum optics*. Springer: Berlin New York, 2007.
- 32 285. Hoffmann, N. M.; Schafer, C.; Rubio, A.; Kelly, A.; Appel, H., Capturing vacuum fluctuations and
33 photon correlations in cavity quantum electrodynamics with multitrajectory Ehrenfest dynamics. *Physical Review
34 A* **2019**, *99* (6), 063819.
- 35 286. Hoffmann, N. M.; Schäfer, C.; Säkkinen, N.; Rubio, A.; Appel, H.; Kelly, A., Benchmarking
36 semiclassical and perturbative methods for real-time simulations of cavity-bound emission and interference. *The
37 Journal of Chemical Physics* **2019**, *151* (24), 244113.
- 38 287. Li, T. E.; Chen, H. T.; Nitzan, A.; Subotnik, J. E., Quasiclassical modeling of cavity quantum
39 electrodynamics. *Physical Review A* **2020**, *101* (3), 033831.
- 40 288. Levine, B. G.; Ko, C.; Quenneville, J.; Martinez, T. J., Conical intersections and double excitations in
41 time-dependent density functional theory. *Molecular Physics* **2006**, *104* (5-7), 1039-1051.
- 42 289. Halcrow, M. A., Jahn-Teller distortions in transition metal compounds, and their importance in functional
43 molecular and inorganic materials. *Chem Soc Rev* **2013**, *42* (4), 1784-1795.
- 44 290. Bersuker, I. B., The Jahn-Teller and Pseudo-Jahn-Teller Effects: A Unique and Only Source of
45 Spontaneous Symmetry Breaking in Atomic Matter. *Symmetry-Basel* **2021**, *13* (9).
- 46 291. Qin, A.; Lam, J. W. Y.; Tang, B. Z., Luminogenic polymers with aggregation-induced emission
47 characteristics. *Prog Polym Sci* **2012**, *37* (1), 182-209.
- 48 292. Schneider, R.; Domcke, W., S1-S2 Conical intersection and ultrafast S2->S1 Internal conversion in
49 pyrazine. *Chemical Physics Letters* **1988**, *150* (3-4), 235-242.
- 50 293. Hacker, B.; Welte, S.; Daiss, S.; Shaukat, A.; Ritter, S.; Li, L.; Rempe, G., Deterministic creation of
51 entangled atom-light Schrödinger-cat states. *Nature Photonics* **2019**, *13* (2), 110-+.
- 52 294. Vlastakis, B.; Petrenko, A.; Ofek, N.; Sun, L. Y.; Leghtas, Z.; Sliwa, K.; Liu, Y. H.; Hatridge, M.;
53 Blumoff, J.; Frunzio, L.; Mirrahimi, M.; Jiang, L.; Devoret, M. H.; Schoelkopf, R. J., Characterizing
54 entanglement of an artificial atom and a cavity cat state with Bell's inequality. *Nature Communications* **2015**, *6*,
8.

1
2
3
4
5
6
7
8
9
10
11
12
13
14
15
16
17
18
19
20
21
22
23
24
25
26
27
28
29
30
31
32
33
34
35
36
37
38
39
40
41
42
43
44
45
46
47
48
49
50
51
52
53
54
55
56
57
58
59
60



Quantum dynamical effects are decisive in reproducing the experimental isotropic Raman spectrum of liquid water at room temperature, as illustrated by the LSC-IVR simulation where the infinite (Wigner) phase space for nuclear DOFs is used. Converged results were obtained with 216 water molecules in a box with periodic boundary conditions. (Reprinted with permission from ref 19. Copyright 2018 Taylor & Francis.)

180x106mm (300 x 300 DPI)



Molecular vibrational spectra produced by more advanced trajectory-based dynamics methods with infinite (Wigner) phase space used for nuclear DOFs, which satisfy the two fundamental criteria: conservation of the quantum Boltzmann distribution for the thermal equilibrium system and being exact for any quantum thermal correlation functions in the classical and harmonic limits. (a) Vibrational spectrum of the H₂O molecule at 100K and that at 300K. Adapted with permission from ref 41. Copyright 2016 American Institute of Physics Publishing. (b) Vibrational spectrum of the H₂O₂ molecule at 100K. Adapted with permission from ref 44. Copyright 2021 American Institute of Physics Publishing.

249x479mm (144 x 144 DPI)

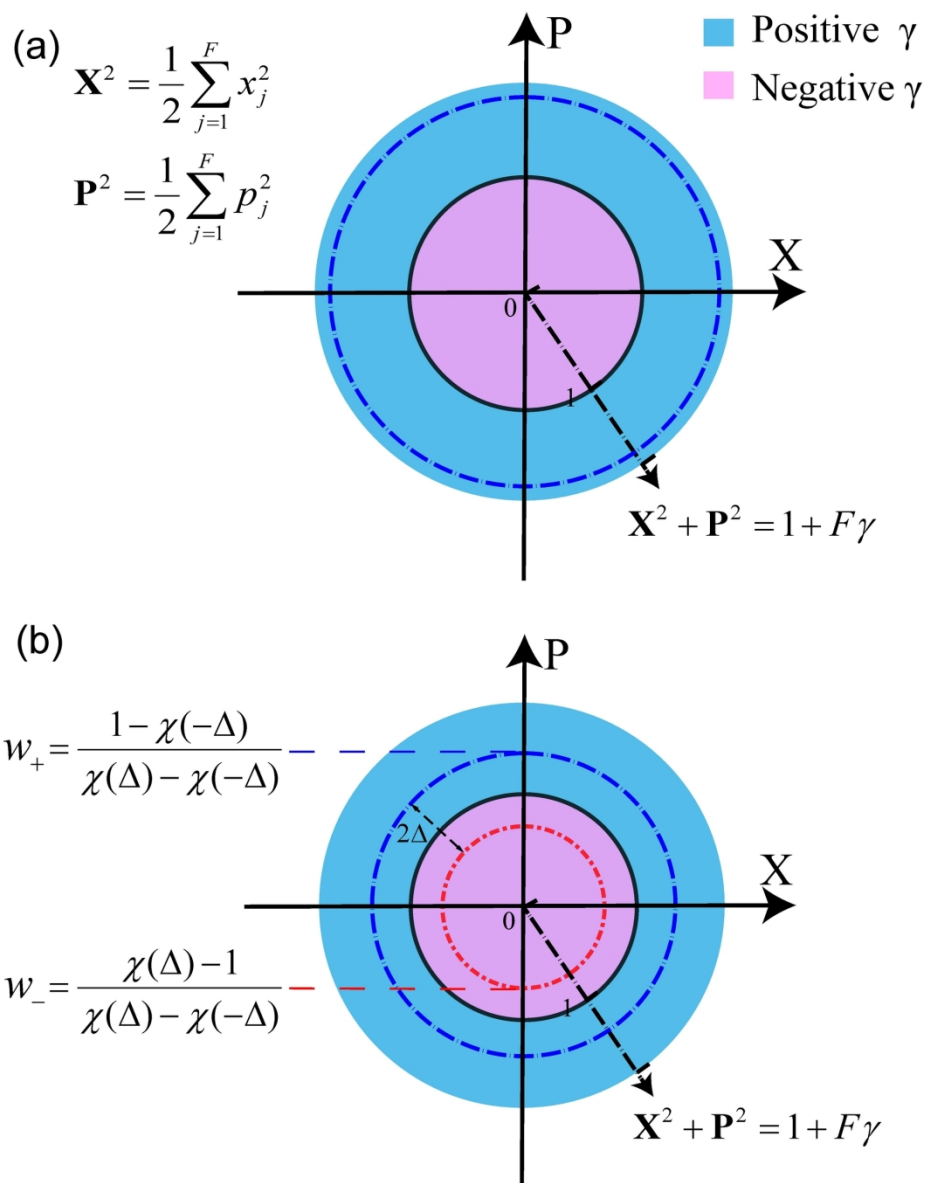
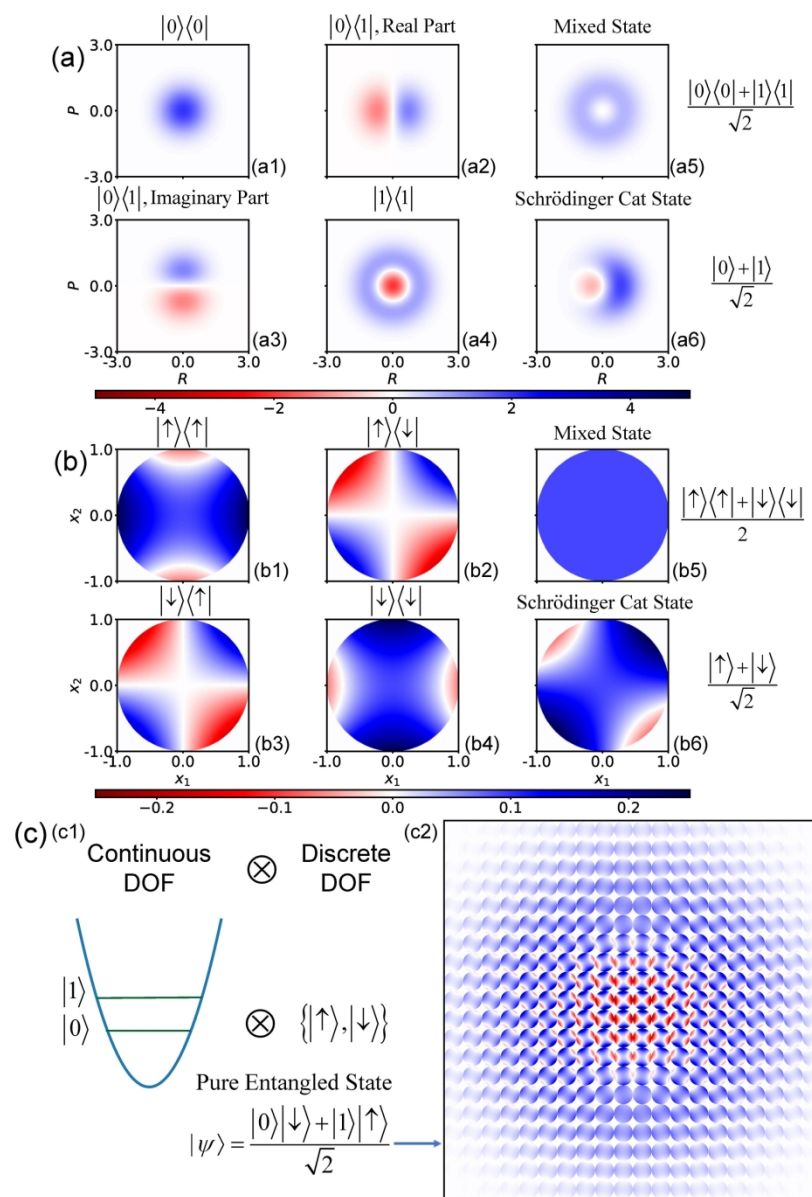


Illustration of the exact mapping formulation with constraint coordinate-momentum phase space. Panel (a) presents constraint phase space with only a single value of parameter γ . Panel (b) demonstrates weighted constraint phase space with two values of parameter γ , where the quasi-probability distribution function is $w(\gamma) = w_+ \delta(\gamma - \Delta) + w_- \delta(\gamma + \Delta)$. Constraint phase space with the positive weight is blue-dashed, while that with the negative weight is red dot-dashed. (Panel (a) is adapted with permission from ref 134. Copyright 2021 American Chemical Society.)

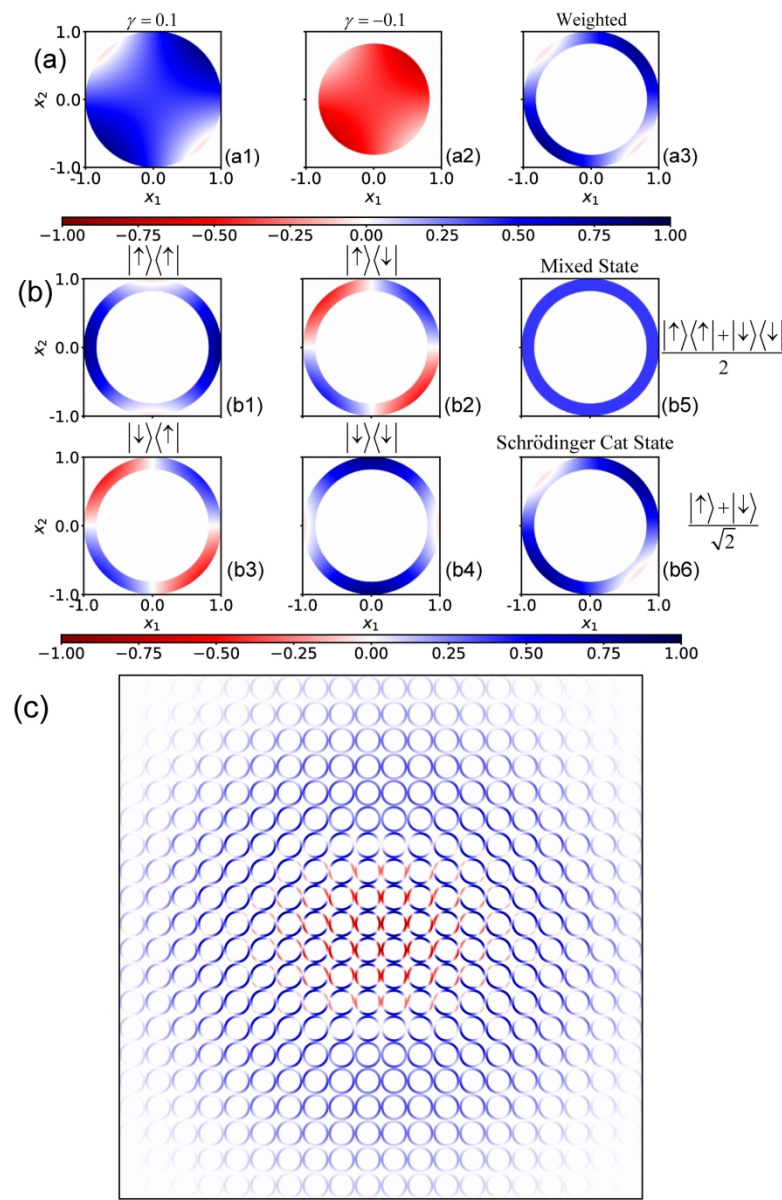
180x212mm (300 x 300 DPI)



Illustrations of (a) Wigner representation of a continuous-variable system, (b) constraint phase space representation of a discrete-variable system, and (c) hybrid coordinate-momentum phase space representation of a composite system with both discrete and continuous DOFs. (a) Wigner distribution for $|0\rangle\langle 0|$ (Panel a1), that for $|1\rangle\langle 1|$ (Panel a4), real part (Panel a2) and imaginary part (Panel a3) of the Wigner distribution for $|0\rangle\langle 1|$, wigner distribution for mixed state $(|0\rangle\langle 0| + |1\rangle\langle 1|)/2$ (Panel a5), and that for Schrödinger cat state $(|0\rangle + |1\rangle)(\langle 0| + \langle 1|)/2$ (Panel a6). Here, $|0\rangle$ and $|1\rangle$ are two energy levels of a continuous-variable system. (b) Marginal distribution of constraint phase space coordinates (x_1, x_2) for $|\uparrow\rangle\langle\uparrow|$ (Panel b1), $|\downarrow\rangle\langle\downarrow|$ (Panel b4), that for $|\uparrow\rangle\langle\downarrow|$ (Panel b2), that for $|\downarrow\rangle\langle\uparrow|$ (Panel b3), that for mixed state $(|\uparrow\rangle\langle\uparrow| + |\downarrow\rangle\langle\downarrow|)/2$ (Panel b5), and that for Schrödinger cat state $(|\uparrow\rangle + |\downarrow\rangle)(\langle\uparrow| + \langle\downarrow|)/2$ (Panel b6). Here, $|\uparrow\rangle$ and $|\downarrow\rangle$ represent two discrete states of a discrete-variable system. (c) Panel c1: Schematic representaton of the composite system and the pure entangled state $(|0\rangle|\downarrow\rangle + |1\rangle|\uparrow\rangle)/\sqrt{2}$; Panel c2: hybrid coordinate-momentum phase space representation of the entangled state. The grid is on the Wigner phase space (R, P) for the continuos DOF, and each circle of a grid stands for the local marginal distribution

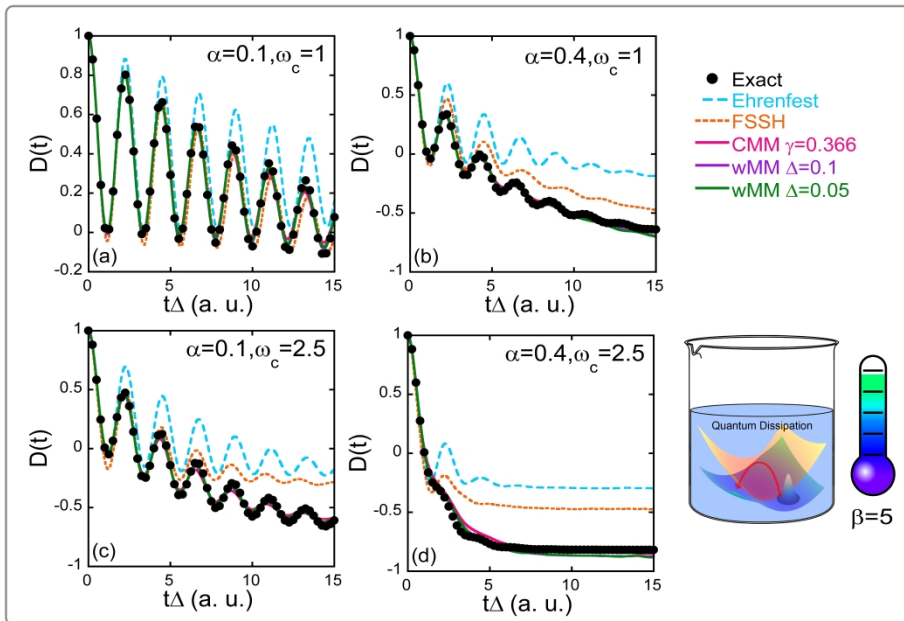
function of constraint phase space variables (x_1, x_2). The notations are identical to those in Panels (a)-(b).

180x251mm (300 x 300 DPI)



Illustrations of (a) components and (b) marginal distribution functions of the weighted constraint phase space representation of a discrete-variable system, and (c) weighted hybrid representation of the same composite system as that of Figure 4(c). (a) Marginal distribution of constraint phase space coordinates (x_1, x_2) for Schrödinger cat state ($| \uparrow \rangle + | \downarrow \rangle \langle \uparrow | + \langle \downarrow | / 2$) with $\gamma = \Delta$ weighted by w_+ (Panel a1), with $\gamma = -\Delta$ weighted by w_- (Panel a2). The sum of the two components yields the marginal distribution of constraint phase space coordinates (x_1, x_2) of the weighted representation with two values of parameter γ for the Schrödinger cat state (Panel a3). Coordinates are scaled by the larger radius $\sqrt{2(1+F\Delta)}$. (b) Weighted marginal distribution of constraint phase space coordinates (x_1, x_2) for the same properties as those in Figure 4(b). (c) Same as Figure 4(c), but using weighted marginal distribution for the discrete DOF.

180x274mm (300 x 300 DPI)



Results of population difference $D(t)=P_1(t) - P_0(t)$ between two states for the spin-boson model at low-temperature ($\beta=1/(k_B T)=5$) with the Ohmic bath. Panel (a) reports the population dynamics of the spin-boson model with parameter $\varepsilon=\Delta_c=1$, $\beta=5$, $\omega_c=1$, $\alpha=0.1$ in Panel (a). Solid circles: Exact results produced by eHEOM reported in ref 134. Cyan dashed lines: Ehrenfest dynamics. Orange dashed lines: FSSH. Magenta solid lines: CMM with $\gamma=0.366$. Purple and green solid lines: wMM with $\Delta=0.1$ and 0.05 , respectively. Panel (b) is similar to Panel (a) but for $\alpha=0.4$; Panel (c) is similar to Panel (a) but for $\omega_c=2.5$; Panel (d) is similar to Panel (a) but for $\omega_c=2.5$, $\alpha=0.4$. In each model 300 continuous DOFs (i.e., effective bath modes) are used.

579x515mm (600 x 600 DPI)

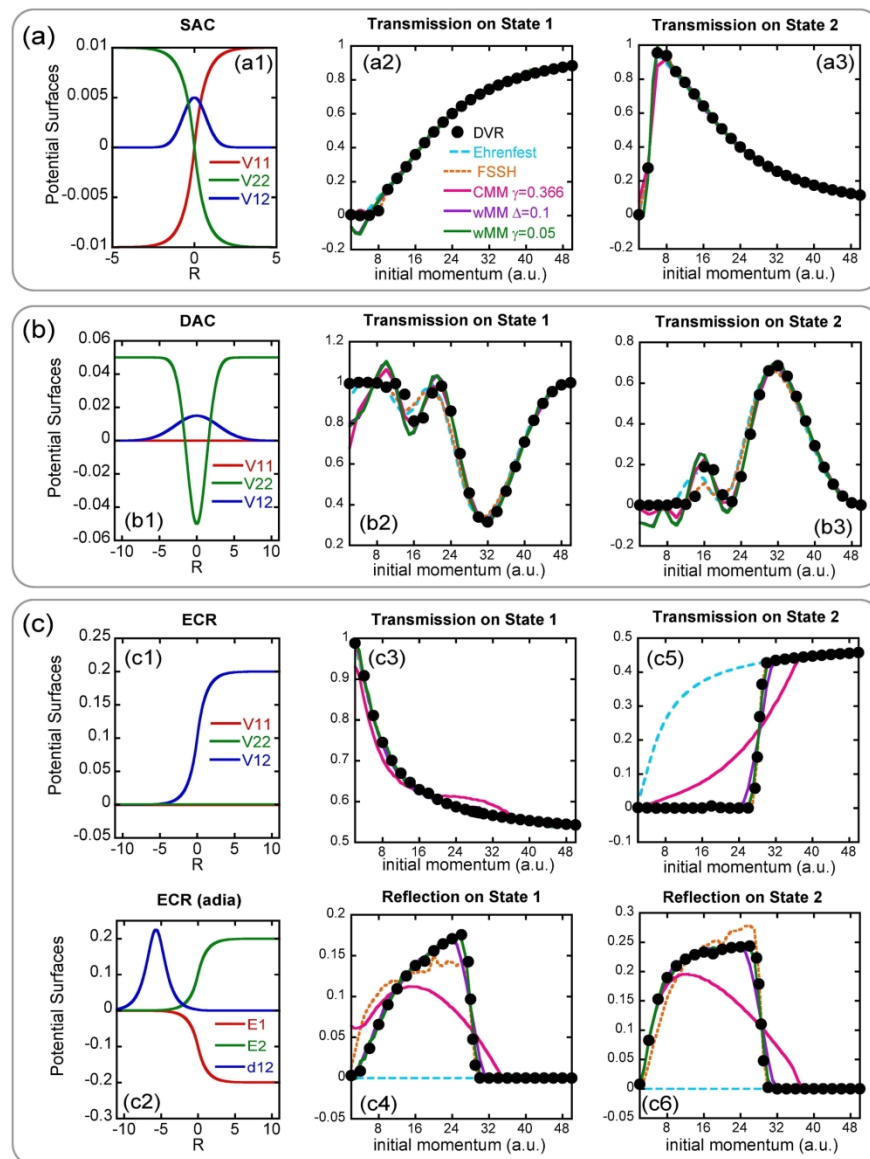
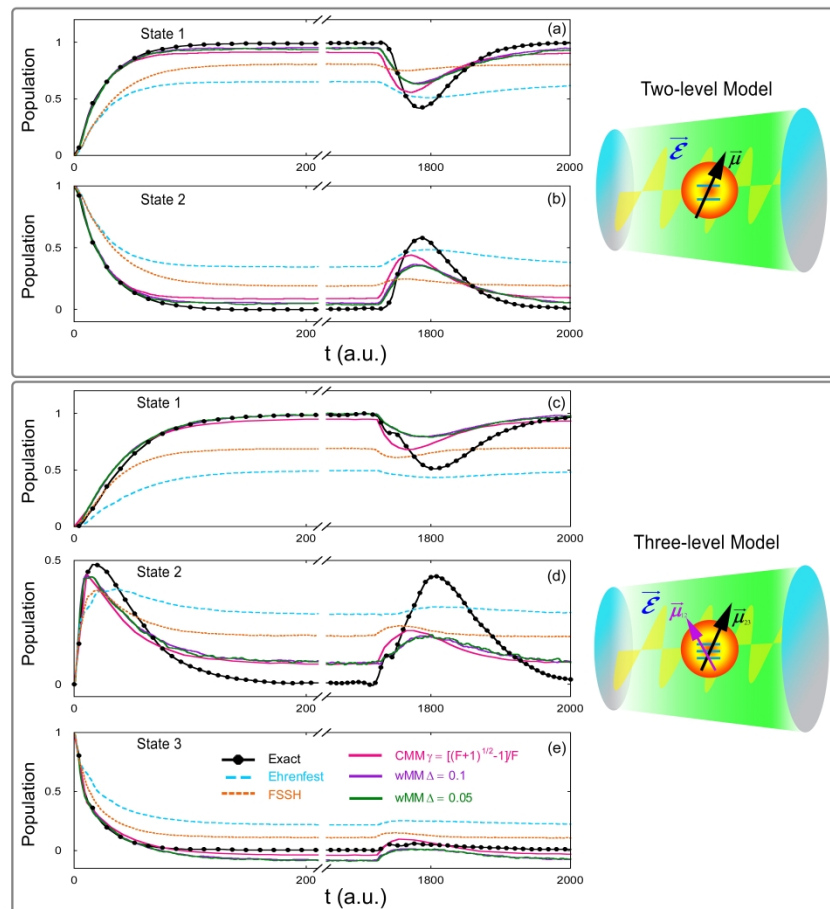


Illustration of three Tully models and simulation results. Panel (a1) denotes diabatic PESes $V_{11}(R)$ and $V_{22}(R)$, as well as coupling term $V_{12}(R)$ for the SAC model; Panel (b1) does so for the DAC model; Panel (c1) does so for the ECR model. Panel (c2) demonstrates adiabatic PESes $E_1(R)$ and $E_2(R)$, as well as nonadiabatic coupling vector $d_{12}(R)$. Panels (a2)-(a3): transmission coefficients on diabatic state 1, and those on diabatic state 2 of the SAC model, respectively. Panels (b2)-(b3): similar to Panels (a2)-(a3), but for the DAC model. Panels (c3) and (c4): transmission/reflection coefficients on adiabatic state 1 of the ECR model; Panels (c5) and (c6): those on adiabatic state 2. In Panels (a2)-(a3), (b2)-(b3), and (c3)-(c6), magenta, purple and green lines stand for transmission coefficients results for CMM with $\gamma=0.366$, wMM with $\Delta=0.1$, and wMM with $\Delta=0.05$, respectively. Long-dashed blue lines: Ehrenfest dynamics; Short-dashed orange lines: FSSH; Black points: exact DVR benchmarks.

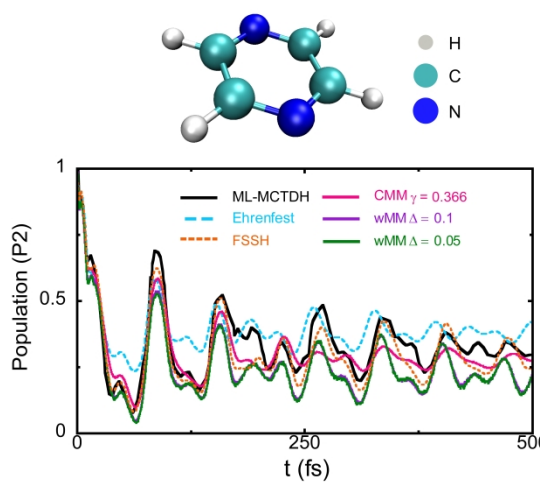
180x239mm (300 x 300 DPI)

1
2
3
4
5
6
7
8
9
10
11
12
13
14
15
16
17
18
19
20
21
22
23
24
25
26
27
28
29
30
31
32
33
34
35
36
37
38
39
40
41
42
43
44
45
46
47
48
49
50
51
52
53
54
55
56
57
58
59
60



Results of population dynamics for the atom-in-cavity models. Panels (a)-(b) represent data of the first and second states of the two-level model, respectively. Panels (c)-(e) denote data of the first, second and third states of the three-level model, respectively. Magenta solid lines: CMM with $\gamma = (\sqrt{F+1}-1)/F$; Purple solid lines: wMM with $\Delta = 0.1$; Green solid line: wMM with $\Delta = 0.05$; Cyan long-dashed lines: Ehrenfest dynamics; Orange short-dashed lines: FSSH; Black solid-dotted lines: exact results of refs 285-286. In each model 400 continuous DOFs (i.e., standing-wave modes) are involved.

840x1188mm (600 x 600 DPI)



Results of population dynamics of the second electronic state of the 2-level 3-mode pyrazine model.
Magenta solid lines: CMM with $\gamma = (\sqrt{F+1}-1)/F \approx 0.366$; Purple solid lines: wMM with $\Delta = 0.1$; Green solid lines: wMM with $\Delta = 0.05$. Cyan dashed lines: Ehrenfest dynamics; Orange short-dashed lines: FSSH; Black solid lines: ML-MCTDH results of ref. 212.

979x515mm (600 x 600 DPI)